A STUDY OF ELECTRON EFFECTS IN SOLID SOLUTION ALLOYS OF TITANIUM

Thesis by

Joseph Myers Denney

In Partial Fulfillment of the Requirements

for the Degree of

Doctor of Philosophy

California Institute of Technology

Pasadena, California

1955

ACKNOWLEDGMENT

The writer is extremely grateful to Professor Pol Duwez for his advice and encouragement during the course of this investigation. He is also indebted to Professors R. B. Leighton and H. V. Neher for the use of some of the facilities of the Norman Bridge Laboratory of Physics. Professor B. G. Bergman kindly read and criticized the manuscript. Mr. J. McClelland provided valuable assistance in the magnetic susceptibility measurements; Mr. J. Wyman assisted in the preparation of some of the titanium-gallium alloys; and Mr. J. Varady prepared tracings of the figures. Gratitude is due the Office of Naval Research for its support of this study.

ABSTRACT

Anomalous behavior of the lattice parameters of solid solution alloys of aluminum and gallium in titanium were observed at approximately 3 atomic percent solute. Alloys of silver in titanium did not exhibit similar anomalies. Anomalies also were observed in the resistivity and in the coefficient of magneto-resistance for solutes of Al and Ga. No significant evidence of anomalous behavior of the Hall coefficient or the magnetic susceptibility with solute concentration was found.

The effect of solute valency in producing the observed anomalous changes in physical properties is interpreted, using the Bloch-Brillouin approximation, as evidence of interaction between the Fermi surface and the Brillouin Zones. The effects produced by monovalent Ag and trivalent Al and Ga solutes indicate that titanium has an alloying valency between 1 and 3 in these alloys. The Brillouin Zone interpretation indicates that the alloying valency of titanium is about 1.5 electrons per atom.

The absence of an effect of solute addition on the susceptibility, the susceptibility-temperature data of Squire and Kaufmann, and the magnitude of the susceptibility indicate that titanium is antiferromagnetic. The suggested antiferromagnetism is in agreement with the interpretation of the effects of solute additions on the other observed physical properties. It is, therefore, concluded that titanium

has approximately 2 electrons per atom in antiferromagnetic coupling between neighboring atoms, and about 2 electrons per atom in the conduction band. Neutron diffraction experiments to verify the suggested existence of a simple hexagonal antiferromagnetic superlattice in titanium are urged.

TABLE OF CONTENTS

TABLE OF CONTENTS (cont'd.)

TABLE OF CONTENTS (cont'd.)

LIST OF FIGURES

LIST OF FIGURES (cont'd.)

LIST OF FIGURES (cont'd.)

LIST OF TABLES

I. INTRODUCTION

Metals are distinguished from other solids in nature by certain outward characteristics which permit them to be easily identified as metals. These characteristics, which are well known, include such properties as ductility, metallic luster, and electrical conductivity. Metals possess certain internal characteristics, responsible for their outward appearance, which are unique in the general class of solids. Addition of a second atomic species to a metal may cause the original crystalline array to be abandoned in favor of some other crystalline array. The degree to which the second atomic species can be added to the first without changing the characteristic crystal structure of the pure metal is determined largely by the difference between the two atomic species. The atomic characteristics most important in this respect are: atomic size, valency, and position in the periodic table. Other considerations are due to the atoms being arranged in the metal; these are: crystal structure of the pure metal and the number of electrons which are not bound to a particular atom in the metal. These outer, "free", electrons, it is well known, are responsible for the metallic properties of metals. In general, the extent to which alloying is possible, the concentration of metal atoms B on the crystal lattice of A , depends on the similitude of A and B in the respects listed above. Since the effects of the free electrons on solid solution

formation is not as readily understood as the other requirements, special attention appears to be indicated. The purpose of the present study is to examine the effect of the outer electrons on solid solution alloys of titanium.

Introduction of solute atoms substitutionally into the solvent lattice changes the number of free electrons in the alloy at a rate proportional to the difference in the number of outer electrons of the solute and solvent atoms. The alkali metals contribute 1 electron per atom, the alkaline earth metals 2, and so on. For the simple metals, with a few outer electrons above a noble gas structure, the number of "free" electrons contributed by each atom, the alloying valency, is well defined. The transition metals, however, present the question of how many of the outer electrons are actually "free" in the sense of the simpler metals. Sufficient latitude exists in the formal definition of alloying valency for the transition metals that the alloying valency is variously defined between 0 and 5.8 electrons per atom (1), (2). This difficulty is discussed in more detail in Section VI.

Jones (3), (4), in about 1934, applied considerations of the outer electrons, developed earlier by Peierls (5) and Brillouin (6), to explain the occurrence of the γ-phase in Cu-Zn and other binary alloys. Jones concluded that the limiting concentrations of Cu and Zn in the γ-phase are determined by the electron-atom ratio, the number of "free" electrons per atom.

Following Jones' work on the Cu-Zn phases, anomalous

lattice parameter changes in magnesium alloys were reported by Hume-Rothery and Raynor (7), Raynor (8), (9), (10), (11), (12), Jones (13), and Busk (14). The lattice parameter changes reported by these investigators were found to depend on the difference between the valency of magnesium and the solute valency. Magnesium crystallizes in the hexagonal close packed structure which is characterized by the parameters a, the atom to atom distance in the basal plane, and c, the atom to atom distance in the axial direction of the hexagonal prism. In addition to the volume change due to the solute size, it was found that the axial ratio, c/a, depended monotonically on the solute valency. This effect was explained with the same considerations employed by Jones on the Cu-Zn alloys. Busk, in his extensive review of the magnesium alloys (14), found that the shear strain in the magnesium alloys, the change in the axial ratio, could be simultaneously described for all solutes provided he assigned an alloying valency, slightly different than the chemical valency, to the solutes.

Titanium, since it crystallizes in the hexagonal close packed structure, provides an opportunity for solute effects similar to those found in the Mg alloys. The hexagonal close packed lattice is unique among the most common crystal structures of metals (h. c. p., b. c. c., and f. c. c.) in the ability to exhibit shear strain in addition to dilatation with solute addition. The present study describes the effect of solute additions on the lattice parameters of the titanium lattice.

The changes in the lattice parameters of the titanium lattice are found to be similar to those found in the Mg alloys. Theoretical interpretation of the lattice parameter changes suggests that changes in other physical properties, accompanying the lattice parameter anomalies, should be found. Titanium, being a transition element (with the atomic configuration $3d^2\ 4s^2$), offers an opportunity to correlate the effects of solute additions in a non-transition element (Mg) with a transition element.

Sections II and III describe the preparation and measurement of lattice parameter, resistivity, magnetic susceptibility, Hall coefficient, and coefficient of magneto-resistance of titanium alloys with solutes of aluminum, gallium, and silver. These solutes were selected because of their wide range of solubility in titanium. The observed physical properties were selected for their sensitivity to electron-atom ratio in the alloys. The results of these measurements are presented in Section IV. In Section V the Brillouin zones and energy zones are derived from fundamentals as a basis for the interpretation of the experiments. The space group and point group symmetry elements of crystal lattices require, in general, additional symmetry of the Brillouin zones. These requirements are discussed and the energy zones for the hexagonal close packed lattice are calculated. Section VI presents a discussion of the experimental results of Section IV in terms of the energy zones developed in Section V. The work is summarized and conclusions are presented

in Section VII.

II. EXPERIMENTAL METHODS

A. Alloy Preparation:

The alloys employed in this study were prepared from the pure metals. Titanium metal, prepared from the tetraiodide, was obtained from the New Jersey Zinc Company. Aluminum, employed in all but the initial survey alloys, is of spectroscopic quality supplied by the Jarrel-Ash Company. The Eagle Pitcher Sales Company supplied the pure gallium metal. Spectroscopic quality silver was obtained from the Jarrel-Ash Company. The impurity analyses of these metals is presented in Table 1.

Alloy preparation was accomplished by melting the pure metals in a Kaufmann type furnace (15). This furnace consists of a water-cooled copper hearth and an adjustable water-cooled molybdenum electrode contained in a pyrex cylinder mounted on rubber gaskets in brass end plates. The assembly is provided with a connection to a vacuum manifold and a source of helium. Melting is accomplished by striking an arc between the molybdenum electrode and the metals on the hearth in an atmosphere of helium at a few pounds per square inch above atmospheric pressure.

Clark's studies (16) indicate that the lattice parameters of titanium are sensitive to contaminants. The lattice parameters of remelted specimens were found to be independent, within experimental accuracy, of melting. Changes in ductility and hardness, which are

Table 1

IMPURITY ANALYSIS OF TITANIUM, ALUMINUM, GALLIUM, AND SILVER

Titanium from New Jersey Zinc Co., Lot No. IT-417

Impurity	Concentration
N	0.002%
Mn	0.015
Fe	0.005
Al	0.008
Mo	0.001
Pb	0.0045
Ni	0.0035
Cu	0.0025
Mg	0.0015

Rockwell F average 77.

Aluminum from Jarrel-Ash Co.; Johnson, Matthey & Co., Ltd., London; Suppliers

Spectroscopic Analysis

Impurity	Concentration
Mg	0.001%
Cu	0.0005
Si	0.0005
Ag	0.0003
Fe	0.0002
Mn	0.0001
Cd	0.0001

Gallium from Eagle-Pitcher Sales Co., Joplin, Mo.
Lot No. 2-3694-900 - Guaranteed Purity 99.95%
principal impurity: Pb 0.02%

Table 1 (continued)

Silver from Jarrel-Ash Co.; Johnson, Matthey & Co., Ltd., London; Suppliers

Spectroscopic Analysis

Impurity	Concentration
Cu	0.0001%
Ca	0.0001
Na	0.0001
Fe)	
Mg)	
Mn)	
Pb)	trace: faint spectroscopic evidence
Si)	
Cd)	
Sn)	

also sensitive to impurity content, were found to be only slightly changed after melting. Therefore, it was concluded from the examination of several pure titanium specimens, which were repeatedly melted, that no significant contamination occurred during melting.

Extreme care was exercised throughout all stages of alloy preparation in handling and cold forming to prevent the inclusion of surface contaminants in the alloys. The pure metals and alloys were washed in a solution of HF, HNO_3, and H_2O, followed by an acetone rinse.

The titanium alloys with aluminum and silver were melted by placing the pure metals in the furnace together. In order to melt the alloys with gallium, it was necessary to diffuse the gallium into the titanium prior to melting. This was accomplished by making a crucible and tight fitting cover of titanium. The gallium metal was placed in the titanium crucible, and the crucible was sealed in an evacuated vycor capsule. The crucible was slowly heated to 700°C during 6 hours and held at 700°C for 18 hours. During this treatment the gallium diffused completely into the titanium capsule. The weight change for the 5 gram assembly was less than 0.3 milligram in each case. After the diffusion treatment the alloy was melted in the same manner as the other alloys. Mixing of the metals was accomplished by convection currents in the molten alloy, and by repeatedly remelting the alloy ingot, turning it over each time.

Alloy analysis was provided by the weights of the alloy

constituents prior to melting and the requirement of a total weight change of two milligrams or less in the five gram specimen during melting. No chemical analyses were made; the requirement of a small weight change during melting was considered adequate. Alloys exhibiting a weight change in excess of two milligrams during melting were abandoned. The composition of each specimen, determined from the constituent weights, is presented in Table 2.

The alloy specimens were cold rolled after melting to break up columnar grains formed in cooling from the melt. Annealing and local homogenization of the cold worked alloys was accomplished by heating in evacuated quartz capsules at a temperature of the order of 1000°C for approximately twenty-four hours. Zirconium strip or wire was included in each capsule to act as a getter to reduce contamination to a minimum. It was intended that this first anneal be performed in the beta phase. However, for the titanium alloys with gallium, there was no available phase diagram. Therefore, the temperature for annealing the alloys with gallium was based on experience with the other solutes and repeated trial.

After the first anneal the alloy specimens were formed to the desired shape. Thin foil, desired for the experiments was formed from the small annealed ingots by cold rolling. Only in the alloys of low solute concentration was it possible to obtain foil 0.020 to 0.040 inches thick without cracks by cold rolling. Therefore, the alloys were cold rolled to 0.040 inch foil or until cracking began. The cold

Table 2

ALLOY HEAT TREATMENT

Spec. No.	Atomic % Solute	Melting Wgt. Chng. ΔW/W	Homogenize °C, Hrs.	Anneal °C, Hrs.
Ti #1	0	not melted	-----	-----
Ti #2	0	not melted	-----	-----
Ti #4	0	0.001	950°, 10 hr.	-----
Ti #5	0	0.0003	950°, 24 hr.	-----
Ti #6	0	0.0001	950°, 24 hr.	-----
TiAl #24	0	0.0002	950°, 24 hr.	-----
TiAl #9	1.466	0.0002	950°, 24 hr.	800°, 4 hr.
TiAl #14	1.897	0.0001+	950°, 24 hr.	800°, 4 hr.
TiAl #15	2.194	0.0001	950°, 24 hr.	800°, 4 hr.
TiAl #16	2.661	0.0001-	950°, 24 hr.	800°, 4 hr.
TiAl #17	3.153	0.0001-	950°, 24 hr.	800°, 4 hr.
TiAl #18	3.480	0.0001-	950°, 24 hr.	800°, 4 hr.
TiAl #7	4.386	0.0001-	950°, 24 hr.	800°, 4 hr.
TiAl #19	5.509	0.0001-	1000°, 24 hr.	850°, 8 hr.
TiAl #12	6.696	0.00008	1000°, 24 hr.	850°, 8 hr.
TiAl #10	8.267	0.00009	1050°, 24 hr.	850°, 8 hr.
TiAl #20	9.410	0.0001	1050°, 24 hr.	850°, 8 hr.
TiAl #13	10.372	0.00007	1050°, 24 hr.	850°, 8 hr.
TiAl #8	12.310	0.0001	1080°, 24 hr.	900°, 8 hr.
TiAl #22	13.421	0.0001	1080°, 24 hr.	900°, 8 hr.
TiAl #23	15.185	0.0001	1080°, 24 hr.	900°, 8 hr.
TiAl #36	18.10	0.0001	1100°, 24 hr.	900°, 8 hr.
TiAl #28	22.04	0.0001	1125°, 24 hr.	900°, 8 hr.
TiAl #32	23.89	0.00006	1160°, 24 hr.	900°, 8 hr.
TiAl #30	25.13	0.0001	1180°, 24 hr.	900°, 8 hr.
TiAl #34	27.96	0.00009	1200°, 24 hr.	900°, 8 hr.
TiAl #33	29.81	0.0001	1220°, 24 hr.	900°, 8 hr.
TiAl #29	32.41	0.0001	1250°, 24 hr.	900°, 8 hr.
TiAl #31	34.50	0.0001	1250°, 24 hr.	900°, 8 hr.
TiAl #35	39.75	0.0001	1250°, 24 hr.	900°, 8 hr.

Table 2 (cont'd.)

Spec. No.	Recrystallize °C, Hrs.	Powder Specimen Anneal	Final Anneal °C, Hrs.
Ti #1	600°, 1 hr.		-----
Ti #2	600°, 1 hr.		-----
Ti #4	600°, 1 hr.		-----
Ti #5	600°, 1 hr.		-----
Ti #6	600°, 1 hr.		800°, 24 hr.
TiAl #24	600°, 1 hr.		800°, 24 hr.
TiAl #9	620°, 1 hr.		800°, 24 hr.
TiAl #14	625°, 1 hr.		800°, 24 hr.
TiAl #15	640°, 1 hr.		800°, 24 hr.
TiAl #16	650°, 1 hr.		800°, 24 hr.
TiAl #17	650°, 1 hr.		800°, 24 hr.
TiAl #18	670°, 1 hr.		800°, 24 hr.
TiAl #7	690°, 1 hr.		800°, 24 hr.
TiAl #19	700°, 1 hr.		800°, 24 hr.
TiAl #12	725°, 1 hr.		-----
TiAl #10	725°, 1 hr.		-----
TiAl #20	750°, 1 hr.		-----
TiAl #13	750°, 1 hr.		-----
TiAl #8	775°, 1 hr.		-----
TiAl #22	775°, 1 hr.		-----
TiAl #23	800°, 1 hr.		-----
TiAl #36	800°, 1 hr.		-----
TiAl #28		900°, 1 hr.	-----
TiAl #32		900°, 1 hr.	-----
TiAl #30		900°, 1 hr.	-----
TiAl #34		900°, 1 hr.	-----
TiAl #33		900°, 1 hr.	-----
TiAl #29		900°, 1 hr.	-----
TiAl #31		900°, 1 hr.	-----
TiAl #35		900°, 1 hr.	-----

Table 2 (cont'd.)

Spec. No.	Atomic % Solute	Melting Wgt. Chng. $\Delta W/W$	Homogenize °C, Hrs.	Anneal °C, Hrs.
TiGa #6	0.4825	0.0001	975°, 24 hr.	800°, 4 hr.
TiGa #1	1.090	0.0001	975°, 24 hr.	800°, 4 hr.
TiGa #7	1.135	0.0001	975°, 24 hr.	800°, 4 hr.
TiGa #9	1.815	0.0001	975°, 24 hr.	800°, 4 hr.
TiGa #2	1.833	0.0001	975°, 24 hr.	800°, 4 hr.
TiGa #3	2.570	0.0001	975°, 24 hr.	800°, 4 hr.
TiGa #10	2.694	0.0001	975°, 24 hr.	800°, 4 hr.
TiGa #11	2.804	0.0001	975°, 24 hr.	800°, 4 hr.
TiGa #12	3.146	0.0001	975°, 24 hr.	800°, 4 hr.
TiGa #5	3.493	0.0001	975°, 24 hr.	800°, 4 hr.
TiGa X	3.72	0.0002	975°, 24 hr.	800°, 4 hr.
TiAg #5	0.53	0.0001	1000°, 12 hr.	825°, 8 hr.
TiAg #2	1.09	0.0001	1000°, 12 hr.	825°, 8 hr.
TiAg #1	1.53	0.0001	1000°, 12 hr.	825°, 8 hr.
TiAg #6	1.94	0.0001	1000°, 12 hr.	825°, 8 hr.
TiAg #10	2.54	0.0002	1000°, 12 hr.	825°, 8 hr.
TiAg #7	2.97	0.0001	1000°, 12 hr.	825°, 8 hr.
TiAg #9	3.51	0.0002	1000°, 12 hr.	825°, 8 hr.
TiAg #3	3.94	0.0002	1000°, 12 hr.	825°, 8 hr.
TiAg #8	4.95	0.0002	1000°, 12 hr.	825°, 8 hr.
TiAg #4	5.70	0.0002	1000°, 12 hr.	825°, 8 hr.

Table 2 (cont'd.)

Spec. No.	Recrystallize °C, Hrs.	Final Anneal °C, Hrs.
TiGa #6	600°, 1 hr.	800°, 24 hr.
TiGa #1	620°, 1 hr.	800°, 24 hr.
TiGa #7	625°, 1 hr.	800°, 24 hr.
TiGa #9	650°, 1 hr.	800°, 24 hr.
TiGa #2	650°, 1 hr.	800°, 24 hr.
TiGa #3	680°, 1 hr.	800°, 24 hr.
TiGa #10	690°, 1 hr.	800°, 24 hr.
TiGa #11	700°, 1 hr.	800°, 24 hr.
TiGa #12	720°, 1 hr.	800°, 24 hr.
TiGa #5	720°, 1 hr.	800°, 24 hr.
TiGa X	720°, 1 hr.	800°, 24 hr.
TiAg #5	550°, 1 hr.	825°, 24 hr.
TiAg #2	600°, 1 hr.	825°, 24 hr.
TiAg #1	600°, 1 hr.	825°, 24 hr.
TiAg #6	600°, 1 hr.	825°, 24 hr.
TiAg #10	600°, 1 hr.	825°, 24 hr.
TiAg #7	620°, 1 hr.	825°, 24 hr.
TiAg #9	640°, 1 hr.	825°, 24 hr.
TiAg #3	640°, 1 hr.	825°, 24 hr.
TiAg #8	650°, 1 hr.	825°, 24 hr.
TiAg #4	650°, 1 hr.	825°, 24 hr.

rolled foil was trimmed to sheets approximately 3/4 x 2 inches, washed in acid, and sealed in evacuated vycor capsules with a Zr getter for further annealing.

The second homogenizing anneal was begun by heating in the beta phase for one hour, followed by cooling to the alpha phase. The alloys were held in the alpha phase near the α, $\alpha + \beta$ boundary for approximately eight hours to insure complete transformation of the alloy to the alpha phase. The annealing temperature for each specimen is given in Table 2. The alloys were quenched in the vycor capsules following this anneal.

The thin foils, previously cold rolled to 0.040 inches thick, were cold rolled slightly, to promote recrystallization with further annealing, and bent to the radius of the X-ray camera. The foils, too brittle to be cold rolled to 0.040 inches thick, were cold rolled slightly, but not enough to cause any additional cracking. Since these thick alloy specimens could not be bent to the radius of the X-ray camera, the cylindrical surface was generated by grinding these specimens. A brass disc, machined to the diameter of the X-ray camera, was fitted with #400 waterproof polishing cloth and mounted on the spindle of a 14-inch lathe. The alloy specimen was mounted in a lucite disc in the manner of a metallurgical specimen. The lucite disc, in turn, was mounted in a holder on the lathe tool post. The alloy specimen was held against the turning polishing cloth with the lathe cross feed. A small mount of water applied during the

grinding was found to be helpful in removing debris from the polishing cloth. After the cylindrical surfaces were generated, the specimen was removed from the lucite disc by notching the lucite and striking it sharply with a hammer. All traces of lucite were removed by prolonged washing in acetone. A final washing in HF and HNO_3 was employed to remove possible surface contaminants and prepare the specimens for the subsequent recrystallizing anneal.

The temperature and time of the recrystallization anneal were determined from trial X-ray diffraction patterns. In general, increased solute concentration required a higher annealing temperature to develop sharp X-ray diffraction lines. Since solid specimens were used, small grains were necessary to prevent spotty diffraction lines. The time and temperatures yielding the best results on trial X-ray patterns, and used for the lattice parameter determinations, are given in Table 2. The titanium-aluminum alloys above 20 atomic percent aluminum were too brittle to be rolled, and hence required different preparation methods described in Section II B.

Attempts to prepare single crystals of these alloys met with failure. It was felt desirable to examine single crystals at later stages of the investigation, especially to evaluate the extent of the anisotropy. Due to the allotropy, a straight-forward application of Bridgman methods (17) cannot be expected to be profitable. The strain-anneal method (18) was attempted, but it was only partially successful in the pure iodide titanium specimens. In the aluminum

alloys even 1/2 atomic percent aluminum proved to increase the nucleation rate prohibitively for any further attempt. The development of single crystals of titanium alloys evidently requires elaborate investigation which is considered beyond the scope of this study.

B. X-Ray Diffraction Techniques:

A careful survey of available diffraction techniques indicated that care was necessary to achieve the desired accuracy in the lattice parameters. As a result of work published by Clark (16), it was apparent that even small concentrations of oxygen or nitrogen have a pronounced effect on the lattice parameters, especially c, of titanium. A comparison of Clark's results with those of others, together with the experimental methods, suggested that powder specimens as used in Debye-Scherrer type cameras are unsuitable. This conclusion was supported in preliminary determinations of lattice parameter. The proposed explanation, which was not extensively investigated, is that in preparing the alloy powder to be used in a Debye-Scherrer camera, oxygen and nitrogen are adsorbed on the surface of the powder. Such a surface condition is probably also achieved in the case of solid specimens. The primary consideration is a large difference in the surface to volume ratio between powder specimens and solid specimens. For powder grains of the order of 10 microns in diameter, a surface to volume ratio of 0.6×10^6 cm per cc is obtained. A smooth metal surface will present about 10^{14} surface

atoms per square centimeter. If a mono-molecular surface layer of oxygen atoms is formed on the presentation of a surface of titanium to air at room temperature, then from above it is seen that this layer will contain about 0.6×10^{20} oxygen atoms per cc of titanium powder (at the density of solid titanium). This amounts to an oxygen concentration of the order of 0.5 atomic percent. For a suitable solid X-ray specimen an atomic concentration of the order of 10^{-7} to 10^{-8} can similarly be expected. On the basis of Clark's results, a variation in lattice parameter of 0.01 Å in the c parameter and 0.003 Å in a parameter can be expected for the powder specimen. The expected variation in the case of the solid specimen due to surface adsorbed contaminants is much less than the desired accuracy of 0.00003 Å in parameter determination. Therefore, it is concluded that lattice parameter accuracy of the order of plus or minus 5×10^{-5} Å requires the use of solid specimens for X-ray diffraction measurements.

1. Solid Specimen Method

Of the two common methods of obtaining X-ray diffraction results from solid specimens, it was found that employing a focusing camera was superior to the back-reflection method using a Laue camera and monochromated X-rays. The focusing camera permitted the application of statistical methods to the determination of lattice parameter from the diffraction lines to a degree not possible with

flat film methods. The determination of lattice parameters is discussed in detail in Section III.

The focusing camera employed in this study was a 21 cm asymmetrical camera of the type designed by Jette and Foote (19), manufactured by George Wyland, Ramsey, New Jersey. Film calibration, which is normally accomplished by the use of calibrated knife edges at the ends of the film, was achieved by the use of molybdenum powder painted on the edge of the specimen, the diffraction lines from the molybdenum powder serving as calibration lines on the film. The calibrated knife edges built into the body of the camera were found to shift slightly (of the order of a few minutes of a degree) upon disassembling and remounting the specimen. This shift was thought to be due to a very small displacement occurring between the specimen and film holder and the body of the camera. A convenient solution was found in the addition of a calibrating material. Molybdenum was chosen for its accurately known lattice parameter, and a desirable number and location of diffraction lines with respect to the titanium lines. The molybdenum employed was in the form of a fine powder obtained from the Westinghouse Electric Corporation. Purity of the Mo powder was certified to be better than 99.99 percent. Accurate lattice parameter determinations of Mo are due to Spieser (20) at Ohio State giving $\underline{a}$ equal 3.14665 $\mathring{A}$. The average of a series of 6 determinations of lattice parameter of the molybdenum powder with a Norelco 11 cm powder camera was found to be 3.14667 $\mathring{A}$ at 27°C

with a standard deviation for this series of 0.00009 Å. Accordingly, the parameter of the molybdenum was taken as 3.14665 Å in all subsequent calculations.

The solid specimens, either bent foil or cylindrically ground and prepared in a manner previously described, were painted with a mixture of the Mo powder and banana oil in a narrow stripe on the cylindrical face. The diffraction of X-rays from the specimen in the camera occurred both from the titanium alloy and the stripe of Mo powder.

The X-ray target was copper in all lattice parameter determinations presented, using the $K_{\alpha 1}$ and $K_{\alpha 2}$ characteristic radiation. In order to improve definition of the diffraction pattern on the film, the nickel filter was placed immediately in front of the film to reduce noncoherent scattering and fluorescence by the specimen in a manner discussed by Barrett (21).

It was found impractical to attempt to control specimen temperature at some arbitrary temperature; however, after about one hour the heating due to the camera motor and the X-ray power supply caused the camera and specimen to reach a stable maximum temperature of 27°C. Temperature control was accomplished by maintaining a specimen and camera temperature of 27°C in all exposures by adjusting the amount of ventilation around the camera.

It is well known that the use of single emulsion film in asymmetrical X-ray cameras is desirable in reducing parallax of the

diffraction lines on the film. In this case, however, it was found that single emulsion film offered no improvement in accuracy over double emulsion film for the diffraction lines employed in the analysis. The increased parallax in double emulsion films was compensated by increased contrast and improved film grain size in the double emulsion film employed. In addition, the diffraction lines used in the analysis occurred at Bragg angles where the effect of parallax between the two emulsions of the film was low, Figure 1. Since the errors due to parallax are systematic, they are largely eliminated by the statistical methods employed in the analysis of the films. After a survey of available X-ray films with the above considerations in mind, it was found that Eastman "No-Screen" X-ray film offered the best compromise between the advantages displayed by various types. Accordingly, the double-emulsion type was used in all diffraction studies.

2. Debye-Scherrer Studies

Lattice parameter measurements extended to the solubility limit were accomplished with the powder method, by necessity. Recognizing the previously mentioned objection to the powder method in this study, it was hoped that at higher aluminum concentrations the expansion of the lattice due to absorbed gases would decrease. Estimation of the error incurred by this method was achieved by comparing the lattice parameters obtained by the powder method with

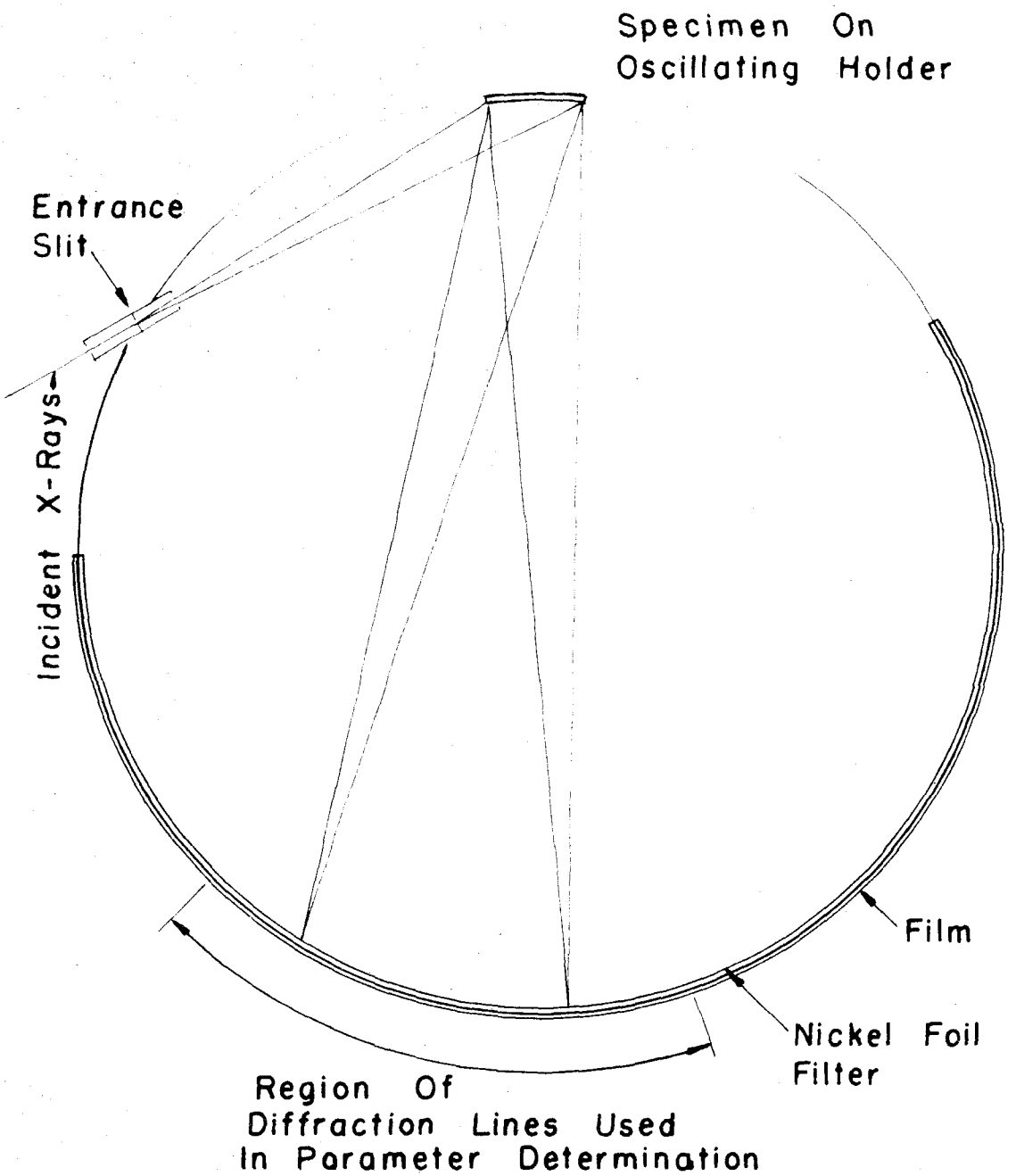

Figure 1

Schematic Of 21 cm. Asymmetrical Focusing Camera

the lattice parameters of solid alloy specimens. At 18 atomic percent aluminum the difference between the c parameter determined from a powder specimen and a solid specimen is 0.0015 Å, while for pure titanium the difference is 0.005 Å or more. It was assumed, therefore, that the error due to using powder methods was less than 0.003 Å in the range 22 to 36 atomic percent aluminum.

The preparation of the powder specimens duplicated the methods employed on the solid specimens up to the point of fitting the solid specimens to the camera. At this point in the preparation powder was obtained by filing the specimen. After screening and magnetically separating any file particles, the powder was sealed in evacuated vycor capsules for annealing. The powder was annealed at 900°C for one hour (Table 2).

After annealing, the powder was placed in small, thin wall quartz tubes for X-ray diffraction. The camera used in this study was an 11 cm Norelco (North American Phillips Co.) powder camera. Filtered copper characteristic radiation was used. Realizing the errors inherent in the powder method employed here, no attempt was made to control the specimen temperature during exposure. Monitored specimen temperatures were observed to be 25°C ± 3°C.

C. Physical Properties:

The alloys which were sufficiently ductile to be rolled to thin foil were further treated prior to the determination of electronic

properties. The previous annealing treatment developed a very fine grain structure suitable for X-ray diffraction studies. To minimize the grain boundary area in these alloys they were subjected to a further anneal. The specimens were sealed in individual evacuated vycor capsules with a small strip of Zr getter and held at 800°C for 24 hours.

1. Resistivity

The alloy specimens were trimmed to rectangular foils suitable for mounting in the specimen holder illustrated in Figure 2. Realizing the limiting errors in the resistivity measurements arise in the dimensional measurements, extreme care was exercised in obtaining smoothly trimmed specimens.

The resistance measurements were obtained using a Kelvin Double Bridge (Leeds & Northrup Co.). The foils were approximately 0.020 inches thick and 3/8 inch wide. The distance between the potential probes was 0.500 inch. During the resistivity measurements temperature was controlled by immersing the specimen and holder in an oil bath at 23°C.

2. Magneto-Resistance

The change of resistance in a magnetic field, perpendicular to the field, was measured for the specimens used in the resistivity determination. The apparatus is illustrated in Figures 2, 3, and 4. The magnet used has a 4-inch square soft iron core with Armco iron

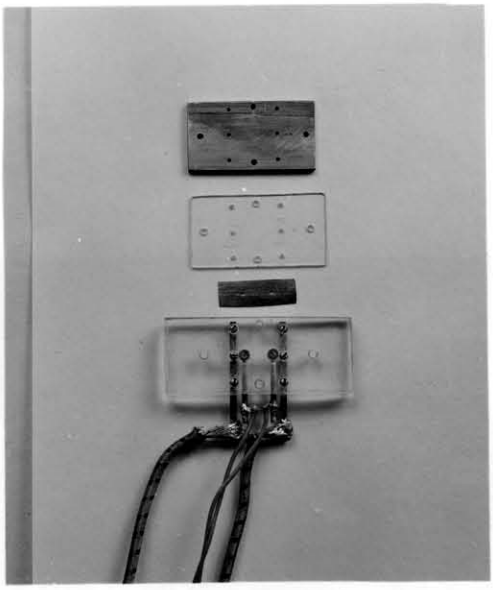

Figure 2

Magneto-Resistance
Specimen Holder

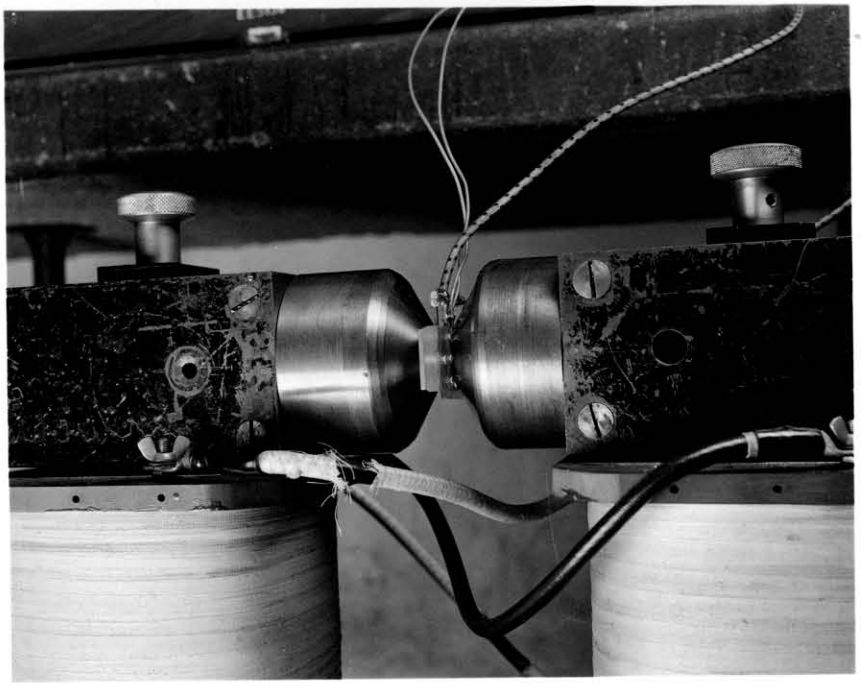

Figure 3

Magneto-Resistance
Specimen and Magnet

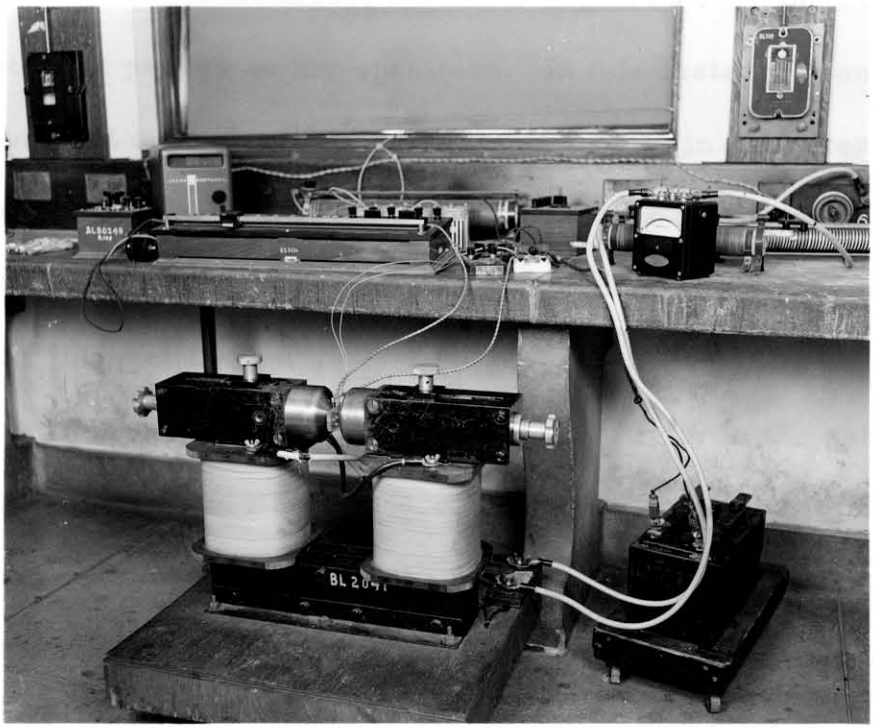

Figure 4

Magneto-Resistance
Apparatus

pole tips. Power was supplied from a regulated motor-generator set at 80 volts and 20 amperes maximum.

A uniform magnetic field is required over the area between the potential probes on the specimen. In this instance a uniform field was obtained over a cylindrical volume 3.5 cm in diameter and 1.2 cm long by the use of 120 degree conical pole tips of Armco iron. The design details and field profiles are presented in the paragraph entitled "Magnet Design".

In order to obtain sufficient sensitivity in the galvanometer circuit of the Kelvin Bridge a d. c. amplifier was substituted for the galvanometer. The output of the amplifier was used to drive a 0-1 volt vacuum tube voltmeter (Figure 5). While this system provided sufficient sensitivity, it had poor drift characteristics. Thus the "null" adjustment at zero field had to be checked both before and after making the resistance measurements in the magnetic field. The bridge slide wire was employed for the "coarse" adjustment of the bridge, a "fine" adjustment was provided by a 1000 ohm "Helipot" connected in parallel with the bridge slide wire. In this fashion resistance changes of the order of 10^{-7} were observable.

Thermal drift of the resistance was considered to be the most troublesome error encountered. A partial solution was effected by enclosing the specimen, holder, and pole faces in an oil bath (not shown in Figures 2 and 3). Thermal drift was not completely removed however, and satisfactory reproducibility of experimental

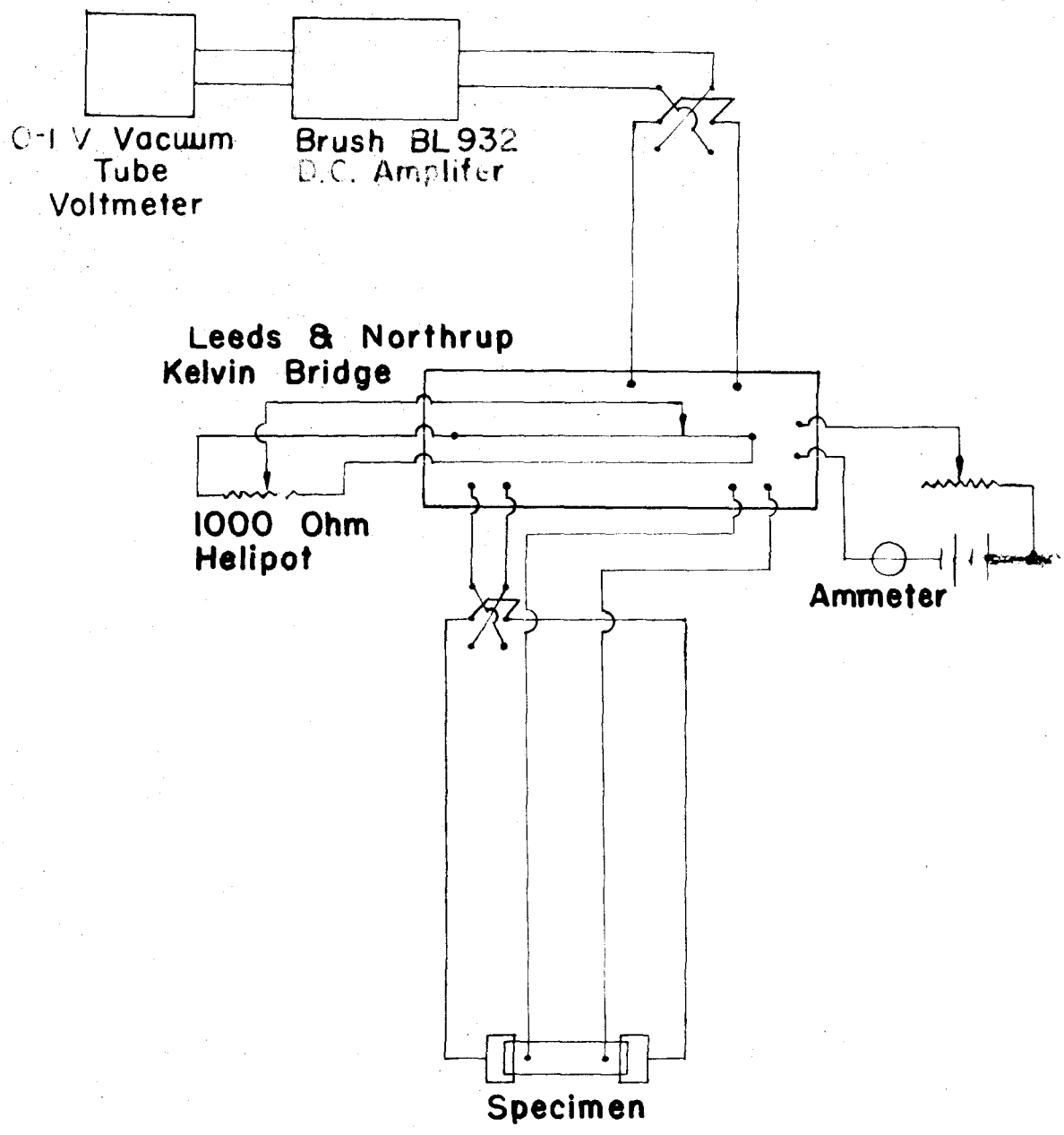

Figure 5 Schematic Of Magnetoresistance Circuit

data required that readings be taken rapidly. The standard deviation of B_t, the coefficient of magneto-resistance, was found to be of the order of $\pm 5 \times 10^{-14}$ oersted^{-2} and adequate for the purposes of the present study.

3. Hall Coefficient

The Hall coefficient, a measure of the shift in equipotential surfaces in a conductor due to an applied magnetic field, was measured with apparatus similar to that used for magneto-resistance. Tungsten potential probes 0.030 inch diameter were mounted in the lucite specimen holder in such a manner that a potential difference normal to both the current and applied magnetic field was measured. The potential appearing between the tungsten probes was amplified by a d.c. amplifier whose output was read on a 0 - 1 volt vacuum tube voltmeter (Figure 6). Providing the input impedance of the d.c. amplifier is sufficiently high, the Hall voltage can be read as the amplifier output. A Brush (Brush Instrument Co.) model BL-932 d.c. amplifier was used which provides an input impedance of 9 megohms. Calibration of this amplifier permitted the output to be read directly in input microvolts.

Temperature control of the specimen was accomplished by immersing the specimen and holder in an oil bath in the manner described under "Magneto-resistance". Thermal drift was not troublesome in this instance, since the Hall potential is rather

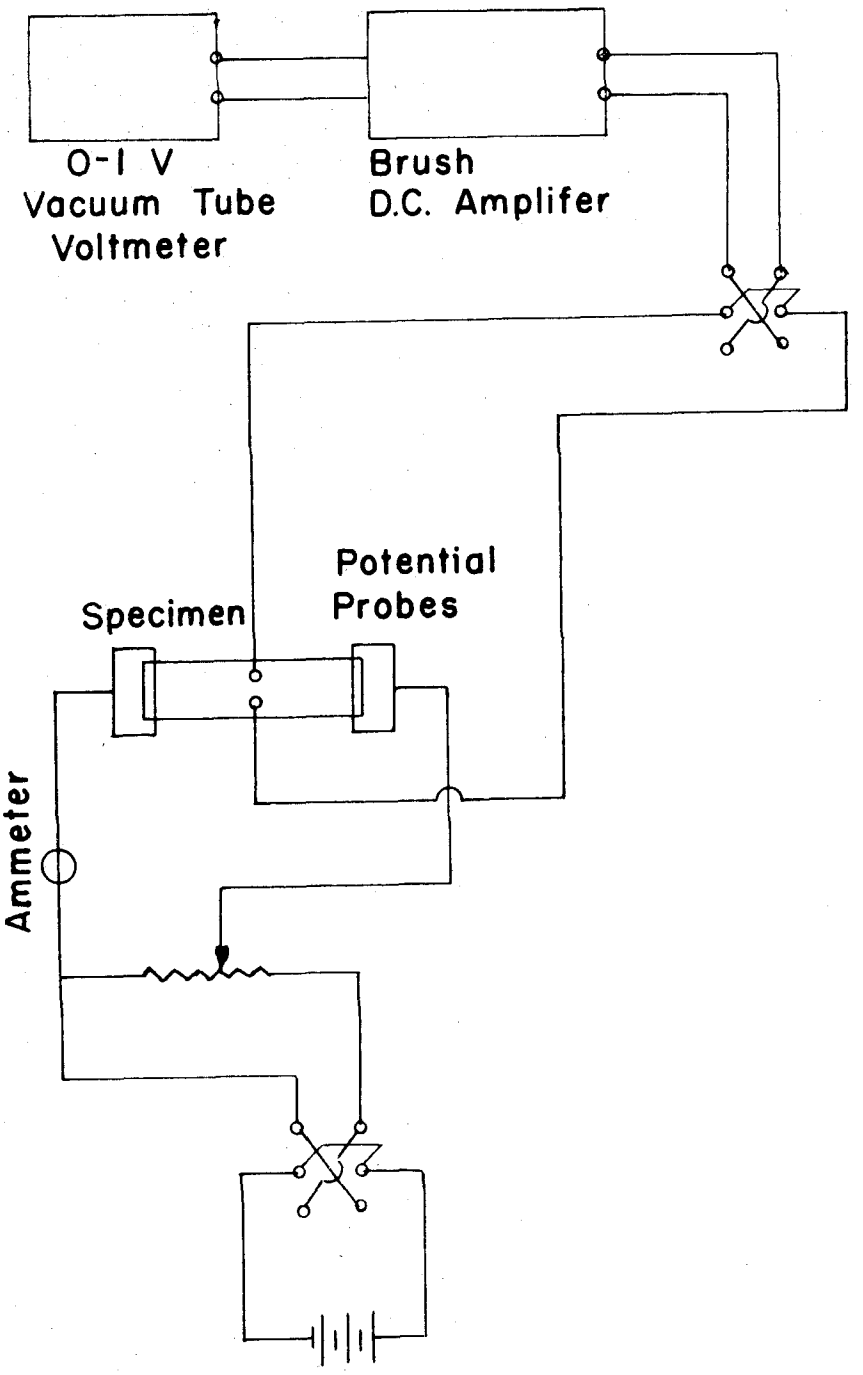

Figure 6 Schematic Of Hall Coefficient Circuit

insensitive to small temperature changes.

4. Magnetic Susceptibility

The experimental determination of magnetic susceptibility in weakly paramagnetic or diamagnetic materials requires elaborate equipment. The writer is indebted to the Atomic Energy Research Department of North American Aviation for provision of susceptibility apparatus. The apparatus employs the Fereday method of determining the susceptibility (22), in which the force on a specimen placed in a constant magnetic force field is determined.

The measurement of the small forces from paramagnetic titanium and titanium alloys was found to be best accomplished by an electrodynamic balance. In such a balance a small coil of wire is flexibly supported about a permanent magnet core (much like the voice coil in a speaker - in fact it was found convenient later to use the magnet and coil from a 10-inch speaker). The coil then supports the specimen in the magnetic field. By use of a mirror system attached to the moving coil, the magnetic force on the specimen can be balanced by a small current in the coil. A microammeter measuring the current in the coil can be calibrated in dynes by the use of standard weights in place of the specimen (Figure 7).

Any ferromagnetic impurities contribute heavily to the observed magnetic forces on the specimen. However their dependence on field strength differs from the paramagnetic specimens and thus

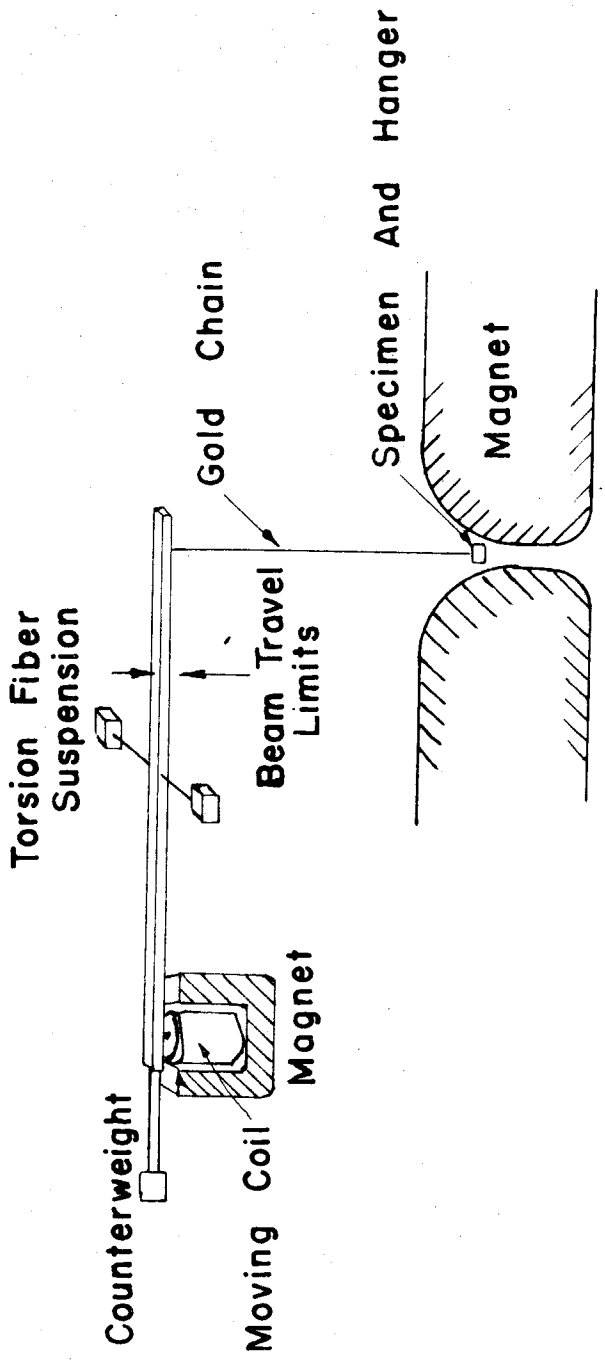

Figure 7 Schematic Of Susceptibility Balance

may be corrected by the use of an analytic method described in Section III. The use of the Fereday method in this manner provides susceptibility determinations which are estimated to be accurate to $\pm 0.1 \times 10^{-6}$ cgs.

D. Magnet Design:

The determination of the coefficient of magneto-resistance and the Hall coefficient requires a uniform magnetic field. The design of suitable pole tips can be accomplished from the following simple consideration. Clearly a symmetrical field will be produced by a solid of revolution. If a cone is taken then the only parameter to be determined is the cone angle. In Figure 8 such a conical pole tip is shown with the half cone angle θ. The field H at 0 along the cone axis due to the surface magnetization I of an element on the surface of the cone is:

$$dH = I \frac{2\pi r x}{(r^2+x^2)^{3/2}} dr \qquad (2-1)$$

The total field is then:

$$H = 2\pi I \int_{r_o}^{r_m} \frac{r x \, dr}{(r^2+x^2)^{3/2}} \qquad (2-2)$$

Assuming r_o and r_m are fixed by the magnet dimensions, the field is maximized if:

$$\frac{\partial H}{\partial x} = 0$$

Hence:

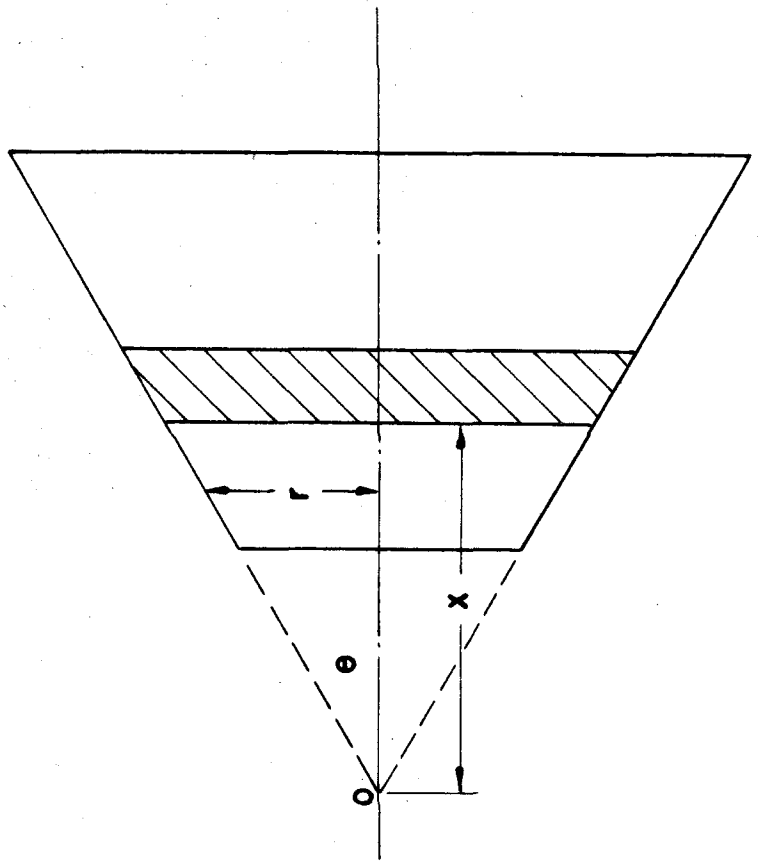

Figure 8 Pole Tip Design To Produce Maximum Uniform Field In Gap

$$x = \frac{1}{\sqrt{2}} r. \qquad (2\text{-}3)$$

θ is found to be:

$$\theta = 55^\circ . \qquad (2\text{-}4)$$

The total field from both pole tips is then:

$$H = 4.84\, I \ln \frac{r_m}{r_0} . \qquad (2\text{-}5)$$

For high fields it is found convenient to increase the cone angle slightly to compensate for saturation at the pole faces. It is estimated that a 60° cone half-angle is a suitable compromise.

A typical field plot is presented in Figure 9. Since it was inconvenient to monitor field strengths simultaneously with magnetoresistance and Hall coefficient measurements, the field strength was determined as a function of magnet current and gap distance. Representative data are presented in Figure 10.

The determination of the magnetic susceptibilities by the Fereday method requires that the specimen be located in a region where the translational magnetic force is constant. For a paramagnetic material this requires that:

$$\text{grad } (H^2) = \text{constant} \qquad (2\text{-}6)$$

where H is the field intensity.

The mathematical formalism for the calculation of the

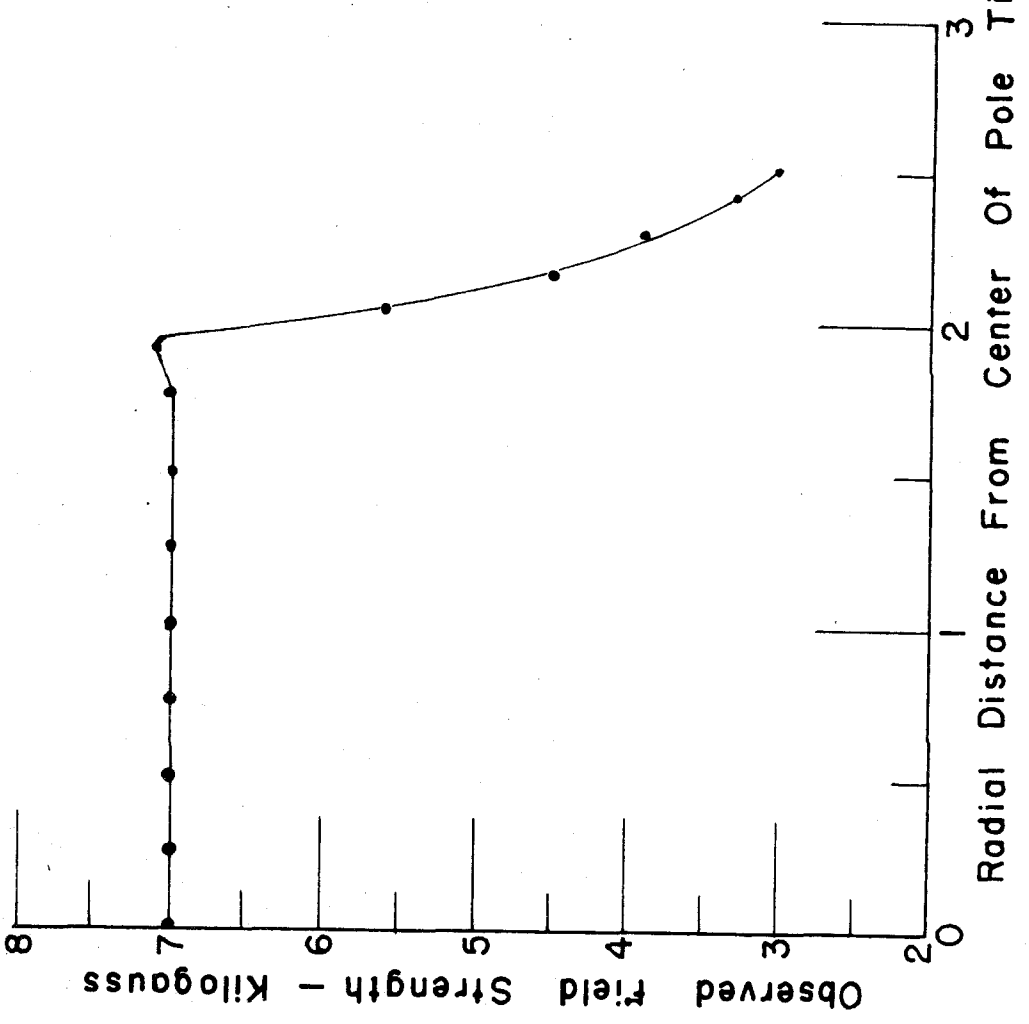

Figure 9 Radial Field Profile — 120° Pole Tips

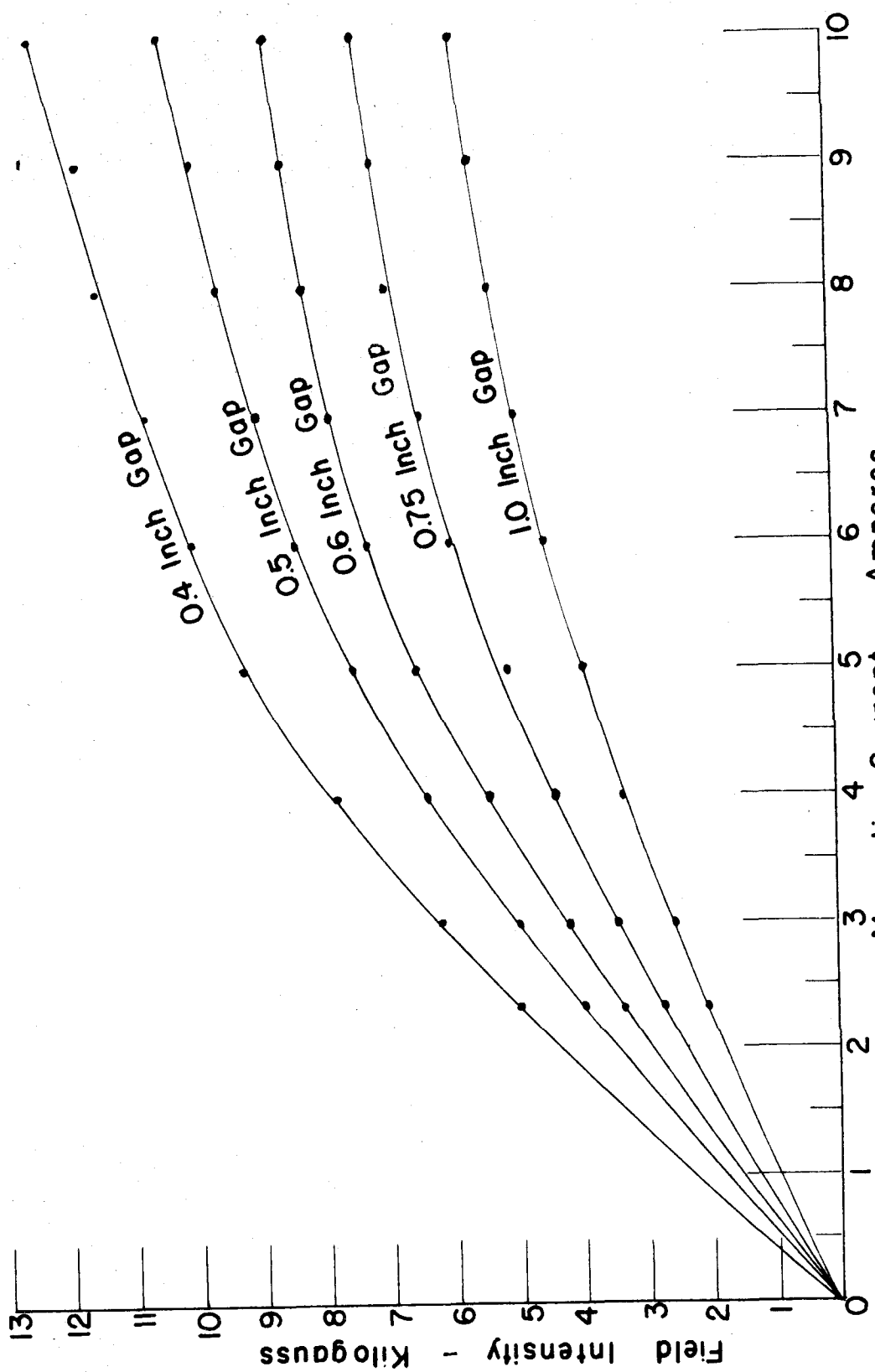

Figure 10 Variation Of Field Intensity With Magnetic Current
120° Conical Pole Tips

appropriate pole tip contours is given by Davy (23). Davy gives the transformation:

$$\zeta^{3/2} = A r^{3/2} e^{3i\theta/2} \qquad (2\text{-}7)$$

where ζ, r and θ are shown in Figure 11, and A is an arbitrary constant.

Davy relates the imaginary part of (2-7) to the equipotential lines, so that these are:

$$A\, r^{3/2} \sin\left(\frac{3\theta}{2}\right) = \text{constant} \qquad (2\text{-}8)$$

Thus the equation of pole tip profile is given by (2-8) since H will be normal to the equipotential surfaces. It is shown by Davy that profiles of the form (2-8) satisfy the requirement (2-6) of the Fereday method.

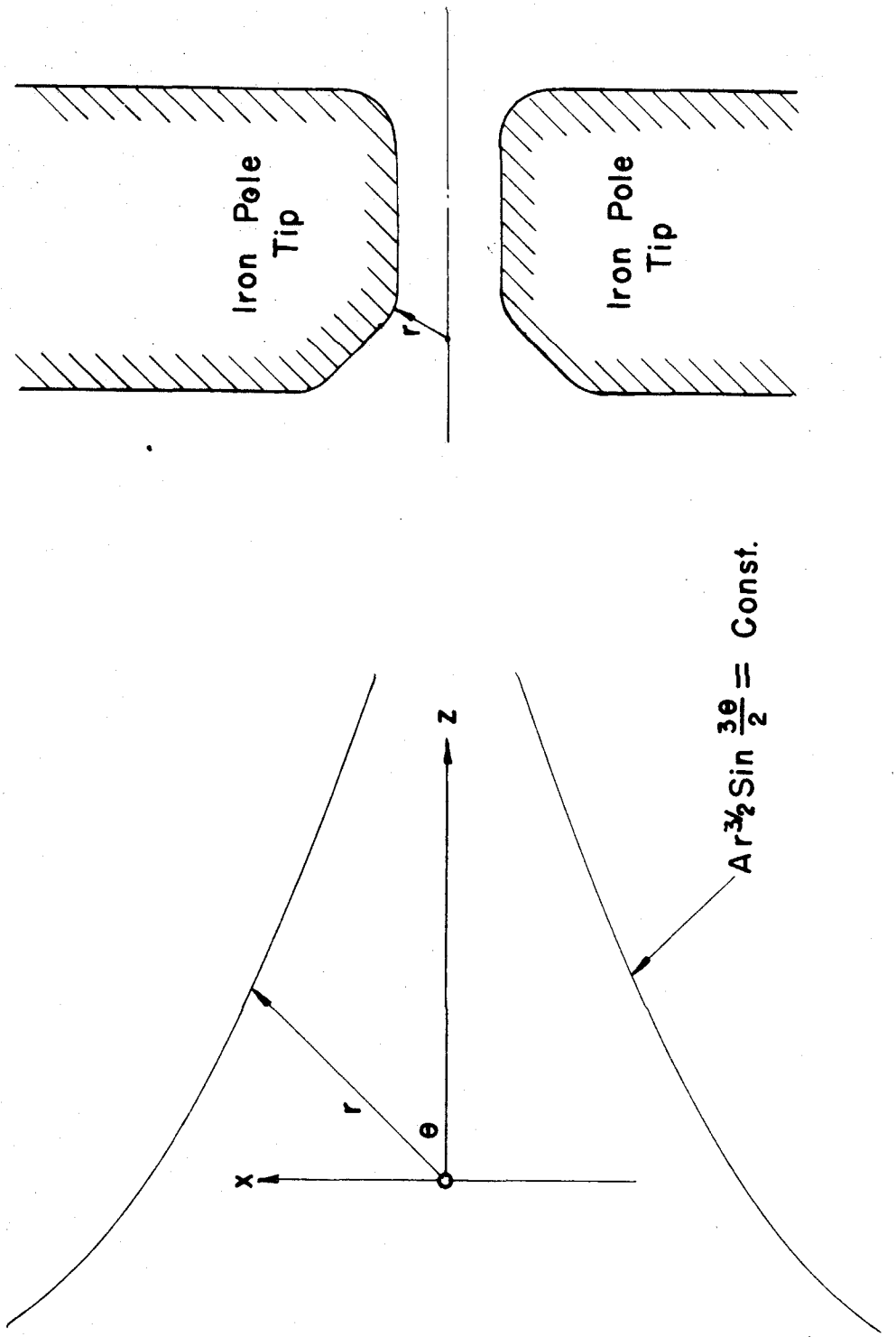

Figure 11 Susceptibility Pole Tip Profile

III. CALCULATION METHODS

A. Determination of Lattice Parameter:

The determination of lattice parameter from the diffraction lines on a film may be accomplished in a variety of ways. The method developed by M. U. Cohen (24) appears to be most desirable from the standpoint of accuracy of lattice parameters. This method provides a means of employing the data themselves for correction of systematic errors while simultaneously achieving the best fit for the random errors. Cohen combined the method of least squares (25), (26), with a correction for systematic errors in the diffraction pattern. Various treatments of the systematic errors have been suggested (27), (28), (29). Following Cohen's analysis, the systematic errors due to finite slit width, absorption, and displacement of the specimen from the camera circumference were estimated to vary as:

$$\delta \sin^2\theta \propto \phi \sin\phi , \qquad (3\text{-}1)$$

where θ is the Bragg angle and ϕ is $\pi - 2\theta$.

Combining the systematic errors with a least squares calculation, in the manner used by Cohen, yields:

$$\left.\begin{aligned}
\frac{\lambda^2}{3a^2}\sum_i \alpha_i^2 + \frac{\lambda^2}{4c^2}\sum_i \alpha_i\gamma_i + D\sum_i \alpha_i\delta_i &= \sum_i \alpha_i \sin^2\theta_i \\
\frac{\lambda^2}{3a^2}\sum_i \alpha_i\gamma_i + \frac{\lambda^2}{4c^2}\sum_i \gamma_i^2 + D\sum_i \gamma_i\delta_i &= \sum_i \gamma_i \sin^2\theta_i \\
\frac{\lambda^2}{3a^2}\sum_i \alpha_i\delta_i + \frac{\lambda^2}{4c^2}\sum_i \gamma_i\delta_i + D\sum_i \delta_i^2 &= \sum_i \delta_i \sin^2\theta_i
\end{aligned}\right\} \qquad (3\text{-}2)$$

where: $\alpha_i = h_i^2 + h_i k_i + k_i^2$

$\gamma_i = \ell_i^2$

$\delta_i = \phi_i \sin \phi_i$

h, k, l are the indices of the diffracting planes, θ is the Bragg angle, a and c are the lattice parameters, and D is the magnitude of the systematic error.

This result can be further improved by removing the implicit assumption that a and c are independent parameters in the least squares calculation. Efforts in this direction add greatly to the amount of work required and do not appear to significantly increase the accuracy. The interested reader is referred to articles by E. R. Cohen (30) and R. T. Birge (31) in the literature. The value D is a measure of the amount of systematic error in the measured values of θ_i. In all determinations it was found that a large D value, indicating a large systematic error, was coincident with obvious camera misalignment as evidenced by careful examination of the film.

The random error can be checked by recomputing $\sin^2\theta_i$ from the calculated values of a and c. It was found that the random errors in $\sin^2\theta_i$ (corrected for systematic errors) amount to less than 0.0005. The resultant lattice parameters are judged accurate to at least one part in 10^5.

The determination of lattice parameter for the Debye-Scherrer specimens was accomplished by similar methods. Due to the inherent errors of powder specimens of titanium alloys mentioned

earlier, the correction of systematic errors was considered unjustified. The observed values of θ were substituted in the equations:

$$\left.\begin{aligned} \frac{\lambda^2}{3a^2}\sum_i \alpha_i^2 + \frac{\lambda^2}{4c^2}\sum_i \alpha_i \gamma_i &= \sum_i \alpha_i \sin^2\theta_i \\ \frac{\lambda^2}{3a^2}\sum_i \alpha_i \gamma_i + \frac{\lambda^2}{4c^2}\sum_i \gamma_i^2 &= \sum_i \gamma_i \sin^2\theta_i \end{aligned}\right\} \quad (3\text{-}3)$$

where the symbols have the same meaning as previously ascribed.

Equation (3-3) corresponds to Equation (3-2) for the case of focusing camera, and was obtained in a similar manner.

Random and systematic errors were not evaluated for the Debye-Scherrer results because they are overwhelmed by the error due to the presence of adsorbed gases in the specimen. Experimental comparison between powder and solid specimens indicated the Debye-Scherrer parameters are in error of the order of +0.002 Å in the c parameter.

B. Resistivity:

The resistivity of the foils was determined from the relation:

$$\rho = \frac{R \cdot A}{\ell} \quad (3\text{-}4)$$

where ρ is the resistivity in ohm-cm, R is the specimen resistance in ohms, A is the area

normal to the current in cm^2, and l is the distance between the Kelvin bridge potential probes in cm.

The maximum error in ρ may be estimated from:

$$\frac{\delta(\rho)}{\rho} = \frac{\delta(R)}{R} + \frac{\delta(A)}{A} + \frac{\delta(l)}{l} \qquad (3\text{-}5)$$

where δ indicates the maximum error of the variable enclosed in brackets.

For the specimen size used in resistivity measurements (0.030 x 1/2 x 1/2 inches) and an uncertainty of 0.0003 inches in thickness and 0.001 inches in length and width, Equation (3-5) indicates an uncertainty of 0.014 in the resistivity.

C. Magneto-Resistance:

The classical theory of magneto-resistance was first developed by Peierls (32). For isotropic materials there are, in principle, two magneto-resistance parameters B_t and B_p for resistance measured transverse and parallel, respectively, to the magnetic field. Peierls defines B_t for isothermal specimens in moderate fields to be:

$$\rho = \rho_o \left(1 + B_t H^2\right) \qquad (3\text{-}6)$$

where ρ is the resistivity in the magnetic field,

ρ_o is the resistivity in the absence of the field,

and H is the field intensity.

Evidently the units of B_t as defined in Equation (3-6) are oersted^{-2}.

Clearly (3-6) can be written in terms of specimen resistance in order to eliminate the determination of resistivity:

$$R = R_o (1 + B_t H^2). \tag{3-7}$$

The magneto-resistance coefficient is then given by:

$$B_t = \frac{R - R_o}{R_o} \frac{1}{H^2} \tag{3-8}$$

The resistance was determined with the field off and then with the field on. Using the Kelvin bridge for resistance determinations and field intensity of the order of 20 kilogauss the uncertainty in B_t was of the order of 5×10^{-13} oersted^{-2}. Increased sensitivity provided by employing the Brush d. c. amplifier reduced the uncertainty in B_t to of the order of 0.5×10^{-13} oersted^{-2}.

Evidently the uncertainty in B_t can be further reduced by requiring a parabolic dependence of resistance change with field strength, and applying least square methods similar to those employed in the lattice parameter determinations. This is expressed by the relation:

$$\frac{1}{n} \sum_{i=1}^{n} \frac{R_i - R_o}{R_o} \frac{1}{H_i^2} = B_t \tag{3-9}$$

where R_i and H_i are the transverse resistance in the field and the field intensity respectively for

the i th measurement.

By making a series of determinations of the resistance and field intensity for varying field intensities the uncertainty in B_t was reduced to of the order of 0.3×10^{-13} oersted^{-2}.

D. Hall Coefficient:

The Hall coefficient relates the magnitude of an e.m.f. developed across a conductor in a magnetic field, where the Hall e.m.f., the current in the conductor, and the magnetic field are mutually perpendicular. The effect was at first classically defined to be proportional to the current in the conductor and to the magnetic field intensity (33). In the absence of the magnetic field H, the potential observed between two points P and P′ (Figure 12) on opposite sides of the specimen is:

$$V_o = i r_o \qquad (3\text{-}10)$$

where r_o is the resistance between P and P′ in the direction of the current i.

When a magnetic field is added in the direction shown in Figure 12 the potential between P and P′ is:

$$V = V_H + i r_o \qquad (3\text{-}11)$$

where V_H is the Hall potential.

The Hall potential is defined classically according to:

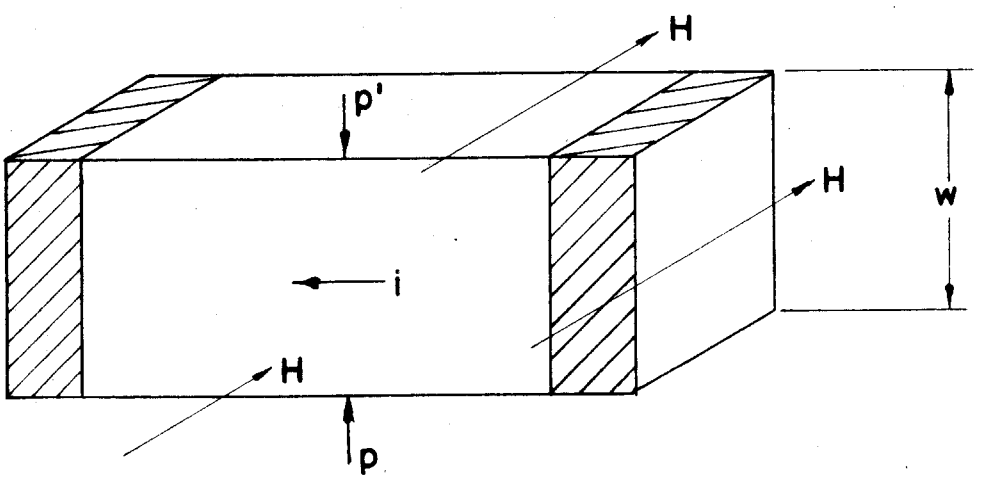

Figure 12 Schematic Of Hall Coefficient Specimen

$$V_H = R \frac{|\vec{H} \times \vec{i}|}{w} \qquad (3\text{-}12)$$

where H is the magnetic field intensity, i is the current, w is the specimen thickness, and R is the Hall coefficient.

In terms of the experimentally observed quantities the Hall coefficient is:

$$R = \frac{w(V - V_o)}{|\vec{H} \times \vec{i}|} \qquad (3\text{-}13)$$

In practice it was found quite easy to reduce V_o, the potential difference in the direction of the current i, to a very low value. A zero adjustment on the amplifier was employed to bias the amplifier the amount V_o, thus eliminating the necessity of taking the difference manually.

A magnetothermal effect contributing to uncertainties in the Hall coefficient is the Ettingshausen effect. The Ettingshausen effect produces a temperature gradient across the Hall specimen and thus a temperature difference between Hall potential probes. The tungsten probes and the titanium specimen form a thermocouple circuit in which the Ettingshausen temperature difference produces a thermal e.m.f. additive to the Hall e.m.f. Experimental data on the Ettingshausen effect are not available for Ti, but assuming that titanium behaves in this respect like Cr and Fe, the contribution to the Hall coefficient is of the order 2×10^{-14} volt-cm/amp-oersted.

Since all the specimens were quite thin ($\sim$ 0.050 inch) and surrounded by an oil bath for temperature stabilization, it was estimated that the Ettingshausen contribution to the Hall coefficient was less than 2×10^{-14} v-cm/amp-oersted. Since the Ettingshausen contribution to the Hall coefficient was of the order of the accuracy of the determination of R it was neglected.

E. Magnetic Susceptibility:

In determining the magnetic susceptibility of paramagnetic materials by the Fereday method, the magnetic force on the specimen F_χ and the magnetic field intensity H have the relation:

$$F_\chi = \frac{v}{2} \nabla \left[(K - K_A) H^2 \right] \qquad (3\text{-}14)$$

where v is the volume of the specimen, and K and K_A are volume susceptibilities of the specimen and surrounding medium respectively.

In terms of the specific susceptibilities Equation (3-14) can be written:

$$F_\chi = \frac{m}{2} \nabla \left[(\chi - \chi_A) H^2 \right] \qquad (3\text{-}15)$$

where $\chi = \frac{K}{\rho}$ and $\chi_A = \frac{K_A}{\rho_A}$ are the specific susceptibilities, m is the mass in grams, and ρ is the density.

Providing the magnetic field has a constant grad (H^2) and

the specimen is magnetically isotropic Equation (3-15) reduces to:

$$F_\chi = \frac{m}{2}\left(\chi - \chi_A\right) \nabla H^2 \qquad (3\text{-}16)$$

In order to proceed from Equation (3-16) to a determination of susceptibility, the electromagnetic force balance must be calibrated. It was found that methods developed by Hutchison and Reekie (34) and McGuire and Lane (35) were suitable for the present experiment. Briefly these methods consist of measuring the coil current by observing the voltage drop across a temperature-compensated standard resistor with a potentiometer, and determining the force using calibrated weights in place of the specimen. Field measurements complete the requirements implicit in Equation (3-16) to the determination of the susceptibility.

Experimentally the susceptibility obtained from Equation (3-16) is too large due to ferromagnetic impurities. Large errors are possible with apparently negligible concentrations of ferromagnetic impurities. It can be computed that five parts per million (5×10^{-4} atomic percent) of ferromagnetic impurity contribute a 70 percent error in the apparent susceptibility of silver at a field intensity of 10,000 oersteds. A modification of a method suggested by Honda (36), Owen (37), and Vogt (38) may be employed to eliminate the contribution of ferromagnetic impurities. Providing the ferromagnetic impurities are saturated, the force due to them is:

$$F_f = mc\sigma \frac{\partial H}{\partial s} \qquad (3\text{-}17)$$

where F_f is the force due to the ferromagnetic impurity, m is the specimen mass, c is the impurity concentration, σ is the specific saturation intensity, and s is the direction of the divergence of the field H (in the direction of grad (H^2) in this case).

Combining (3-16) and (3-17) and dividing by m grad (H^2) yields:

$$\chi_a = \chi + \frac{c\sigma}{H} \qquad (3\text{-}18)$$

where F_t is the total force, χ_a is the apparent susceptibility from the force measurement, and χ is the true susceptibility (less χ_{air}, of course). Equation (3-18) defines a linear dependence between χ_a and $^1/H$ whose intercept at $^1/H = 0$ is χ.

The systematic errors originating from ferromagnetic impurities were eliminated by a linear least squares fit of χ_a to $^1/H$. A typical case is presented in Figure 13 for pure titanium.

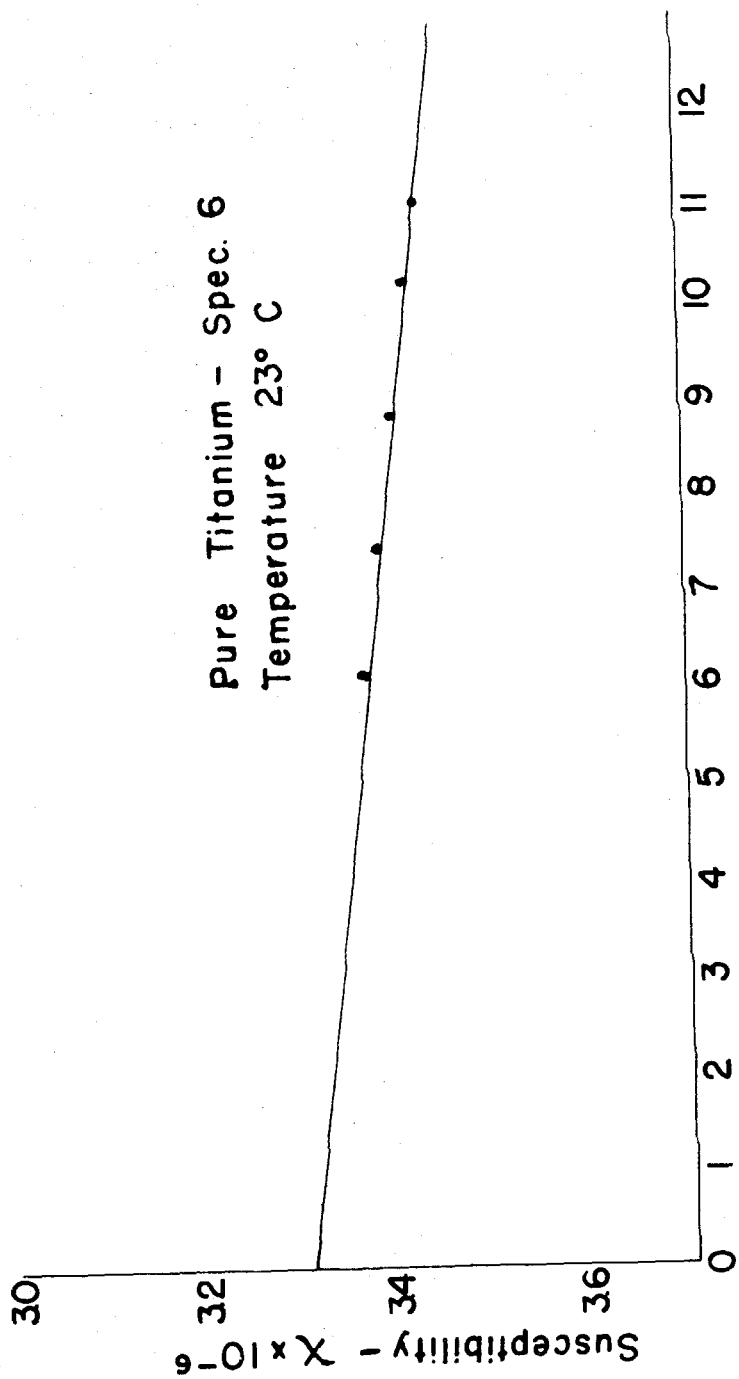

Figure 13 Honda - Owen Plot For The Determination Of Magnetic Susceptibility Of Titanium

IV. EXPERIMENTAL RESULTS

The experimental results for titanium rich alloys of aluminum, gallium, and silver are presented below. The solute concentrations in the solid solution region are shown in the phase diagram of the titanium-aluminum system, due to Bumps, Kessler, and Hansen (39), and in the titanium-silver phase diagram, due to Adenstedt and Freeman (40), Figures 14 and 15 respectively. The titanium rich end of the titanium-silver phase diagram has also been investigated by Worner (41), and found to be similar to Adenstedt's and Freeman's diagram. The titanium-gallium system has not been investigated; however, it is thought to bear some resemblance to the titanium-aluminum system at the titanium rich side.

A. Lattice Parameter:

The lattice parameters of pure titanium are $\underline{c}$ = 4.68321 Å and $\underline{a}$ = 2.95030 Å; these values are accurate within ± 0.00005 Å. The agreement with the values given by Clark (16), namely: $\underline{c}$ = 4.6833 Å and $\underline{a}$ = 2.9504 Å, is quite satisfactory.

The change in the lattice parameters with solute concentration is shown in Figures 16, 17, 18, and 19. These data are presented in tabular form in Tables 3, 4, and 5.

The curves of lattice parameters with aluminum concentration display an unusual behavior at 2.9 atomic percent aluminum (Figure 16). The $\underline{a}$ parameter decreases uniformly with aluminum

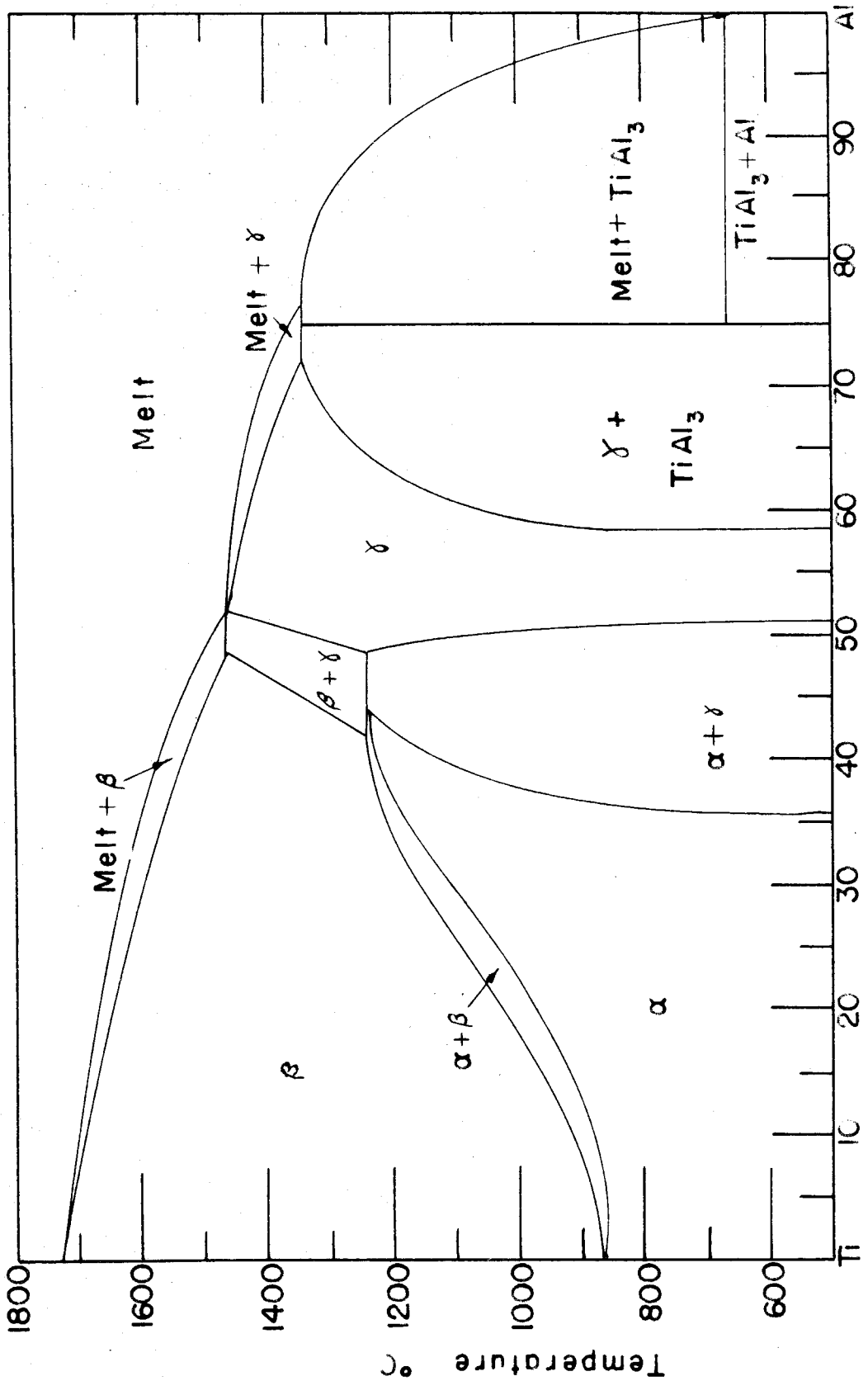

Figure 14 Titanium-Aluminum Phase Diagram

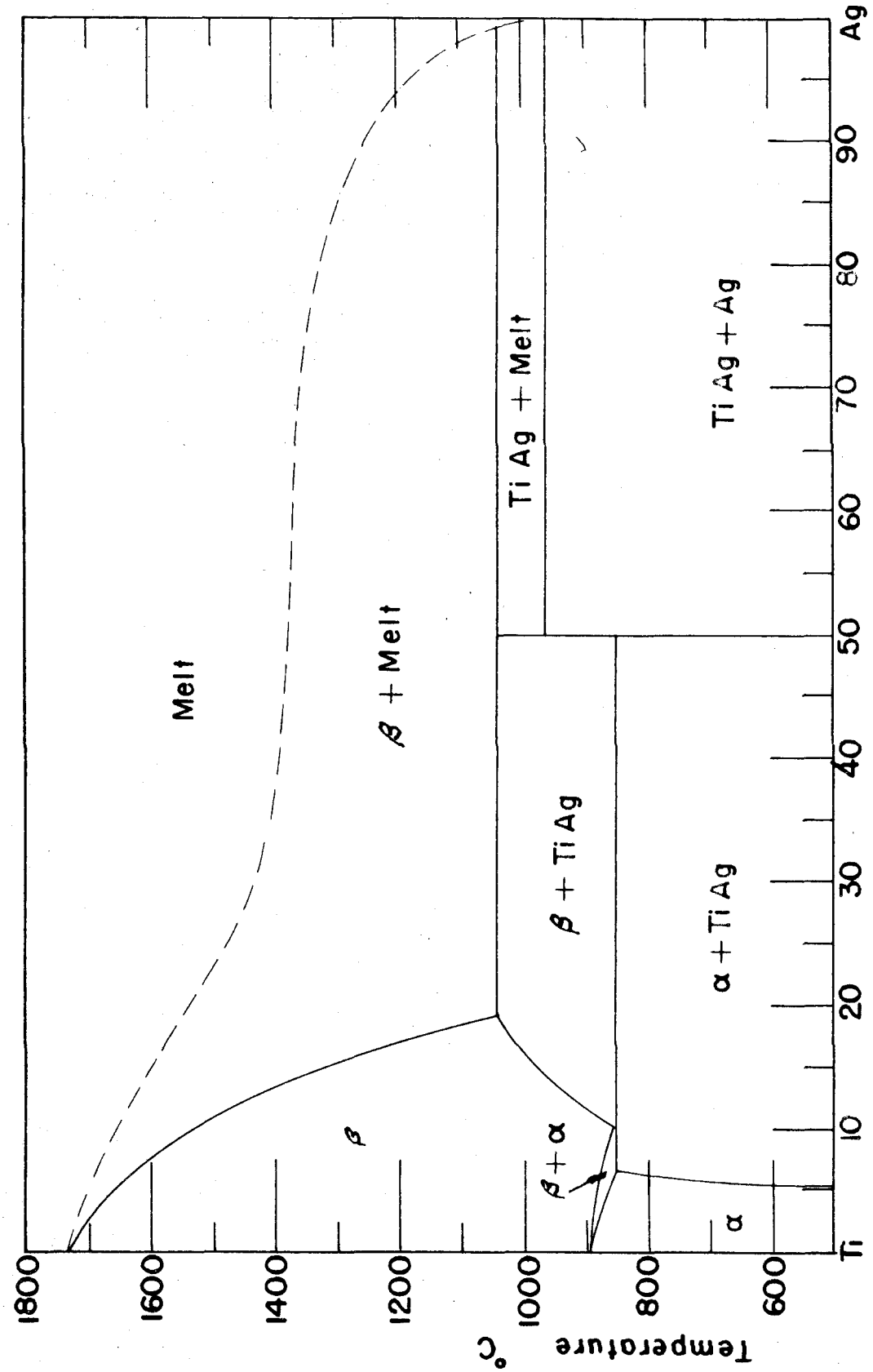

Figure 15 Ti - Ag Phase Diagram

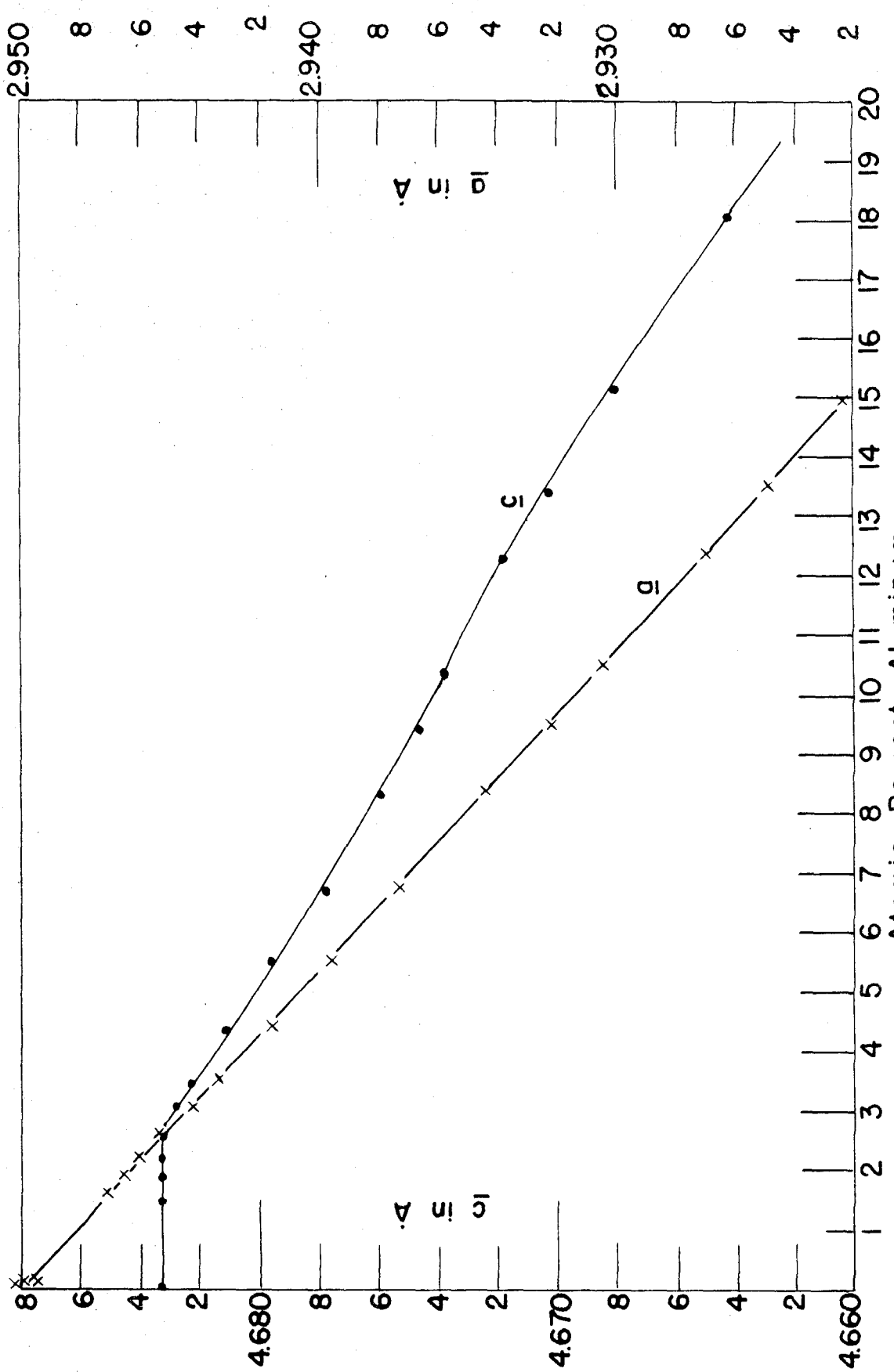

Figure 16 Titanium – Aluminum Lattice Parameters

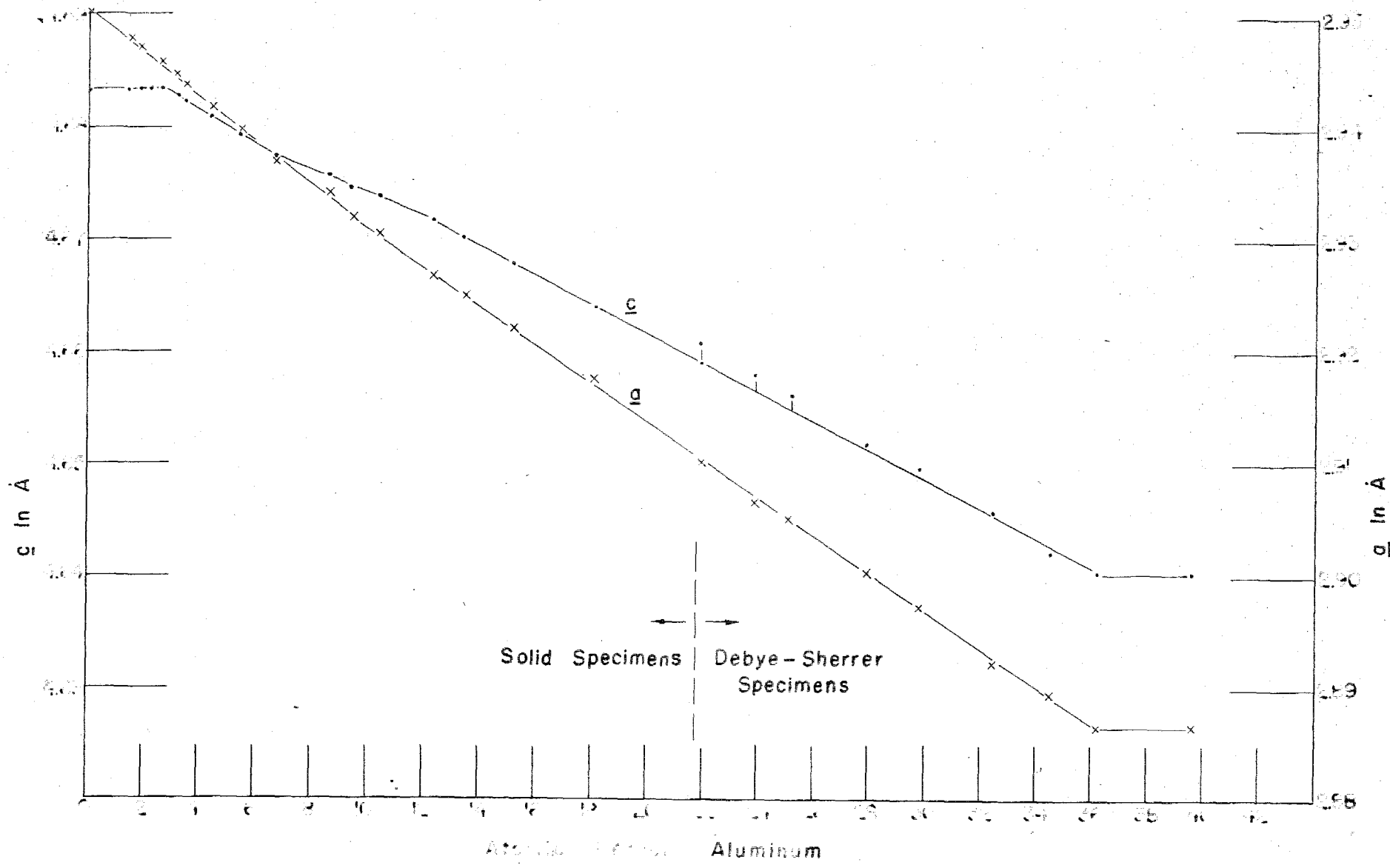

Figure 17 Lattice Parameters In Titanium – Aluminum Alpha Solid Solution

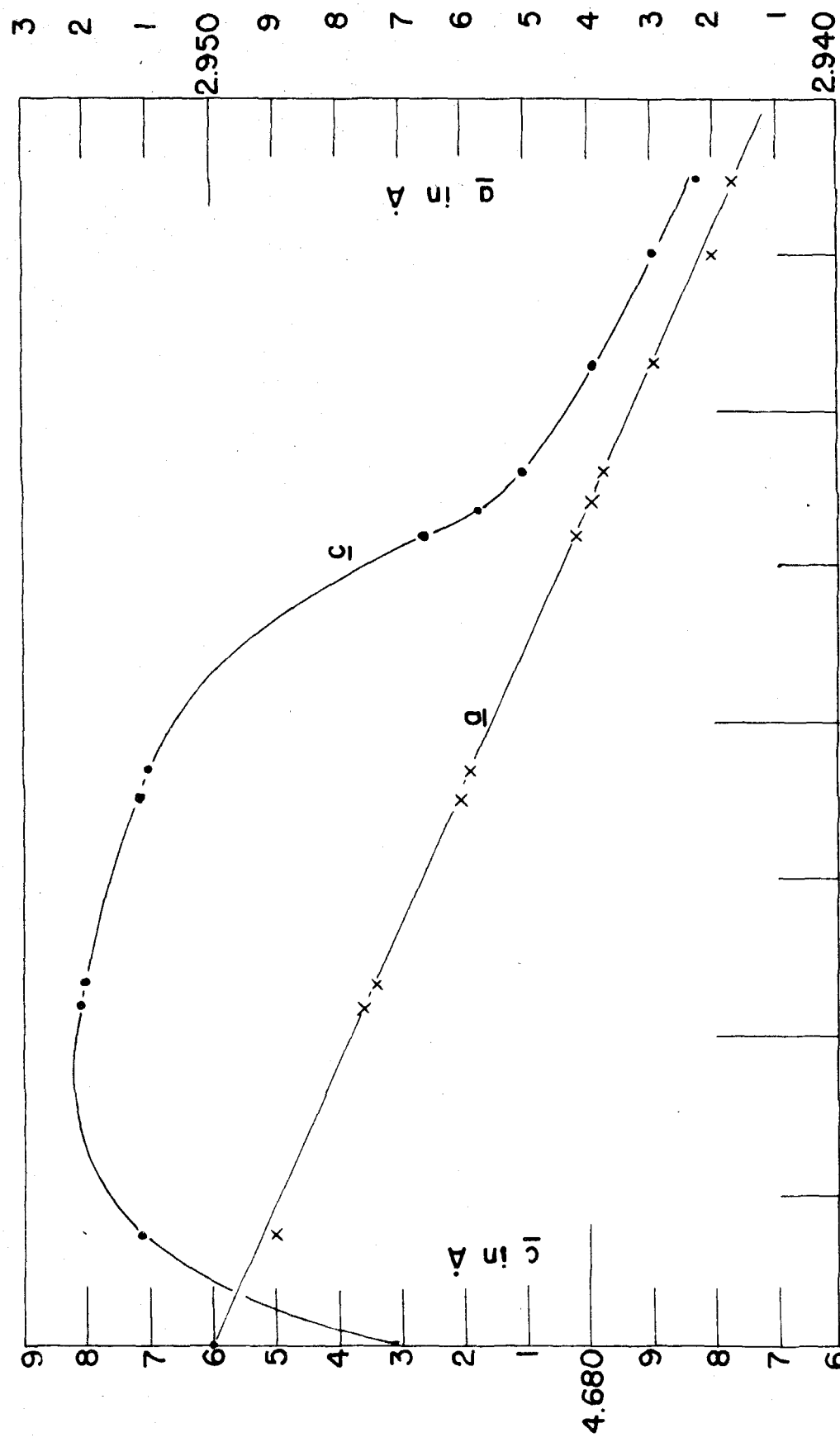

Figure 18 Titanium – Gallium Lattice Parameters

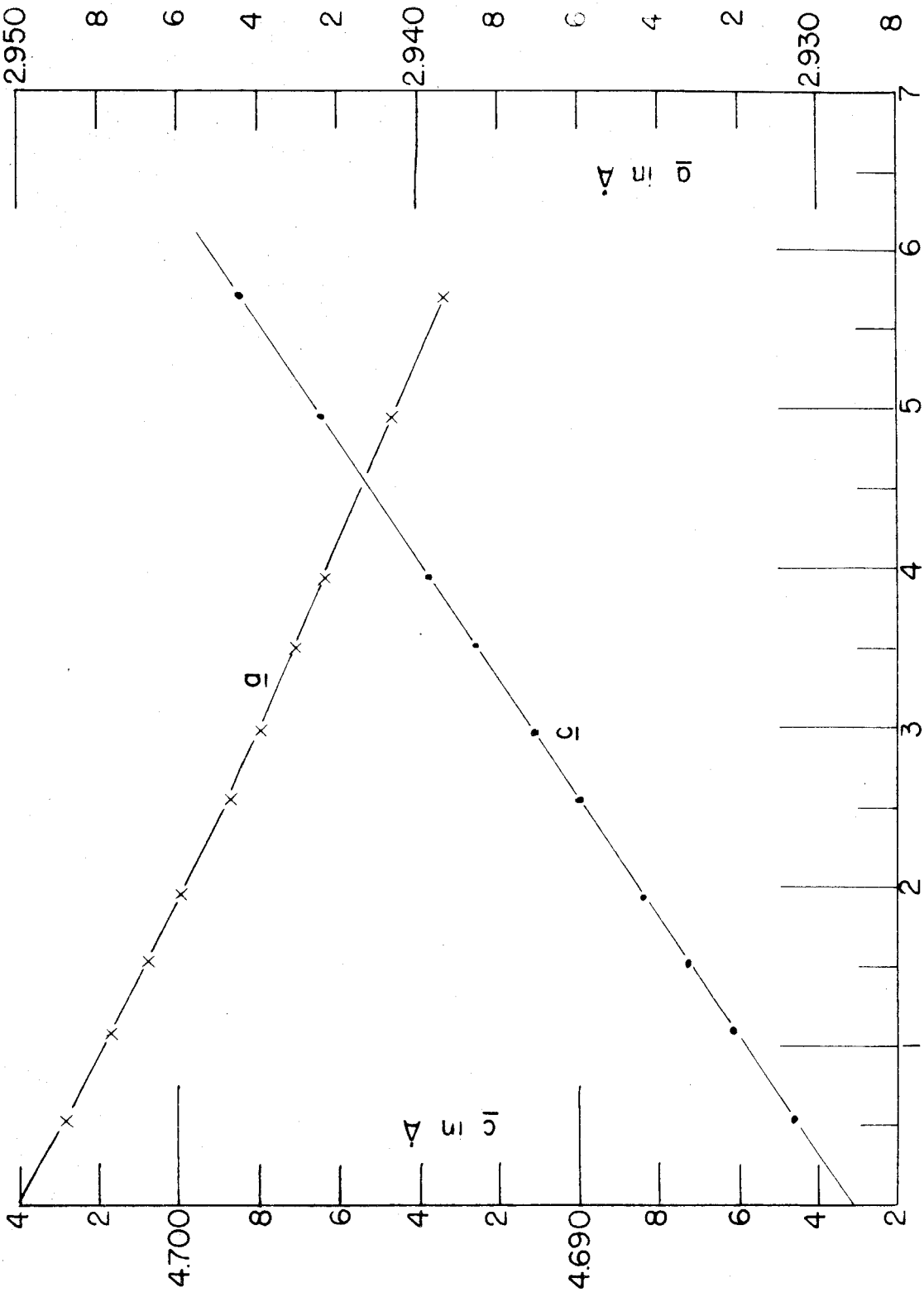

Figure 19 Titanium – Silver Lattice Parameters

Table 3

TITANIUM-ALUMINUM LATTICE PARAMETERS

Spec. No.	At. % Al.		c	a
1	0		4.68302	2.95075
2	0		4.68299	2.95024
5	0		4.68295	2.94994
6	0		4.68312	2.95010
24	0		4.68310	2.95023
9	1.466		4.68318	2.94758
14	1.897		4.68313	2.94680
15	2.194		4.68316	2.94629
16	2.661		4.68314	2.94552
17	3.153		4.68278	2.94441
18	3.480		4.68211	2.94370
7	4.386		4.68096	2.94161
19	5.509		4.67912	2.93664
12	6.696		4.67742	2.93435
10	8.267		4.67575	2.93431
20	9.410		4.67448	2.93215
13	10.372		4.67385	2.93055
8	12,310		4.67334	2.92690
22	13.421		4.67017	2.92512
23	15.185	↑	4.66802	2.92211
36	18.10		4.66420	2.91750
28	22.04	solid	4.65911	2.91040*
32	23.89	powder	4.65812	2.90672
30	25.13	↓	4.65620	2.90528
34	27.96		4.65198	2.90026
33	29.81		4.64981	2.89733
29	32.41		4.64573	2.89240
31	34.50		4.64214	2.88949
35	39.75		4.64023	2.88680

*Lattice parameters from a powder pattern of specimen number 28 were: c = 4.66082, a = 2.91041.

Table 4

TITANIUM-GALLIUM LATTICE PARAMETERS

Ti Ga No.	At. % Ga	c	a
6	.4825	4.68721	2.94910
1	1.090	4.68808	2.94763
7	1.1345	4.68796	2.94750
9	1.8152	4.68715	2.94604
2	1.833	4.68706	2.94600
3	2.570	4.68261	2.94430
10	2.6941	4.68163	2.94400
11	2.8042	4.68097	2.94361
12	3.1459	4.67990	2.94282
5	3.493	4.67901	2.94208
X	3.72	4.67838	2.94170

Table 5

TITANIUM-SILVER LATTICE PARAMETERS

Ti Ag No.	At. % Ag.	c	a
5	0.53	4.68459	2.94882
2	1.09	4.68602	2.94771
1	1.53	4.68724	2.94673
6	1.94	4.68838	2.94597
10	2.54	4.69002	2.94478
7	2.97	4.69110	2.94390
9	3.51	4.69252	2.94302
3	3.94	4.69371	2.94223
8	4.95	4.69640	2.94070
4	5.70	4.69842	2.93933

concentration, but the c parameter remains constant (within $\pm$ 0.0001 Å) up to 2.9 atomic percent and then decreases uniformly. On the basis of Vegard's law and the smaller atomic diameter of aluminum, a linear decrease in both parameters is expected. A further deviation of the c lattice parameter from a linear dependence on solute concentration occurs in the alloys with aluminum at approximately 10 atomic percent aluminum. The deviation from a linear dependence is small (of the order of 0.05 percent change in slope), but is believed to be real. The a parameter does not appear to deviate significantly from the linear dependence on solute concentration; behaving in this aspect as it does at the c parameter abnormalities at lower solute concentration. No additional deviations in the lattice parameters from a linear dependence on aluminum concentration occur within experimental accuracy.

The (α,$\alpha+\gamma$) phase boundary at 900°C in the titanium-aluminum system is determined from the intercept of the lattice parameters (Figure 17) to be located at 36.2 atomic percent aluminum. This agrees well with investigation by Bumps, Kessler, and Hansen (39), which locates the phase boundary at 36.5 atomic percent Al.

The lattice parameters for solid solutions of gallium in titanium are shown in Figure 18. The a parameter decreases linearly with gallium concentration, but the c parameter increases at first, and then decreases. While no abrupt discontinuity in slope is apparent, the linear dependence of lattice parameter on solute

concentration does not begin until a concentration of about 2.8 atomic percent gallium is reached. The lattice parameters decrease linearly with gallium concentration from 2.9 to 3.8 atomic percent Ga.

In the alloys of silver in titanium the lattice parameters change linearly with the concentration of silver in the range 0 to 5.5 atomic percent Ag. The c parameter increases with silver concentration and the a parameter decreases. The lattice parameter curves of the alloys with silver agree with those given by Worner (41) in the direction of the parameter change, but do not agree in the numerical values of the lattice parameters. The lack of complete agreement is thought to be due to differences in the experimental methods.

B. Resistivity:

The resistivity of pure titanium is found to be 52.7 micro-ohm cm at 23°C. This value is in good agreement with the resistivity given by Wyatt (42) as 54.98 micro-ohm cm at 77°F (25°C).

The addition of solutes to titanium increases the resistivity for solutes of aluminum, gallium, and silver. The curves of resistivity increase with solute concentration are shown in Figure 20. The data are presented in Table 6. The simple theory of electrical resistivity in alloys as developed by Matthiessen (43), (44), Guenther (45), and Linde (46) predicts a linear relationship between resistivity and solute concentration. The curves of resistivity with solute

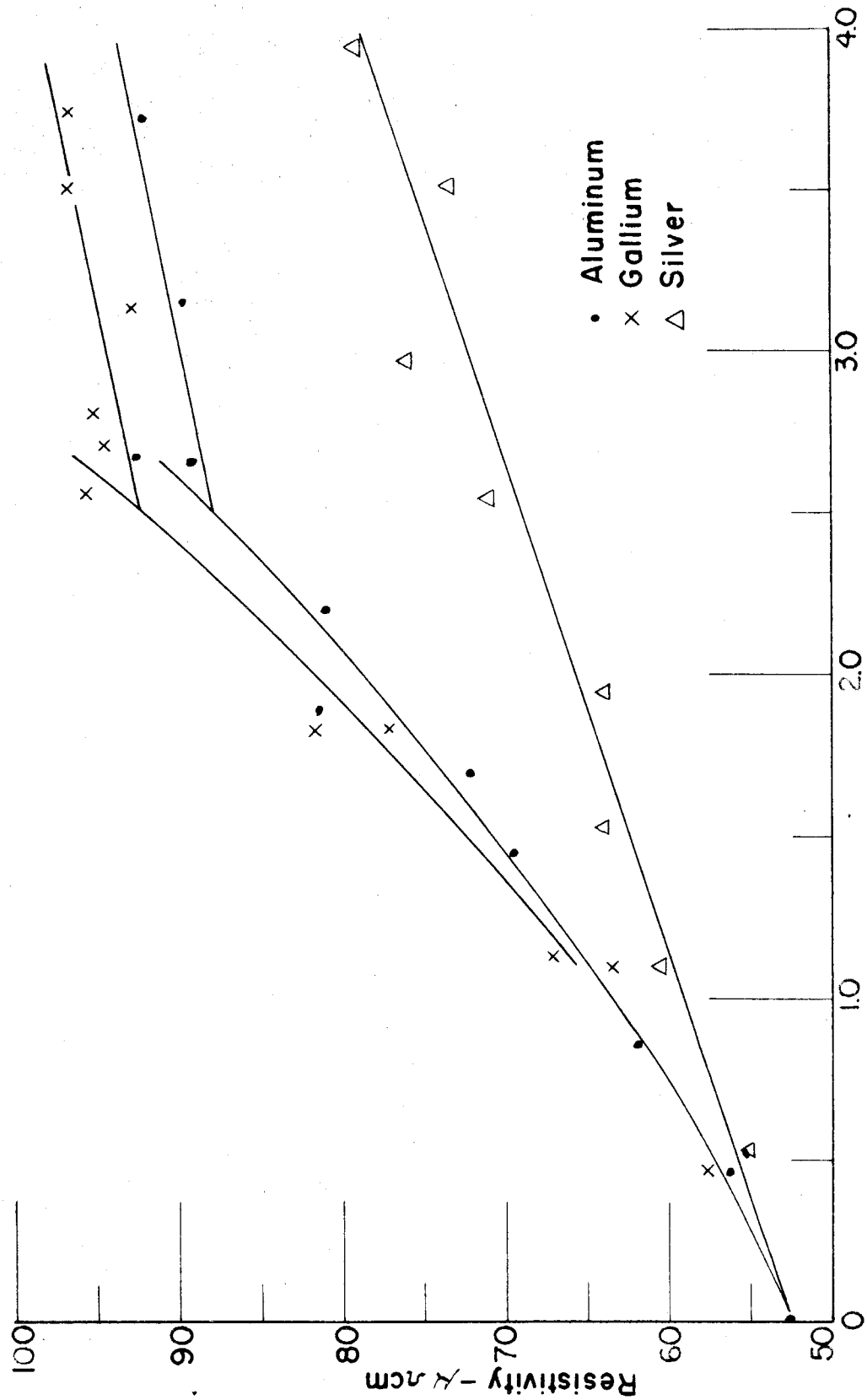

Figure 20 Resistivity Of Titanium Alloys

Table 6

RESISTIVITY OF TITANIUM ALLOYS

Spec. No.	At. %	ρ - $\mu\Omega$ cm
TiAl #6	pure Ti	52.7
TiAl #41	0.46	56.2
TiAl #42	0.86	61.8
TiAl #9	1.47	69.4
TiAl #43	1.70	72.2
TiAl #14	1.89	81.3
TiAl #15	2.19	80.8
TiAl #16-1	2.66	88.9
TiAl #16-2	2.66	92.5
TiAl #17	3.15	89.6
TiAl #18	3.48	92.0
TiAl #7	4.38	96.3
TiGa #6	0.48	57.6
TiGa #1	1.09	63.6
TiGa #7	1.13	67.1
TiGa #9	1.81	77.0
TiGa #2	1.83	81.6
TiGa #3	2.57	95.5
TiGa #10	2.69	94.3
TiGa #11	2.80	95.1
TiGa #12	3.14	92.9
TiGa #5	3.49	96.7
TiGa #X	3.72	96.5
TiAg #5	0.53	55.3
TiAg #2	1.09	60.6
TiAg #1	1.53	64.1
TiAg #6	1.94	63.9
TiAg #10	2.54	71.0
TiAg #7	2.97	75.9
TiAg #9	3.51	73.4
TiAg #3	3.94	79.1

concentration for alloys of aluminum and gallium in titanium increase at a greater than linear rate for Al and Ga concentrations less than about 2.6 atomic percent. In addition, a change in the slope of the resistivity-solute concentration curve occurs at about 2.6 atomic percent for both Al and Ga solutes. Above about 2.6 atomic percent the resistivity increases linearly, in agreement with theory, with Al and Ga concentration. The non-linear parts of the resistivity curves occur at the same concentrations of Al and Ga at which anomalous behavior of the c lattice parameter is observed, except that the resistivity assumes a normal behavior with solute concentration at a lower concentration of Al and Ga (2.6 instead of 2.9 atomic percent).

The resistivity increase due to a silver solute is proportional to the concentration of Ag in agreement with Matthiessen's rule. The linear resistivity change with silver concentration is in accord with the linear change in lattice parameters with Ag concentration, in spite of the violation of Vegard's law in the latter case.

C. Magneto-Resistance

The magneto-resistance coefficient, B_t, for current normal to the magnetic field for the titanium alloys with aluminum, gallium, and silver is displayed in Figure 21 and in Table 7.

The coefficient of magneto-resistance for pure titanium is found to be 6.6×10^{-13} oersted^{-2}. This value is larger than the value for alkali metals, Li, Na, . . ., and the noble metals, Cu, Ag, and Au,

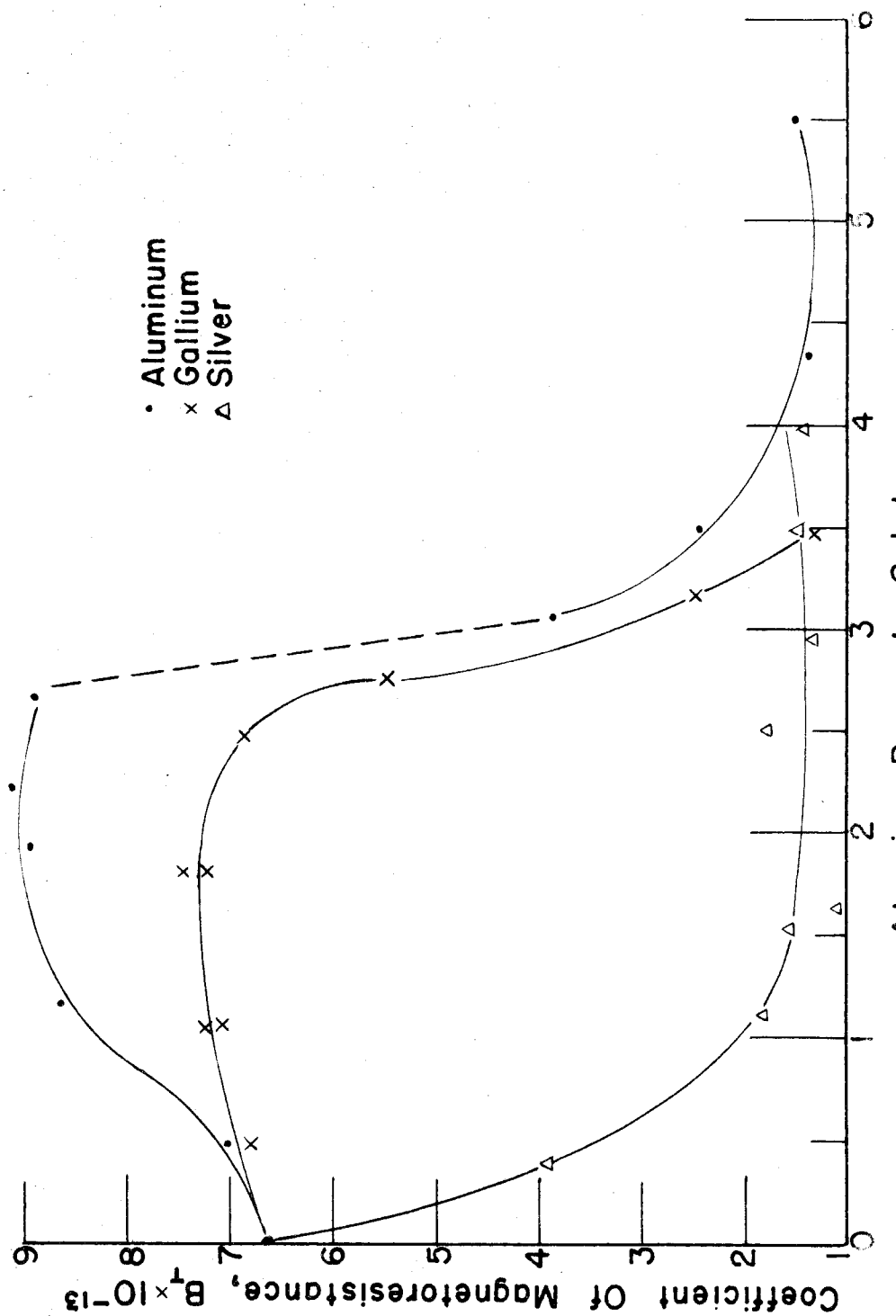

Figure 21 Magnetoresistance Of Titanium Alloys

Table 7

MAGNETO-RESISTANCE OF TITANIUM ALLOYS

Spec. No.	Solute Concentration At. %	$B_t \times 10^{-13}$ (oersted^{-2})
Ti #6	pure Ti	6.6
TiAl #41	0.46% Al	7.0
TiAl #9	1.47% Al	8.6
TiAl #14	1.90% Al	8.8
TiAl #15	2.19% Al	9.2
TiAl #16	2.66% Al	8.8
TiAl #17	3.15% Al	3.9
TiAl #18	3.48% Al	2.5
TiAl #7	4.38% Al	1.4
TiAl #19	5.50% Al	1.5
TiGa #6	0.48% Ga	6.8
TiGa #1	1.09% Ga	7.2
TiGa #7	1.13% Ga	7.0
TiGa #9	1.81% Ga	7.2
TiGa #2	1.83% Ga	7.5
TiGa #3	2.57% Ga	6.9
TiGa #11	2.80% Ga	5.6
TiGa #12	3.14% Ga	2.6
TiGa #5	3.49% Ga	1.4
TiAg #5	0.53% Ag	4.0
TiAg #2	1.09% Ag	1.9
TiAg #1	1.53% Ag	1.6
TiAg #6	1.94% Ag	1.1
TiAg #10	2.54% Ag	1.7
TiAg #7	2.97% Ag	1.4
TiAg #9	3.51% Ag	1.5
TiAg #3	3.94% Ag	1.4

but is less than the values for less metallic elements such as Sb, As, Cd, Ba, and Bi. While the order of magnitude of B_t found in this study is certainly beyond doubt, some question of its exact value exists. B_t is found to be dependent upon specimen orientation in the specimen holder of the order of $\pm 10^{-13}$ oersted^{-2} in the specimens examined for this effect. This is thought to be due to an anisotropy of B_t with crystallographic direction. Movement of the specimen in the specimen holder causes the potential probes to make contact in a different region of the specimen. Since the potential probes are small enough to contact individual grains separately in the specimen, it seems possible the change in B_t, caused by moving the specimen, may be due to the dependence of B_t on crystallographic direction. The use of polycrystalline specimens prevented further investigation of this effect.

The coefficient of magneto-resistance increases slightly in the titanium alloys with aluminum and gallium up to solute concentrations of about 2.9 atomic percent. At about 2.9 atomic percent Al and Ga a rapid decrease in B_t occurs with increasing solute concentration. Further increase in the concentration of Al and Ga above 3 atomic percent does not produce a significant change in B_t.

The addition of silver to titanium causes the coefficient of magneto-resistance to decrease monotonically in the range 0 to 2 atomic percent Ag. Further increase in the silver concentration above 2 atomic percent has little effect on B_t.

D. Hall Coefficient

The Hall coefficient for alloys of aluminum and silver in titanium is presented in Figure 22 and Table 8. The Hall coefficient for pure titanium is found to be $+1.82 \times 10^{-13}$ volt-cm-amp^{-1}-oersted^{-1}. Previously Scovil (47) reported the Hall coefficient for titanium as $+3.0\ (\pm 0.1) \times 10^{-13}$ volt-cm-amp^{-1}-oersted^{-1}. Foner (48) has given the Hall coefficient to be $+0.95 \times 10^{-13}$ volt-cm-amp^{-1}-oersted^{-1}. Foner examined several specimens of varying degrees of purity and concluded that non-metallic impurities decrease the Hall coefficient. One specimen Foner examined, containing of the order of 1 atomic percent oxygen, was found to have a negative Hall coefficient. It is thought that the difference between Foner's result and that of the present study is due to different degrees of purity of the specimens. Scovil's value of 3.0×10^{-13} is not understood; however, it may be due to a high degree of preferred orientation in the specimen, thus incorporating any crystallographic anisotropy heavily in the measurement.

The change in the Hall coefficient with solute additions of Al and Ag is small compared to the changes in lattice parameter, resistivity, and magneto-resistance in these alloys with Al and Ag. In addition, no marked difference in the change of the Hall coefficient occurs between Al and Ag solutes, as observed in the other physical properties. The Hall coefficient does not exhibit any significant change at 3 atomic percent Al.

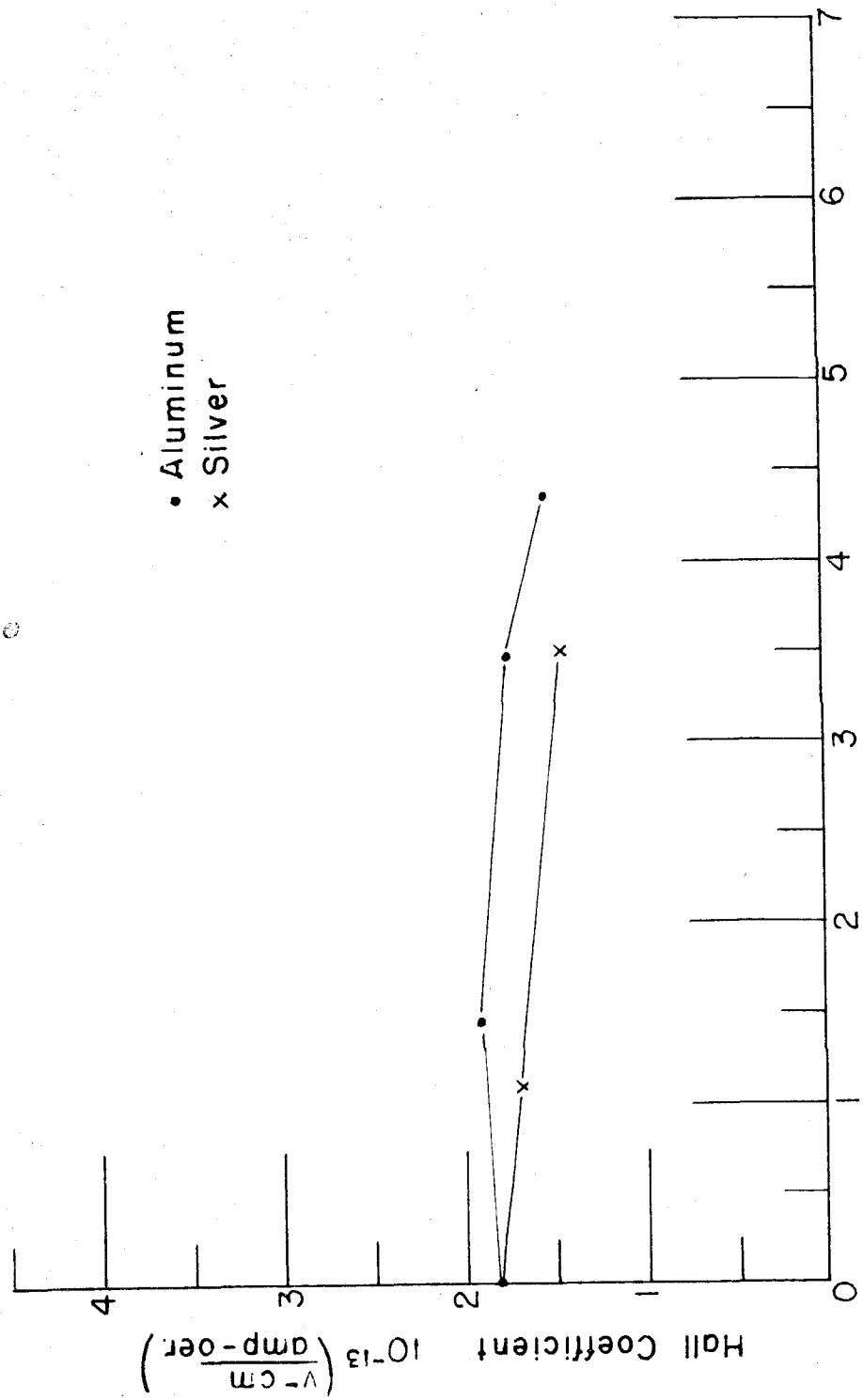

Figure 22 Hall Coefficient Of Titanium Alloys

Table 8

HALL COEFFICIENT OF TITANIUM ALLOYS

Spec. No.	Solute Concentration At. %	R($\frac{\text{v-cm}}{\text{amp-oersted}}$)
Ti #6	pure Ti	1.82×10^{-13}
TiAl #9	1.466% Al	1.90×10^{-13}
TiAl #18	3.48% Al	1.73×10^{-13}
TiAl #7	4.38% Al	1.51×10^{-13}
TiAg #2	1.09% Ag	1.68×10^{-13}
TiAg #9	3.51% Ag	1.44×10^{-13}

E. Magnetic Susceptibility

The magnetic susceptibility of alloys of aluminum and silver in titanium is shown in Figure 23 and Table 9. Pure titanium is paramagnetic with a susceptibility of 3.31×10^{-6} emu (cgs). This susceptibility is in good agreement with the value given by Squire and Kaufmann (49) from measurements on high purity Ti (50). The addition of solutes of Al and Ag to titanium causes almost no change in the susceptibility for solute concentrations less than 5 atomic percent. In addition, there is no significant difference in the susceptibility between alloys with Al and with Ag.

F. Significance of Experimental Results

The experimental results indicate that solute additions in titanium cause anomalous changes in some physical properties with solute additions. The changes in lattice parameter with solute concentration suggest that the lattice parameter anomalies result from an effect of the solute valency. In this respect the lattice parameter changes are similar to those found in the magnesium alloys by Hume-Rothery, Raynor, and Busk. Like the magnesium alloys, the lattice parameter changes in the titanium alloys produced by the trivalent solutes (Al and Ga) are different than those for the monovalent solute (Ag). The different changes in the lattice parameter produced by trivalent and monovalent solutes suggests that the alloying valency of titanium in these alloys is between 1 and 3.

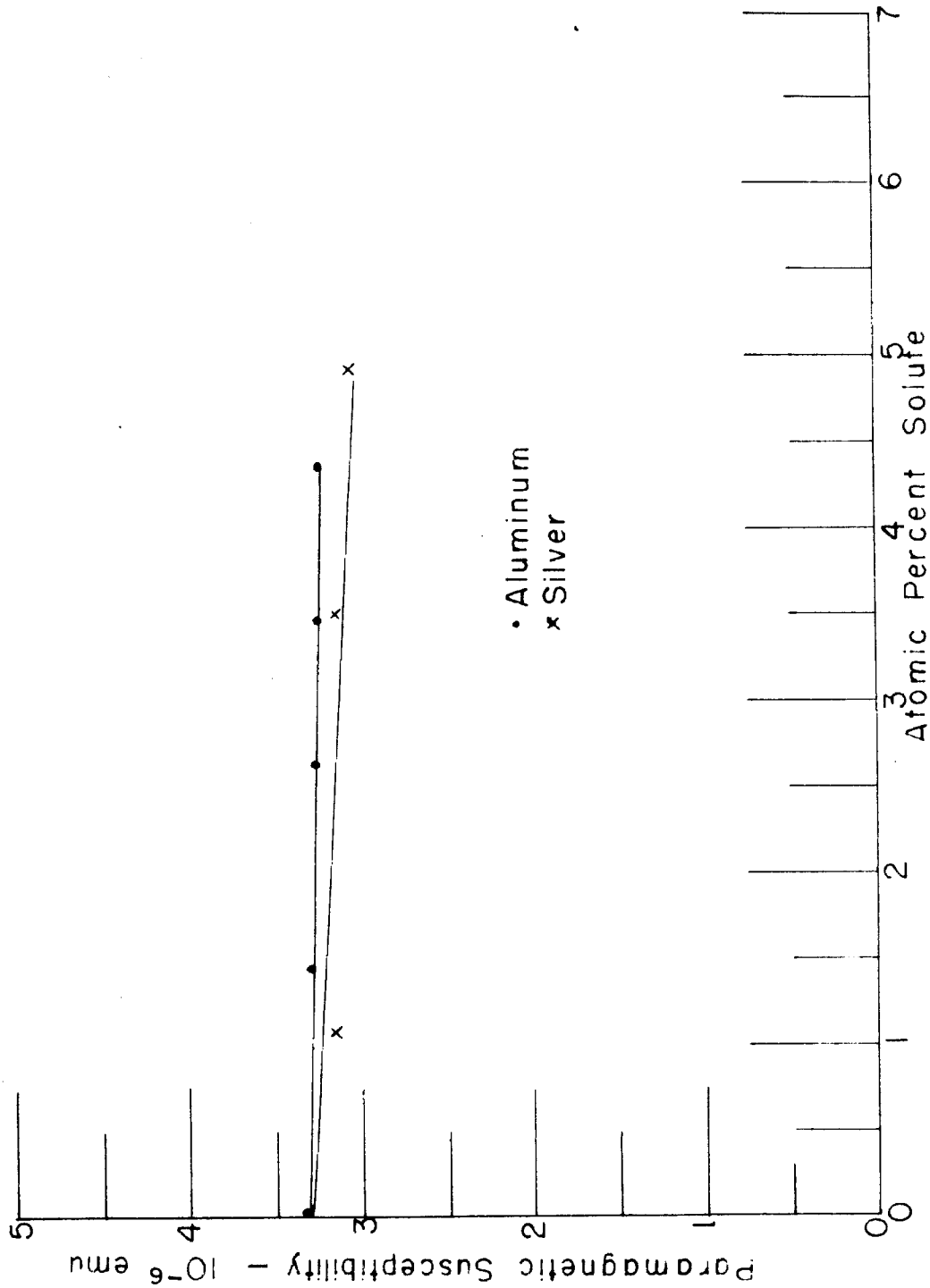

Figure 23 Magnetic Susceptibility Of Titanium Alloys

Table 9

SUSCEPTIBILITY OF TITANIUM ALLOYS

Spec. No.	Solute Concentration At. %	χ
Ti #6	pure Ti	3.31×10^{-6}
TiAl #9	1.466% Al	3.27×10^{-6}
TiAl #16	2.661% Al	3.24×10^{-6}
TiAl #18	3.48% Al	3.22×10^{-6}
TiAl #7	4.38% Al	3.21×10^{-6}
TiAg #2	1.09% Ag	3.11×10^{-6}
TiAg #9	3.51% Ag	3.14×10^{-6}
TiAg #8	4.95% Ag	3.02×10^{-6}

The effects of the solute valency evidently influence the changes in other physical properties of the titanium alloys. The changes in resistivity and magneto-resistance with solute concentrations are similar for the trivalent solutes Al and Ga, but are different for the monovalent solute Ag. The solute valency has a reduced influence on the Hall coefficient and susceptibility of the alloys, whose explanation is not immediately evident. These changes in other physical properties, in addition to the lattice parameters, with solute addition further reinforces the suggestion of the influence of solute valency in the titanium alloys. Since these changes in resistivity and magneto-resistance, with solute concentration in addition to the changes in lattice parameter, are different for monovalent and trivalent solutes, it is concluded that titanium has a valency between 1 and 3 in these alloys.

V. BRILLOUIN ZONES FOR TITANIUM

The interpretation of the experimental results in terms of the electron theory of metals requires the formulation and solution of the appropriate eigenvalue problem. In this section the background and preliminary formulation of the problem is reviewed in preparation for the following detailed discussion. The perturbation calculation, presented in the first part of this section to emphasize the relation between the crystal lattice and the mathematical result, is given in similar form in texts on the theory of metals, e.g., Seitz (51), Wilson (52), and Mott and Jones (53).

The suggestion by Drude (54) and Lorentz (55) that metals contain free electrons, and the application of Fermi-Dirac statistics to this suggestion by Sommerfeld (56), remains the basis of the electron theory of metals. The electrons, in the electrostatic potential well of the metal, can be described by the Schrodinger equation:

$$H\Psi = W_{op}\,\Psi \qquad (5\text{-}1)$$

where H is the Hamiltonian operator, W_{op} is the energy operator, and Ψ is electron wave function. Since only electrons in stationary energy states are of interest, (5-1) may be replaced by:

$$H\psi_k = W_k \psi_k \qquad (5\text{-}2)$$

where W_k is the energy of the kth stationary state, and ψ_k is the corresponding wave function.

An approximation must now be introduced in order to solve Equation (5-2). This is necessary since H in Equation (5-2) contains the coordinates of all the electrons in the solid if electron-electron interactions as well as electron-ion interactions are to be included. If the electron-electron interactions are ignored, then Equation (5-2) can be solved explicitly. There are a number of objections to neglecting the electron-electron interactions, which are examined as the occasion warrants and are discussed briefly later. For the present the calculation can proceed treating the electrons independently (subject, of course, to Fermi-Dirac statistics) in a potential "well", the metal, with a periodic potential perturbation, the local potential in the neighborhood of the metal atoms.

With the above assumption, Equation (5-2) can be separated and written for each electron:

$$\nabla^2 \psi_k + \frac{8\pi^2 m}{h^2}\left(W_k - V(x, y, z)\right)\psi_k = 0 \qquad (5\text{-}3)$$

where m is the electron mass, h is Planck's constant, and V is the potential.

It is to be noted that V(x, y, z) is periodic with the period of the lattice. For example, if V(x, y, z) refers to a cubic lattice with a distance a

between atoms, then:

$$V(x,y,z) = V(x+a,y,z) = V(x,y+a,z) = V(x,y,z+a). \quad (5\text{-}4)$$

Bloch (57) has investigated equations of the form (5-3) and has shown* that the solutions are of the form:

$$\psi_k = \chi_k(x,y,z)e^{2\pi i \bar{k}\cdot\bar{r}} \quad (5\text{-}5)$$

where $\chi_k(x,y,z)$ is a periodic function with the period of the lattice, $\bar{r}$ is the vector from origin to the point (x, y, z), and $\bar{k}$ is a vector of dimension reciprocal length.

While Bloch's development of Equation (5-5) is certainly acceptable and attractive, it is desirable later to examine the dependence of the wave functions ψ_k and the energy eigenvalues W_k on the lattice symmetry. The perturbation method has the desirable property in this respect of displaying the lattice symmetry in the most appropriate manner.

The eigenfunctions and eigenvalues obtained from the perturbation calculation are:

---

*The proof given by Bloch for Eq. (5-5) is very similar to Floquet's theorem; see for example Whittaker & Watson, "Modern Analysis", 4th edition, p. 412, Cambridge Univ. Press, London, 1950.

$$\psi_k = \frac{1}{\sqrt{v}}\psi_k^o + \sum_{k'}{}' \frac{\psi_{k'}^o}{W_k^o - W_{k'}^o} \int \psi_k^{o*} V_p \psi_{k'}^o \, d\tau$$

$$W_k = \frac{h^2 k^2}{2m} + \sum_{k'}{}' \frac{1}{W_k^o - W_{k'}^o} \left| \int_{cell} \psi_k^{o*} V_p \psi_{k'}^o \, d\tau \sum_d{}' e^{2\pi i(\bar{k}-\bar{k}')\cdot\bar{d}} \right|^2 \qquad (5\text{-}6)$$

The energy becomes infinite, according to Equation (5-6), if:

$$\begin{aligned} &a) \quad W_k^o = W_{k'}^o \\ &b) \quad \sum_d{}' e^{2\pi i(\bar{k}-\bar{k}')\cdot\bar{d}} \neq 0 \end{aligned} \qquad (5\text{-}7)$$

The infinity occurring in (5-6) when the conditions (5-7) are satisfied is due to the treatment of the problem by non-degenerate perturbation theory. The "proper" wave functions may be constructed from linear combinations of the zeroth order wave functions. Using the resulting wave functions, the perturbed eigenvalues may be calculated. Corresponding to the conditions (5-7) two energy eigenvalues are obtained:

$$W_k = W_k^o \pm \int \psi_k^{o*} V_p \psi_{k'}^o \, d\tau \qquad (5\text{-}8)$$

with no acceptable eigenvalues lying between the two eigenvalues. The conditions for the energy discontinuity in W_k, Equation (5-8), are exactly the same as those for the infinity in the non-degenerate solution, namely, Equations (5-7).

The relations (5-7) for the energy discontinuity may be related directly to the crystalline properties by examining them in more detail. The first becomes:

$$|\bar{k}| = |\bar{k}'|.$$

The second vanishes unless $e^{2\pi i(\bar{k}-\bar{k}')\cdot\bar{r}}$ has the periodicity of the lattice. Values of $(\bar{k}-\bar{k}')$ satisfying this requirements are called $\bar{K}$. Then:

$$\bar{k} - \bar{k}' = \bar{K}.$$

These last two relations can be combined in a single expression:

$$\bar{k} \cdot \frac{\bar{K}}{2} = \frac{\bar{K}^2}{4} \qquad (5\text{-}9)$$

Equation (5-9) presents the well-known condition for the energy discontinuities. The polyhedra formed in k-space by Equation (5-9) are the equally well-known Brillouin Zones (58).

A. Brillouin Zones:

It is to be emphasized at this point that the preceding development has not employed any detail of the crystal lattices except the general specification of periodicity of the potential, a characteristic common to all crystals. In addition, it is important to note that the conclusions thus far are independent of the exact functional form of the perturbing potential Vp.

From the condition that $\exp 2\pi i\bar{K}\cdot\bar{r}$ has the same periodicity as the lattice and the definition of $\bar{K}$, it can be seen that the space of $\bar{k}$ has the same translation properties as the reciprocal space of the lattice. The primitive translation vectors of the reciprocal lattice are derived from the primitive translation vectors of the real lattice

by the transformation:

$$\left.\begin{aligned} \rho_1 &= \frac{\tau_2 \times \tau_3}{\tau_1 \times \tau_2 \cdot \tau_3} \\ \rho_2 &= \frac{\tau_1 \times \tau_3}{\tau_1 \times \tau_2 \cdot \tau_3} \\ \rho_3 &= \frac{\tau_1 \times \tau_2}{\tau_1 \times \tau_2 \cdot \tau_3} \end{aligned}\right\} \qquad (5\text{-}10)$$

where τ_1, τ_2, and τ_3 are the primitive translation vectors of the real lattice, and ρ_1, ρ_2, and ρ_3 are the primitive vectors of the reciprocal lattice.

In this reciprocal lattice (k-space) the K vectors are primitive translation vectors connecting the reciprocal lattice points. Equation (5-9), then, describes a set of planes in this space. The polyhedra formed by these planes are the Brillouin Zones. Not all of the zones thus formed are unique; in fact a better understanding of the electron behavior is afforded by a reduction of the Brillouin Zones which lie beyond the first.

B. Reduced Zones:

The possibility of representing the Brillouin pattern in a different manner than the extended zones from Equation (5-9) is suggested by the translation properties of the wave functions. By substitution in Equation (5-6) it may be seen that the translation $\bar{k} \rightarrow \bar{k} + \bar{K}$ which transforms the wave function ψ_k to ψ_{k+K} leaves the wave function unchanged, i.e.:

$$\psi_{k+K} = \psi_k \quad . \tag{5-11}$$

Similarly, the translation $\bar{k} \rightarrow \bar{k}+\bar{K}$ transforms the energy surfaces into the first zone. Since, in general, W_k is not equal to W_{k+K}, the energy may be represented as a multivalued function of $\bar{k}$ with $\bar{k}$ restricted to values lying within the first of the planes (5-9). The difference in energy $2\,V_{kk'}$ across the zone face is obtainable from the degenerate perturbation calculation (5-8). The energy gap is solely dependent in this approximation on the matrix element $V_{kk'}$. Some of the conditions which permit the Brillouin conditions (5-9) to be fulfilled and yet require that certain of the $V_{kk'}$ vanish will presently be discussed.

It is important to the proper application of the perturbed free-electron approximation to more complex structures to realize that the only properties of the structure that have been employed in the development to this point are: (1) the translational periodicity of the lattice described by the primitive vectors τ_1, τ_2, τ_3; and (2) the existence of a perturbing potential Vp having the same translational periodicity as the lattice. These properties are sufficient to develop the Brillouin Zones in both the extended and reduced schemes for any translationally periodic lattice. The first four zones for the hexagonal lattice are presented in Figures 24 and 25 together with the appropriate parting lines in the reduced zones. The outer zones may be constructed in various ways, but these are of no real difference since

BRILLOUIN ZONES FOR THE HEXAGONAL LATTICE

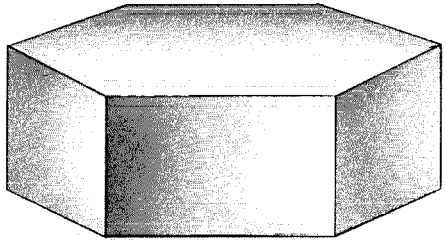

FIRST ZONE

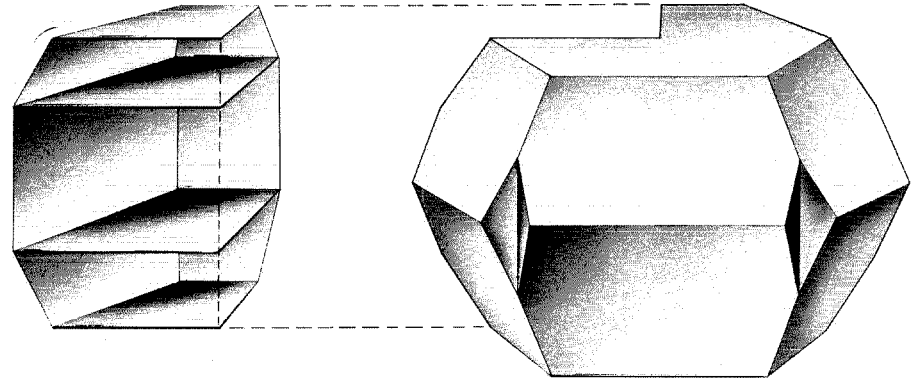

SECOND ZONE

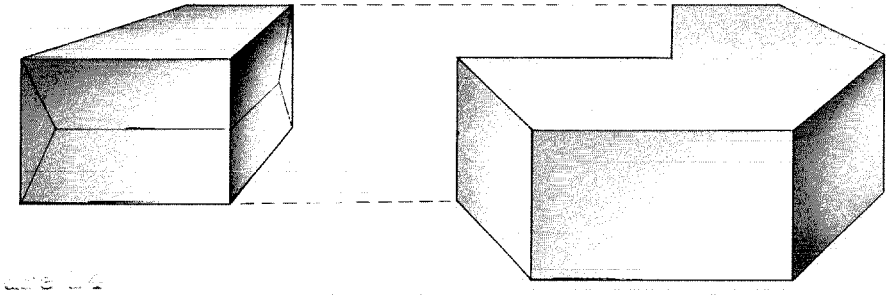

REDUCED SECOND ZONE

BRILLOUIN ZONES FOR THE HEXAGONAL LATTICE

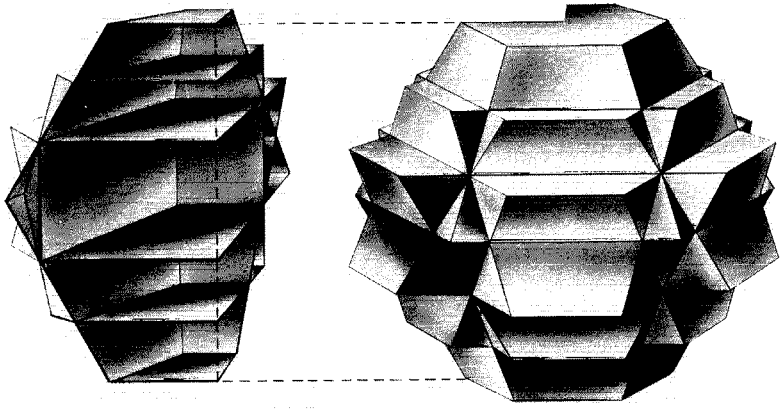

THIRD ZONE

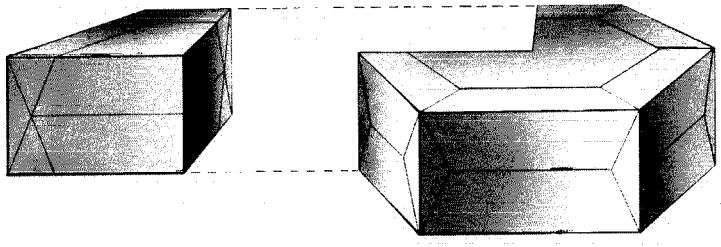

REDUCED THIRD ZONE

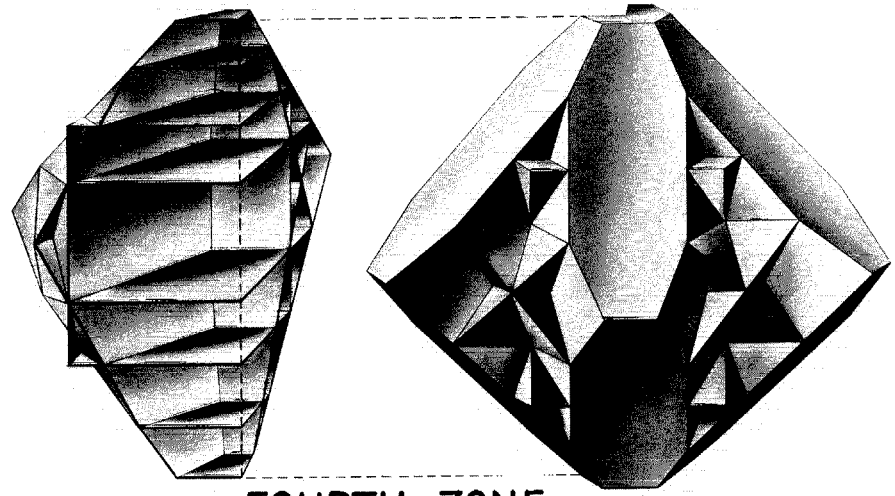

FOURTH ZONE

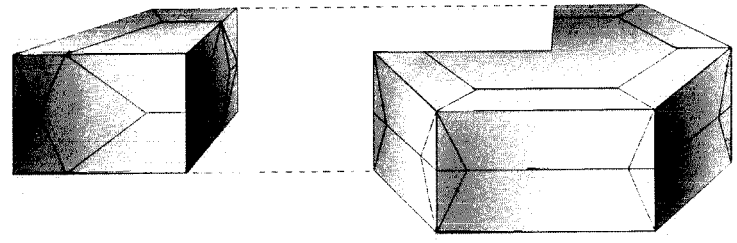

REDUCED FOURTH ZONE

they lead to identical reduced zone figures. For example, all hexagonal lattices (e.g. simple hexagonal, graphite, hexagonal close packed, and Wurtzite lattices) lead to the same Brillouin Zones since they all have the same translational periodicity of the simple hexagonal lattice.

These considerations suggest that there exist further conditions for the existence of energy gaps on the Brillouin planes beyond the Brillouin conditions. An extensive discussion of the properties of energy bands and Brillouin Zones is beyond the scope of this study; however, it appears desirable to develop such concepts which yield significant variations in the energy band structure to be employed in the interpretation of the present experiments.

C. Time-Reversal Symmetry:

The reality of the Hamiltonian can be shown to result in additional symmetry in the representations of the wave functions and the associated eigenvalues W_k. The consequences of the reality of the Hamiltonian on the energy eigenvalues in wave number space have been studied extensively by Wigner (59) and Herring (60) with group theory methods. Herring refers to the additional symmetry due to the reality of the Hamiltonian as time-reversal symmetry since the eigenfunctions are interchanged upon an interchange of the time axis. The additional symmetry which results is the addition of inversion symmetry types to the eigenvalues W_k. Such additional

symmetries, Herring points out, may be accomplished with a center of inversion, two-fold rotation axes, glide plus translation, or a suitable combination of these. Certain other symmetry forms, in addition to these, may be required for eigenvalues for $\bar{k}$ satisfying the Brillouin condition. For the present purpose it is sufficient to recognize that additional symmetry of the eigenvalues is required by the reality of the Hamiltonian, and that this additional requirement is at least inversion symmetry of the eigenvalues, i.e., $W_k = W_{-k}$. The determination of the additional symmetry form required of the W_k, i.e., center of inversion, two-fold axes, etc., requires extensive consideration by group theory or its equivalent if the condition is not automatically satisfied.

The inversion symmetry of the eigenvalues is automatically assured in the hexagonal lattice providing only that the Brillouin planes pass through the points $\bar{k} = \bar{K}/2$. This is always satisfied for the hexagonal lattice when the reduced zone form of specifying the eigenvalues is employed. The use of certain possible outer zone forms may not satisfy this requirement.

D. Structural Symmetry Requirements:

In addition to the symmetry requirements imposed on the wave functions by translational periodicity of the lattice, the Brillouin conditions, and the reality of the Hamiltonian, further symmetrical requirements may be imposed by point group and space group

symmetries of the lattice. All the symmetry elements required of the wave functions can be expressed in group theory form (61). While the application of group theory in this manner relieves the investigator of a certain effort with respect to completeness, it does not present a clear physical picture of the structural analogies and, in general, presents the results in such a way as to be unavailable to the investigator unfamiliar with group theory methods. The point group and space group symmetries, therefore, are discussed only on the basis of individual symmetry element requirements rather than in the abstraction of formal group theory.

The lattice symmetry elements consist of point group symmetry elements, which are those symmetry elements exhibited at a lattice point, and space group elements, which require a spatial element in the symmetry description. The association of point group and space group symmetry elements with the wave functions may be accomplished by the transformation properties of the symmetry element. Consider a particular symmetry element S. This symmetry element has the property that it maps the lattice space R into the lattice space R' in a one-to-one mapping such that R' is indistinguishable from R. Since the wave functions in the original lattice space R must be the same as those in the space R' and since these lattices are indistinguishable, the wave functions must be invariant under the

operation S*. This is:

$$R' = S \cdot R$$

and $$\psi_k(r') = S\,\psi_k(r). \qquad (5\text{-}12)$$

This symmetry requirement on the wave functions must evidently also be imposed on the energy eigenvalues which are determined from the wave functions. Similarly the energy discontinuities $V_{kk'}$ on the zone faces must satisfy a corresponding requirement since the perturbing potential Vp must be unchanged by the operation S.

Consider, for example, a four-fold axis. The symmetry operation S is then a rotation of $n\pi/2$, where n is any integer. The transformation carries the vector $\bar{r}$ into the vector $\bar{r}'$ by a rotation of $n\pi/2$ about the four-fold axis. If the requirement that $\psi_{k'}(r) = \psi_{k'}(r')$ is to be met, the vector $\bar{k}_i$ must be carried into the vector $\bar{k}_{i'}$ by the rotation of $n\pi/2$ about the four-fold axis. Similarly, the energy states must also display the four-fold symmetry since these are developed according to (5-6) from the wave functions and $\bar{k}$ vectors. By analogous considerations it may be seen that if $\bar{k}_i$ is a vector to a Brillouin plane, then $\bar{k}_{i'}$ must also terminate at a similar plane. This latter property is assured if the set of primitive translation vectors possesses the symmetry of the point or space group element. If,

*Actually the wave functions must either be symmetric or antisymmetric under the operation S. Since inversion is required, it is not necessary to consider in detail the antisymmetric case.

however, the symmetry element is not implicitly included in the set of primitive translation vectors, additional considerations will be required to determine the required form of the energy zone.

The Brillouin Zone determined by the planes satisfying (5-9) is to be distinguished from the energy zone which is derived from the conditions (5-9) and further symmetry considerations. It is to be emphasized that the Brillouin Zones resulting from the conditions (5-9) will not be acceptable descriptions of the energy zones for all possible crystal structures. While a complete discussion of this subject is beyond the scope of this dissertation, a brief discussion of this conclusion is presented as a basis for the subsequent development of the appropriate energy zone for the hexagonal close packed lattice. Unfortunately, the available textbooks (51), (52), (53), fail to present a complete description of the symmetry requirements of the energy zones. The interested reader is referred to articles by Herring (62), Bouckaert, Smoluchowski, and Wigner (63), and Hund (64), which treat in some detail certain phases of the general problem of energy zones by advanced group theory.

E. Energy Zone Forms:

Consider, as in the preceding section, that the vector $\bar{k}_i$ terminates on a plane satisfying the Brillouin condition (5-9). The symmetry element that transforms the vector $\bar{r}$ into $\bar{r}'$ preserves the wave function ψ_k and transforms the vector $\bar{k}_i$ into $\bar{k}_i'$. Further,

the unperturbed energy W_k^o is unchanged by this transformation. The energy perturbation $V_{kk'}$ on the Brillouin plane is unchanged by the transformation. The potential perturbation Vp must remain unchanged by the transformation since it has all the symmetry of the lattice. The wave functions ψ_k remain unchanged by the transformation, thus the product $\psi_k^* V_p \psi_k$ must be invariant under the transformation. Hence the matrix element $V_{kk'}$ must be invariant under the symmetry operation since its integrand is invariant. Thus, if $\bar{k}_1$ terminates on a Brillouin plane, either (1) $\bar{k}_{1'}$ also terminates on a similar Brillouin plane, or (2) the Brillouin plane does not represent an energy surface since $V_{kk'}$ must vanish on the surface. The case (1) contributes no really new information to the construction of the energy zones; the conclusion that similar zone faces had equal energy gaps could have been obtained from less fundamental considerations. The case (2), however, constitutes a significant addition to the required properties of energy zones. The degeneracy condition includes all possible planes of degeneracy, and hence the postulate cannot be satisfied in the manner (1) by the construction of zone surfaces in addition to those given by (5-9). The only remaining possibility is that the energy gap, $V_{kk'}$, must vanish on such planes. This principle can reasonably be extended to show that the planes forming the energy zones must satisfy the appropriate point group and space group symmetry elements of the crystal lattice. This requirement is, of course, in addition to the requirements previously stated.

Group theory accomplishes the same result as the above treatment, but in a less intuitive fashion. It provides, in addition, some information about the behavior of the degeneracy of certain states at the edges of the faces of the energy zones. This additional information is of importance in only a small fraction of the interpretive problems where this theory is useful, and hence is not discussed here.

F. Energy Zones in the Hexagonal Close Packed Lattice:

The foregoing theory will now be employed to construct the energy zones for the hexagonal close packed lattice of the titanium alloys of this study. Since the energy zones for the hexagonal close packed lattice which satisfy the symmetry requirements are different than the Brillouin Zones given in some texts (52), (53), the calculation is developed in detail.

The translational periodicity of the hexagonal lattice is described by the vectors:

$$\bar{\tau}_1 = \begin{pmatrix} \sqrt{3}\,a/2 \\ -a/2 \\ 0 \end{pmatrix}, \quad \bar{\tau}_2 = \begin{pmatrix} 0 \\ a \\ 0 \end{pmatrix}, \quad \bar{\tau}_3 = \begin{pmatrix} 0 \\ 0 \\ c \end{pmatrix} \qquad (5\text{-}13)$$

where these vectors are illustrated in Figure 26, and c and a are the hexagonal lattice parameters.

The hexagonal close packed lattice is characterized by an atom at $(\frac{2}{3}\bar{\tau}_1, \frac{1}{3}\bar{\tau}_2, \frac{1}{2}\bar{\tau}_3)$ in addition to the one at (0, 0, 0). The reciprocal lattice is described by the vectors:

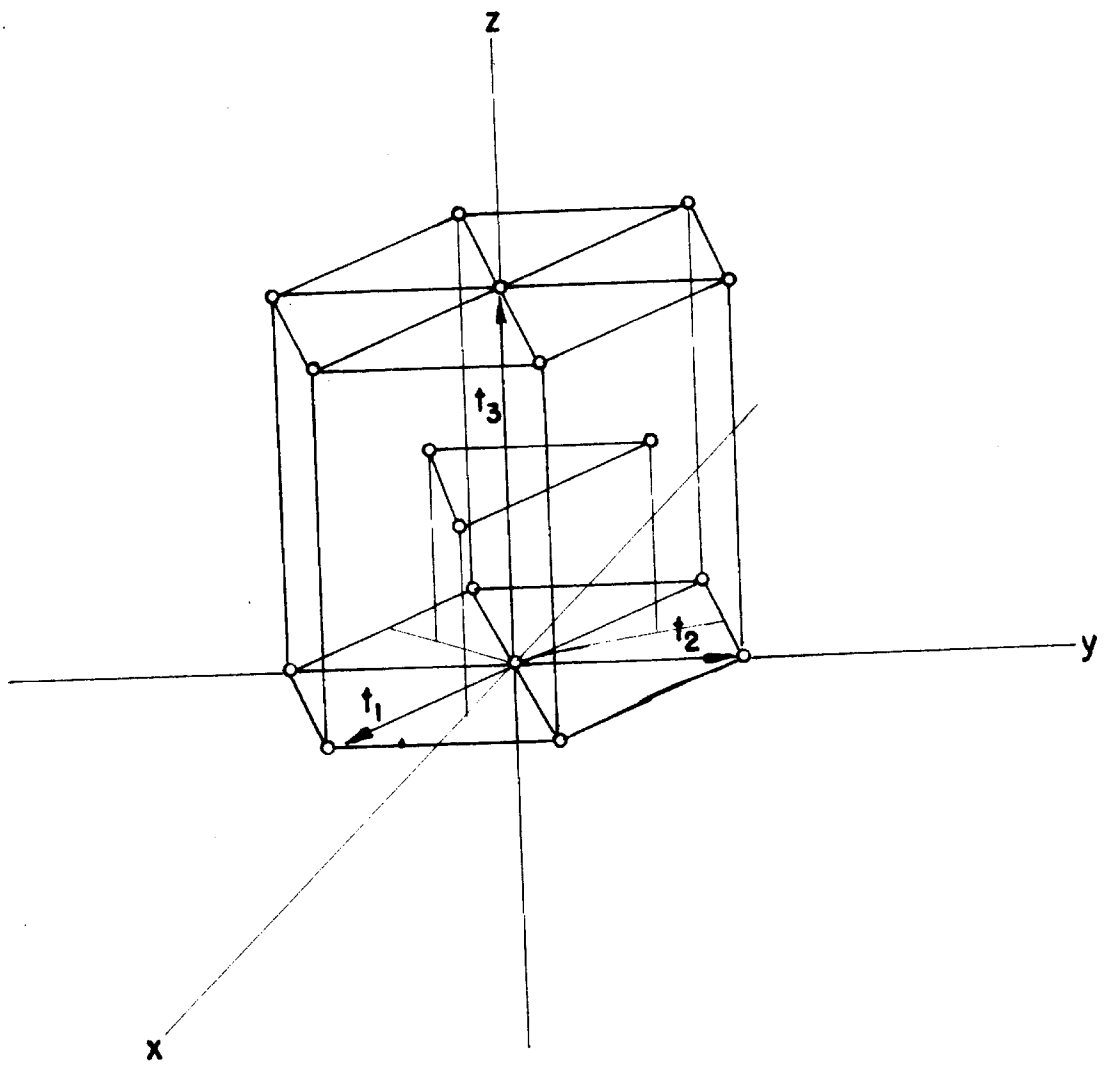

Figure 26

Hexagonal Close Packed Lattice Showing The Primitive Translations

$$\bar{\rho}_1 = \begin{pmatrix} 1/\sqrt{3}a/2 \\ 0 \\ 0 \end{pmatrix}, \quad \bar{\rho}_2 = \begin{pmatrix} -\frac{1}{\sqrt{3}a} \\ -\frac{1}{a} \\ 0 \end{pmatrix}, \quad \bar{\rho}_3 = \begin{pmatrix} 0 \\ 0 \\ 1/c \end{pmatrix}. \qquad (5\text{-}14)$$

Thus the reciprocal lattice is hexagonal with the parameters $2/\sqrt{3}a$ and $1/c$ corresponding to the parameters a and c in the real lattice. This reciprocal lattice is shown in Figure 27 in approximately correct proportion to Figure 26.

The Brillouin Zones are constructed in the reciprocal lattice space by the relations (5-9). The space of $\bar{k}$ and the reciprocal lattice space are taken as identical; thus the set of $\bar{K}$ vectors may be chosen the same as the primitive vectors, $\bar{\rho}$, of the reciprocal lattice. The planes satisfying the Brillouin condition are normal to and bisect the $\bar{K}$ vectors. The first zone is shown in the reciprocal lattice space in Figure 27. The outer zones are shown in Figures 24 and 25. If the reduced zone scheme is used, only the first zone need be constructed and the form of the remaining zones need not be considered further.

The inversion symmetry required of the energy zones is seen to be satisfied by the hexagonal prism in Figure 27. In addition, it is necessary to consider the requirements of the remaining symmetry elements of the hexagonal close packed lattice. All symmetry requirements of the simple hexagonal lattice (D_{6h}^{1}) with 1 atom at the lattice point (000) are automatically satisfied since the set of primitive translations possess all the remaining symmetry elements of the

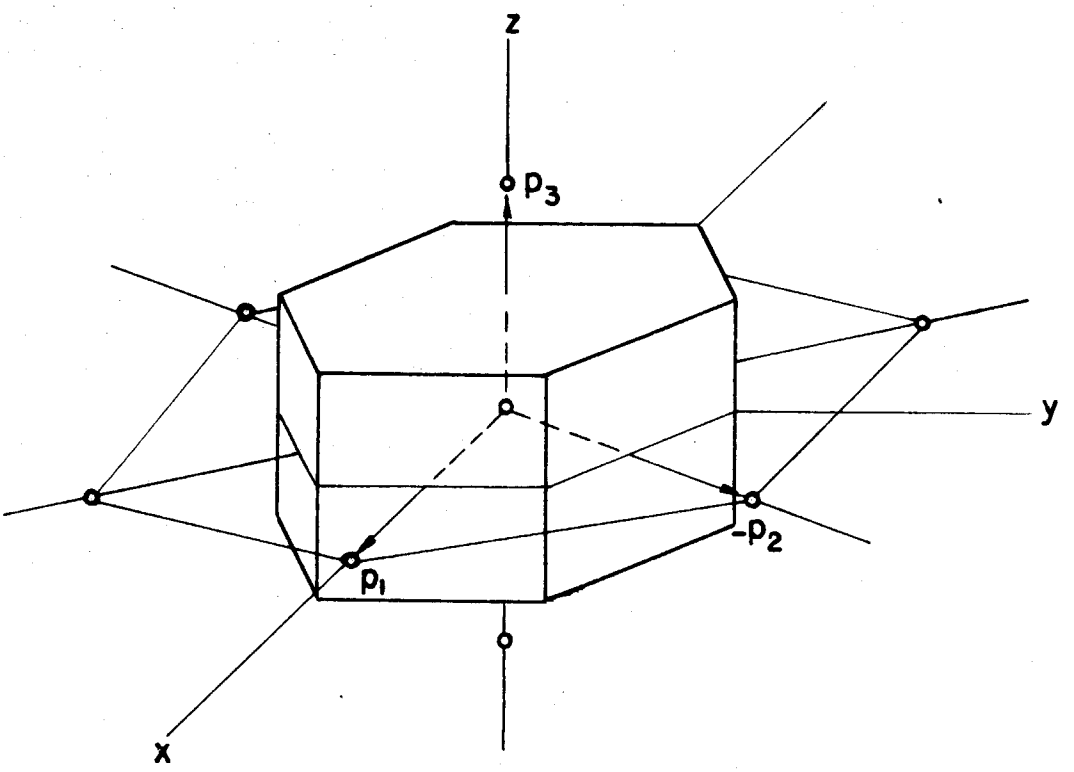

Figure 27

Reciprocal Lattice With The Primitive Vectors And The First Brillouin Zone

lattice. The close packed hexagonal lattice (D_{6h}^4) with an additional atom at (2/3, 1/3, 1/2) has the same set of primitive translations, but has a different set of symmetry elements. The Brillouin Zones are the same in both cases, since the primitive translations are the same. It might, however, be expected that the energy zones in the latter case are different due to the additional symmetry elements. Verification of this intuitive notion may be obtained by carrying out the indicated symmetry operation for each individual symmetry element in the case of the hexagonal close packed lattice. The characteristic symmetry element introduced in the hexagonal close packed lattice over the simple hexagonal is the c glide resulting from the plane of atoms (2/3, 1/3, 1/2). The other symmetry elements do not affect the zone structure in the reduced zone scheme and are not discussed in detail.

The c glide transforms the space lattice into itself by a displacement along the z axis of c/2 and reflection in a plane normal to a vector of the form:

$$\begin{pmatrix} a/2\sqrt{3} \\ 0 \\ 0 \end{pmatrix}, \qquad (5\text{-}15)$$

lying in the basal plane. The reflection in the plane normal to (5-15) takes the vector $\bar{r}$ into the vector whose components are:

$$\frac{a}{\sqrt{3}} - \frac{r_x}{2}, \; r_y, \; r_z .$$

Thus the glide operation transforms the vector:

$$\begin{pmatrix} r_x \\ r_y \\ r_z \end{pmatrix} \quad \text{into} \quad \begin{pmatrix} \frac{a}{\sqrt{3}} - \frac{r_x}{2} \\ r_y \\ r_z + \frac{c}{2} \end{pmatrix}. \qquad (5\text{-}16)$$

Calling the operator which performs this operation Sc, indicating a c glide, the wave function ψ_k must then satisfy:

$$\left.\begin{aligned} \psi_k(r') &= S_c\, \psi_k(r) \\ \psi_k(r') &= \psi_k(r) \end{aligned}\right\} \qquad (5\text{-}17)$$

where the transformed function may be the conjugate of ψ_k without violating the requirement.

Using the relation (5-17), the energy perturbation $V_{kk'}$ at the zone surfaces may be examined. Writing the expression for the energy perturbation

$$V_{kk'} = \int \psi_k^*(r)\, V_p(r)\, \psi_{k'}(r)\, d\tau,$$

it is seen that this must transform as:

$$V_{kk'} = \int S_c\, \psi_k^*(r) S_c V_p(r)\, S_c\, \psi_{k'}(r)\, d\tau. \qquad (5\text{-}18)$$

The periodic potential Vp is invariant under the glide transformation since either (0, 0, 0) or (2/3, 1/3, 1/2) are equivalent origins for the description of the hexagonal close packed lattice*. Thus $V_p(r)$ is identical with $V_p(r')$ and either $V_p(r)$ or $V_p(r')$ may be written in the

*This is evident by considering the hexagonal close packed lattice to be constructed from two identical simple hexagonal lattices, one centered at (0, 0, 0), the other at (2/3, 1/3, 1/2).

expression for $V_{kk'}$.

If Bloch functions are employed in (5-18), the expression becomes:

$$V_{kk'} = \int S_c\left\{\chi_k(r)e^{2\pi i\bar{k}\cdot\bar{r}}\right\} V_p(r)\, S_c\left\{\chi_{k'}(r)e^{2\pi i\bar{k}\cdot\bar{r}}\right\} d\tau \qquad (5\text{-}19)$$

The expression (5-19) becomes appreciable at the zone boundaries, i.e., for $\bar{k}$ satisfying the relations (5-9). For a vector $\bar{k}$ terminating on the planes forming the ends of the hexagonal prism, the planes normal to:

$$\begin{pmatrix} 0 \\ 0 \\ \frac{1}{2c} \end{pmatrix},$$

the expression (5-19) becomes:

$$\int S_c\left\{\chi_k \exp\left(2\pi i\,\bar{k}\left(\tfrac{1}{2c}\right)\cdot\bar{r}\right)\right\} V_p(r)\, S_c\left\{\chi_{k'} \exp\left(2\pi i\,\bar{k}\left(\tfrac{1}{2c}\right)\cdot\bar{r}\right)\right\} d\tau \qquad (5\text{-}20)$$

Equation (5-20) is identical with the expression for the energy perturbation by the assumption that $V_{kk'}$ is invariant under the transformation Sc. Hence the equality:

$$\int \psi_k^*\left(r, \tfrac{1}{2c}\right) V_p\, \psi_{k'}\left(r, \tfrac{1}{2c}\right) d\tau = \int e^{i\frac{\pi}{2}} \psi_k^*\left(r, \tfrac{1}{2c}\right) V_p\, e^{i\frac{\pi}{2}} \psi_{k'}\left(r, \tfrac{1}{2c}\right) d\tau$$

must hold. This can be written:

$$V_{kk'} = e^{i\pi} V_{kk'} = -V_{kk'} \qquad (5\text{-}21)$$

Evidently the matrix element $V_{kk'}$ must vanish on the zone faces $(0,\ 0,\ \pm\frac{1}{2c})$. Therefore the energy must be a continuous function of $\bar{k}$ across the (001) faces of the first Brillouin Zone. The correct

energy zone is thus distinct from the Brillouin Zone since the energy varies continuously from the first to the second zones.

The next zone face in the (001) direction occurs at $z = \pm\frac{1}{c}$. The glide transformation yields a factor of $\exp(2\pi i \cdot \frac{c}{2}\frac{1}{c})$ in the wave functions so that the relation analogous to (5-21) in this case is:

$$V_{kk'} = e^{2\pi i} V_{kk'} = V_{kk'} : \qquad (5\text{-}22)$$

Therefore, the energy difference across the zone faces does not vanish from symmetry requirements.

In the extended zone scheme, planes satisfying the Brillouin condition occur at $\pm\frac{1}{2c}$, $\pm\frac{1}{c}$, $\pm\frac{3}{2c}$, $\pm\frac{2}{c}$, etc. The glide symmetry removes the energy gap on the planes $\pm\frac{1}{2c}$, $\pm\frac{3}{2c}$, $\pm\frac{5}{2c}$, etc. Therefore, the correct energy zones for the hexagonal close packed lattice occur as pairs of the Brillouin Zones.

The volume of each Brillouin Zone for the hexagonal lattice is $\sqrt{3}/2\, a_k^2 c_k$. For a lattice of N_1, N_2, N_3 primitive cells in the x, y, z directions respectively, there are $N_1N_2N_3$ energy states. The total volume of such a lattice is $N_1N_2N_3 \frac{\sqrt{3}}{2} a^2 c$. The total number of energy states in each Brillouin Zone is $N_1N_2N_3$, or one energy state per primitive cell in the crystal. Each energy state accommodates two electrons by the Pauli Principle. Since the primitive lattice cell contains two atoms, each Brillouin Zone corresponds to an electron-atom ratio of 1. Since each energy zone contains two Brillouin Zones, each energy zone contains two electrons per atom when all the energy

states are occupied.

Assuming the energy perturbation at the energy zone faces is small, the approximate electron-atom densities can be computed by geometrical considerations. The inscribed sphere which just touches the first Brillouin plane in the (001) direction contains $\frac{\pi}{6\sqrt{3}}\left(\frac{c_k}{a_k}\right)^2$ energy states/atom. For titanium with an axial ratio of c/a = 1.58 or $c_k/a_k = 0.548$, the electron density is approximately 0.18 electrons per atom. The first planes of the energy zone to be encountered upon further increasing the electron density are planes of the form (100). The volume of the inscribed sphere touching these planes is $4/3\pi\, a_k^3$ and contains $\frac{\pi}{3\sqrt{3}}\,\frac{a_k}{c_k}$ electrons per atom. For titanium this electron density is 1.1 electrons per atom. The next planes of the energy zone to be encountered are planes of the form (001), which correspond to an electron density of 1.46 electrons per atom. These values can be extended to higher energy zone faces by simple analogy with the preceding discussion.

Calculation of exact electron densities is extremely difficult on the basis of present theory and will not be treated in detail. A semi-empirical method, however, may be used which serves only as an approximation to the necessary correction. This correction will be discussed briefly in Section VI.

G. Corrections for Electron-Electron Interactions:

In the foregoing discussion no mention has been made of

electron-electron interactions. While the ad hoc assumption of a small perturbation in potential precludes an exact treatment of these interactions, approximate methods exist which might be employed. Inclusion of these corrections is omitted in the present study since the amount of the correction is small and the methods required are quite complex. The correlation energy has been estimated by D. Pines (65) in titanium and similar metals and found to be small (of the order of 10 percent correction). The exchange correction is of the same order of magnitude as the correlation correction; its inclusion in the present treatment is even less justified (66). A careful consideration of these corrections on the present model in titanium would alter the results less than 20 percent in energy and even less in the other parameters. Inclusion of these effects does not appear to be justified in view of the doubtfulness of the accuracy of the perturbed free electron model in the description of transition metals and additional complexity of theory resulting from even an approximate treatment of the corrections. Detailed discussions of correlation effects have recently appeared by Pines (67) and Stoner (68) to which little could be added. Exchange corrections are treated in detail by Seitz (51). Recently, an excellent review of the application of theoretical methods to transition metals and alloys has been written by Hume-Rothery and Coles (69). The completeness of this review leaves little to be added for application to the present study. It may be noted that the conclusions reached by Hume-Rothery and Coles are

not unfavorable to application of the perturbed free electron treatment to transition metals.

VI. DISCUSSION

Transition metals are characterized in the atomic state by unsaturated "d" quantum states. Titanium has the atomic configuration $3d^2\ 4s^2$ and hence has 4 electrons in quantum states beyond a noble gas structure. In a metal crystal these four outer electrons occupy energy states considerably above the lower states of the argon configuration. The four outer electrons of titanium may be represented in the energy zones developed in the previous section, and occupy energy states in the energy zones up to the number required to accommodate 4 electrons per atom. The maximum number that can be accommodated in any one zone is 2 electrons per atom. Thus the four outer electrons of titanium will occupy at least two energy zones.

The addition of solute atoms substitutionally in the titanium lattice produces a dilatation of the lattice since the solute atoms, in general, are not of the same atomic volume as the titanium atoms. The local dilatation strain around a solute atom is distributed between many neighboring atoms so that the strain energy is minimized. Above very small solute concentrations the dilatation is nearly uniform in the lattice. The dilatation in the lattice is a linear function of the number of solute atoms in the lattice. The linear dependence of atomic volume on the solute concentration (Vegard's Law) is found to be obeyed in many solid solutions.

Addition of solute atoms also changes the number of electrons

which are not bound to a particular atom if the valency of the solute atom is different than the valency of the solvent atoms. Providing the concentration of solute is sufficiently small and the solute and solvent atoms have different valencies, the number of loosely bound electrons changes as the difference in valency and the solute concentration. The solute atoms are also assumed to be randomly distributed in the lattice. If the solute atoms are distributed in a regular pattern, the Brillouin Zones of the alloy are different than the Brillouin Zones of the pure solvent, since the periodicity of the alloy lattice is not the same as the solvent lattice. A common example of such a regular array is the superlattice alloy Cu_3Au. In dilute solutions such ordering, even in local regions, is unlikely.

The dilatation of the solvent lattice by the addition of the solute creates a perturbation of the electron energy in the pure solvent lattice. The form of the energy zones was shown in the previous section to be dependent only upon translational periodicity of the lattice. The energy perturbation at the zone boundaries, however, depends upon the functional form of the perturbing potential. The distribution of electrons near the energy zone boundaries will necessarily be changed by a dilatation of the lattice. The change in the energy distribution is negligible for all the unbound electrons except those in energy states very near surfaces of the energy zones.

The local potential around the solute atoms will usually be different than the potential in the neighborhood of the solvent atoms.

In a perturbed free electron approximation, this difference is usually neglected in its effect on the energy perturbation. Since this amounts to a second order correction in the eigenvalues, neglecting the difference in the local potential in the neighborhood of the solute atoms is probably justified in dilute solutions.

In the following paragraphs the alloy model described above is examined in more detail to develop an explanation of the experimental results presented in Section IV. The discussion, based on the energy zones derived in Section V, is directed first toward mechanical property changes resulting from changes in the electron energy distribution due to solute additions, and then toward electrical property changes. Next the experimental results are compared with the property changes based upon the energy zone model, and a description of the electron structure of pure titanium is developed with the close packed hexagonal energy zones. Finally the resultant energy zone structure is compared with some of the current theories of metals of transition elements.

A. Lattice Strains:

The hexagonal close packed lattice is characterized by the lattice parameters c and a, Figure 26. For ideal close packed lattices these are in the ratio $c/a = \sqrt{8/3} = 1.633$. In most hexagonal close packed metals the axial ratio, $\frac{c}{a}$, is somewhat different than the ideal ratio; in titanium the axial ratio is $c/a = 1.587$. Due to solute-solvent

size difference, solute atoms added to the hexagonal close packed lattice produce a change in the average atomic volume which is linear with solute concentration. The resulting changes in the parameters $\underline{c}$ and $\underline{a}$ vary linearly with the solute concentration, while the axial ratio is invariant with solute concentration.

The energy zone for the hexagonal close packed lattice provides a unique opportunity for non-isotropic lattice deformations. The planes of energy discontinuity are located at different energies in the (100) and (001) directions in the hexagonal lattice. Upon addition of electrons in the hexagonal energy zones, the Fermi surface, the surface of highest occupied energy states, encounters the zone face in the (100) direction before encountering the zone face in the (001) direction. Jones (3) suggests that when the Fermi surface overlaps planes of the energy zones it produces a "stress" on the crystal. If the Fermi surface overlaps the energy zone surface moderately, the total energy of the electrons can be reduced if the surface of the energy zone is shifted to higher energies. Similarly if the Fermi surface lies below the surface of the energy zone, the total energy of the electrons can be reduced if the surface of the energy zone is shifted to lower energies. The number of energy states enclosed in the energy zone must, however, remain constant during any displacement of the energy zone surfaces. Thus only those lattices whose energy zones are not cubically symmetrical about the coordinate axes of reciprocal space can asymmetrically deform in order to lower the

electron energy and maintain a constant volume. In the hexagonal lattice, deformation of the zone can occur by contraction in the (001) direction and expansion in the (100) direction. The distortion of the energy zone in this manner necessitates a shear strain in the crystal lattice in the opposite sense: c expands and a contracts. Jones refers to this effect as a "stress" on the crystal in the appropriate crystallogropic direction produced by the electrons. This terminology is apparent from considering that the "stress", -grad E, acts in such a way as to produce the shear strain in the crystal equivalent to the distortion of the energy zone. Jones has evaluated such a "stress" for γ-phase alloys in the copper-zinc system. Goodenough (70), following Jones' suggestion, calculated the "stress" for other Fermi energies in hexagonal close packed lattices. Both writers found that the electron energy reduction is of the order of magnitude to be expected from the observed shear strain by approximate considerations of the interactions involved. Experimental evidence of this strain is given, in addition to Jones' work, by Hume-Rothery and Raynor (7) in magnesium alloys.

The effect of the perturbation on the energy of the outer electrons can be considered, for convenience, as an interaction between the Fermi surface and the energy zone, as suggested by Jones. Calculation of the interaction between the Fermi surface and the energy zone involves the evaluation of integrals of the form:

$$\int \frac{\partial}{\partial k} V_{kk'} \, dk' , \qquad (6\text{-}1)$$

where the meaning of these symbols is the same as previously ascribed.

The assumptions necessary for quantitative evaluation of integrals of the form (6-1) do not appear to be justified for most real metals; however, a qualitative understanding of the change in the interaction on changes in the Fermi level is easily obtained. The change in energy of a state $\bar{k}$ due to the perturbation is $V_{kk'}$. The energy perturbation for $|\bar{k}|$ less than $|\bar{k}'|$ satisfying the Brillouin condition is negative and increases in magnitude as $\bar{k}$ tends to $\bar{k}'$. At $\bar{k}$ equal $\bar{k}'$ the energy gradient $\frac{\partial E}{\partial k}$ is zero. Thus the Fermi surface will contact the planes of the energy zones orthogonally. The density of energy states is, therefore, increased at the Fermi surface when a contact with the energy zone is made. These states are reduced in energy below the corresponding unperturbed energy states by the amount $V_{k'k'}$. If the Fermi surface is near the surface of the energy zone, the energy of the electrons near the Fermi surface is reduced by the amount (6-1) if a contact can be made. Contact can be achieved by the lattice shearing in such a way that the surfaces of the energy zone near the Fermi surface are shifted toward the Fermi surface while the energy zone surfaces farther from the Fermi surface are shifted away. The "stress" on the crystal suggested by Jones is therefore of the form of (6-1).

The Fermi surface contacts the energy zones for the hexagonal close packed lattice (Figures 24 and 25) on the (100) faces at an electron-atom ratio of about 1.1. The (001) face contacts occur at about 1.5 electrons per atom. While the details of the interactions associated with these contacts are difficult to determine, a qualitative relation between lattice strain and electron-atom ratio can be obtained by examining the nature of the interaction with increasing electron-atom ratio. As the electron-atom ratio increases, the interaction between the (100) faces of the energy zones and the Fermi surface increases. A shear strain increasing the axial ratio c/a will reduce the energy of the energy states near the Fermi surface until the Fermi surface contacts, and overlaps, the (100) faces of the energy zone. Thus an axial ratio greater than 1.63 can be expected for electron-atom ratios near 1.1. As the electron-atom ratio increases, the overlap of the Fermi surface beyond the (100) faces increases. The energy states near the overlapped Fermi surface are reduced by a shear strain reducing the axial ratio below 1.63. As the electron-atom ratio continues to increase, the interaction between the Fermi surface and the (001) faces becomes increasingly important. The shear strain reducing the (001) face interaction increases the axial ratio. The overlapped (100) face interaction and (001) face interaction compete until just before the (001) face contact is made. When the Fermi surface nearly contacts the (001) faces, the (001) interaction is greater than the (100) interaction, and the axial ratio

increases abruptly. After the (001) contact between the Fermi surface and the energy zone at about 1.5 electrons per atom, the axial ratio can be expected to increase, but less rapidly than just prior to the (001) contact. The behavior of the axial ratio with electron-atom ratio is shown schematically in Figure 28. The exact behavior is strongly dependent on $V_{kk'}$, particularly, at high electron-atom ratios, therefore Figure 28 should be regarded as only approximate.

The shear strain produced by the interaction of the Fermi surface and the energy zone provides an explanation of the deviation of the lattice parameter curves (Figures 16, 17, 18, 19) from Vegard's Law. The solutes aluminum, gallium, and silver have atomic diameters 2.86 Å (71), 2.82Å *, and 2.88 Å (71) respectively. Titanium is larger than these solutes with the atomic diameter 2.93 Å (71). Addition of aluminum, gallium, or silver in titanium decreases the atomic volume of the alloy to less than the atomic volume of pure titanium, corresponding to the smaller atomic diameter of the solute. The axial ratio does not remain constant when these solutes are added, and in the case of aluminum and gallium the c parameter does not decrease with increasing solute concentration at low concentrations. The shear strain produced by the interaction of the Fermi surface with the (001) face of the energy zone

*The atomic diameter of gallium was obtained by extrapolating to pure gallium the atomic volume of solid solutions of Cu-Ga (72) and Ag-Ga (73).

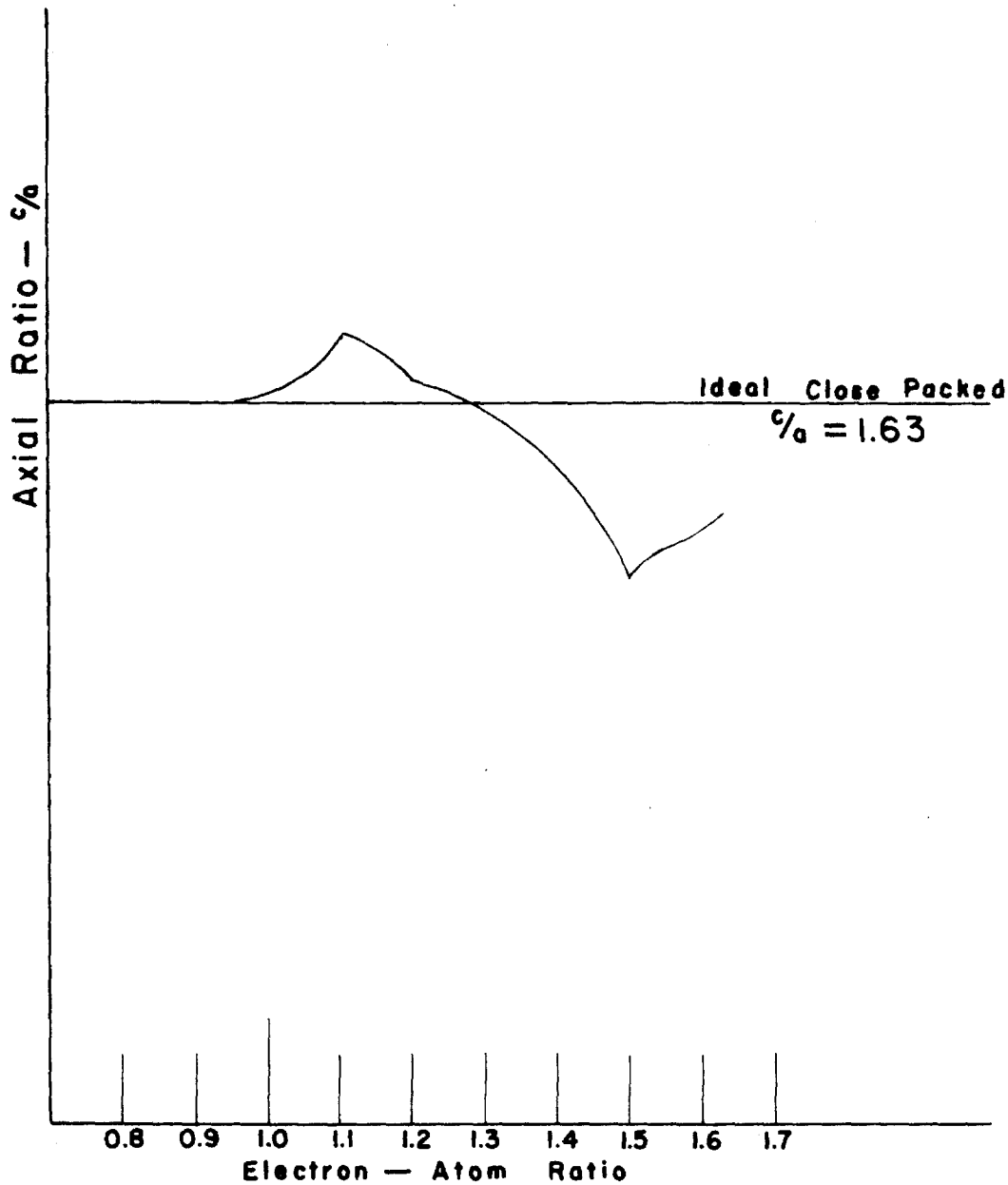

Figure 28

Variation Of Axial Ratio With Electron Concentration In Hexagonal Close Packed Lattice, Schematic

increases the axial ratio as contact between the (001) face and the Fermi surface occurs. The interaction between the (001) face and the Fermi surface decreases as a larger contact area is achieved. Increased contact is provided by increasing the shear strain, i.e., the axial ratio, or by increasing the electron-atom ratio. The solid solutions of aluminum and gallium in titanium (Figures 16 and 18) exhibit such behavior at low solute concentrations. Gallium in titanium (Figure 18), especially, exhibits this change in axial ratio. If the deviation of the c lattice parameter from Vegard's Law is taken as measure of the interaction of the Fermi surface and energy zone, then the addition of aluminum and gallium at first increases the interaction up to a solute concentration of about 2 percent, followed by a decreasing interaction to about 2.8 percent. It is not possible to decide on the basis of the additions of trivalent aluminum and gallium if the parameter variation is due to an increasing or decreasing electron-atom ratio. Nor is it possible to determine from the aluminum and gallium additions whether the (001) face involved is the first zone face at an electron-atom ratio of about 1.5, or the second zone face at an electron-atom ratio of about 3.5. These uncertainties are resolved by additions of a monovalent, divalent, or quadrivalent solute. Divalent and quadrivalent solutes are not soluble in titanium to the extent required for suitable comparison with aluminum and gallium. The monovalent solute, silver, provides a comparison with the trivalent solutes. The c and a parameters change linearly

with solute concentration (Figure 19), and do not exhibit the anomalous behavior of the c parameter with trivalent solute concentration. The uniform parameter change with the concentration of silver indicates that contact of the Fermi surface and the energy zone does not occur with the addition of silver. Together with the parameter changes observed for solutes of aluminum and gallium, this indicates that the electron-atom ratio decreases with the addition of silver and increases with additions of aluminum and gallium. For a decreasing electron-atom ratio, the Fermi surface, overlapping the (100) faces and not in contact with the (001) faces, interacts with the energy zone to increase the axial ratio. This shear strain is superimposed on the change in atomic volume of the alloy with addition of silver. The titanium-silver alloys exhibit this behavior with an increasing c parameter and a decreasing a parameter with addition of silver.

These changes in lattice parameter with solute concentration indicate that titanium has an alloying valency for addition of solutes of aluminum, gallium, and silver of about 1.5 electrons per atom. The Fermi surface, according to this hypothesis, is enclosed by the energy zone in the (001) direction and overlaps the zone in the (100) direction. Increasing the electron-atom ratio in titanium (addition of aluminum or gallium) strongly increases the interaction between Fermi surface and the (001) face of the energy zone, producing anomalous variations of the c lattice parameter. Decreasing the electron-atom ratio (addition of silver) causes the Fermi surface to

shrink and therefore decreases the interaction with the energy zone, hence the axial ratio increases without abrupt lattice parameter changes. Continued increase or decrease of the electron-atom ratio brings the Fermi surface again in the region of the energy zone. The next planes of the energy zone encountered by the Fermi surface by decreasing the electron-atom ratio are the (100) planes at $1/2\ \rho_1$. The Fermi surface contacts these planes at an electron-atom ratio of about 1.1. An electron-atom ratio of 1.1 is reached at a silver concentration of 80 atomic percent silver. Since the solubility of silver in titanium is less than 7 atomic percent silver, no change of slope of the lattice parameters with solute concentration is to be expected in the range of solubility of silver. The lattice parameter curves for the titanium-silver alloys bear out this expectation.

Increasing the electron-atom ratio above 1.5 electrons per atom causes the Fermi surface to overlap planes of the energy zone in both the (001) and (100) directions. The (100) overlap, beginning at an electron-atom ratio of about 1.2, continues to increase, while the (001) overlap can be expected to begin at an electron-atom ratio of about 1.6 electrons per atom depending on the $V_{kk'}$. The occurrence of overlap of the (001) faces changes the interaction of the Fermi surface and the (001) faces of the energy zones a smaller amount than the initiation of the contact between the (001) face and the Fermi surface, at least for small to moderate values of $V_{kk'}$. The shear strain of the crystal to be expected from the overlap interaction is difficult to

predict with any accuracy since it is strongly dependent on $V_{kk'}$. Jones' calculations (3), for a highly idealized situation, indicate a slight Fermi surface overlap of the (001) face of the energy zone should produce a shear strain increasing the axial ratio c/a of the alloy. The lattice parameter curves for the titanium-aluminum alloys show a slight increase in c/a at about 9 atomic percent aluminum, which is manifested particularly by the c parameter. The corresponding electron-atom ratio is approximately 1.6, which shows good agreement with the electron-atom ratio at which the overlap might be expected. The limited solubility of gallium in titanium ($\sim$ 5 atomic percent) prevents an additional experimental comparison of the behavior of the c lattice parameter at 9 atomic percent aluminum.

Increases in the electron-atom ratio above 1.6 electrons per atom do not produce any rapid changes in the interaction of the Fermi surface and energy zones until either contact on the next (100) faces of the energy zone is made, or the last states of the first energy zone become occupied. Whether the (100) face contact or the completion of filling of the first energy zone is accomplished at lower electron-atom ratios is dependent on $V_{kk'}$. However, in either case the electron-atom ratio is of the order of 3 electrons per atom. The solubility limit of aluminum in titanium (36 atomic percent aluminum) corresponds to about 2.0 electrons per atom, therefore no change in slope of the lattice parameter-solute concentration curves is expected above about 10 percent aluminum. The experimental lattice parameter-

solute curves for the titanium-aluminum alloys agree with this hypothesized lattice parameter behavior within experimental accuracy*.

The lattice parameter curves for titanium alloys suggest that the solvent alloying valency of titanium for non-transition solutes is approximately 1.5 electrons per atom. No contradictions to this conclusion are presented by lattice parameter variation with solute concentration for the solutes aluminum, gallium, and silver.

B. Electrical Properties:

The alloying valency of titanium and variations of the lattice parameter curves suggest that anomalous behavior in other physical properties may be found to provide additional support to the conclusions indicated by variations in lattice parameter. In general, the variations in electrical properties can be expected to be less pronounced, and more difficult to interpret, than the lattice parameter changes. In the following paragraphs the experimental curves of resistivity, susceptibility, Hall coefficient, and magneto-resistance coefficient are compared with the conclusions derived from the lattice parameter variations.

C. Resistivity:

While an exact theory of electrical conductivity in metals is

---

*Experimental accuracy above 20 atomic percent aluminum is reduced to $\pm$ 0.002 Å, see Section III.

lacking, qualitative explanations, based on formal theory, seem to acceptably describe most metals. Matthiessen's rule (43), which represents only a first approximation to the electrical conductivity, nevertheless shows good agreement with experiment in many cases. Matthiessen's rule states that the resistivity of a metal or alloy is separable into an ideal resistivity, ρ_i , for the pure metal and a residual, temperature independent resistivity, ρ_r , due to impurities, etc. Thus the observed resistivity may be written:

$$\rho = \rho_i(T) + \rho_r \ . \qquad (6\text{-}2)$$

According to Matthiessen's rule, solute additions, in small concentrations, produce a resistivity increase proportional to the solute concentration. In many instances this proportionality is closely obeyed (74). Qualitatively Matthiessen's rule, in the case of solute additions, states that the scattering cross section of each solute atom is independent of the solute concentration. In most dilute alloys the contribution to the resistivity is largely scattering off the solute ions in the lattice. The interaction of the Fermi surface with the energy zones may, however, contribute significantly to the electron scattering and hence to the resistivity. As the electron-atom ratio increases and the Fermi surface approaches the energy zone, the concentration of holes (empty electron states) increases in the part of the Fermi surface near the energy zone planes. These empty states can contribute to increased resistivity by providing a nonconducting energy state

for transitions by electrons actively participating in the conduction process at a free portion of the Fermi surface. The process is similar to the s-d transitions which are thought to be responsible for the high resistivity of the transition metals (51, p. 271). In this case, however, the s-d scattering is not significantly altered by small concentrations of solutes, but the in-band scattering is thought to change with electron-atom ratio. As the Fermi surface increases with electron-atom ratio the density of states at the Fermi surface also changes. The contribution to the change in the resistivity by the change in the density of states should be very small, probably less than the experimental accuracy.

The slope of the resistivity-solute concentration curves (Figure 20) increases in the range 0 to 2.6 percent for solutes of aluminum and gallium, followed by a smaller constant slope above 2.6 percent aluminum or gallium. The addition of aluminum or gallium in titanium, therefore, does not obey Matthiessen's rule that the scattering from each solute atom is independent of the concentration. The additional resistivity increase can be accounted for by assuming that a resistivity contribution due to in-band scattering is significant, and represents the difference between the observed resistivity dependence on solute concentration and the linear resistivity-solute curve predicted by Matthiessen's rule. When a solute concentration of 2.6 percent is reached, the additional scattering due to in-band transitions begins to decrease. The concentration at which the contact between the

Fermi surface and the energy surface occurs, however, cannot be predicted due to the extreme complication of the in-band scattering problem. The anomalous resistivity dependence on solute concentration for solutes of aluminum and gallium does seem to be related to the valency of the solutes and an interaction of the Fermi surface with the energy zone, since the resistivity increase due to additions of silver is in agreement with Matthiessen's rule.

D. Magneto-Resistance:

The increase of resistance in a magnetic field has been evaluated theoretically in only a few simple cases, which do not strictly apply to the interpretation developed to explain the lattice parameter and resistivity changes. However, an insight into the observed behavior of the coefficient of magneto-resistance can be obtained from the existing theory.

Theoretical treatments of magneto-resistance are given by Mott and Jones (53, p. 280), Davis (75), and Sondheimer and Wilson (76) for nearly free electrons. The coefficient of magneto-resistance is given by Davis for nearly free electrons in the form:

$$B_t = \left(\frac{e}{\ell^2 c}\right)^2 \frac{I_4}{I_1 I_2} \quad , \qquad (6\text{-}3)$$

where:

$$I_1 = -\int S \frac{\partial f_o}{\partial E}\left(\frac{\partial E}{\partial k_1}\right)^2 d\tau$$

$$I_2 = -\int S \frac{\partial f_o}{\partial E}\left(\frac{\partial E}{\partial k_2}\right)^2 d\tau \qquad (6\text{-}4)$$

$$I_4 = -I_2 \int S \frac{\partial f_o}{\partial E}\left\{\Omega\left(S\frac{\partial E}{\partial k_1}\right)\right\}^2 d\tau - \left\{\int S \frac{\partial f_o}{\partial E}\frac{\partial E}{\partial k_2}\,\Omega\left(S\frac{\partial E}{\partial k_1}\right) d\tau\right\}^2 .$$

The symbols appearing in (6-4) are:

S is the relaxation time for the electron distribution,

f_o is the electron distribution function when no fields are present,

Ω is the differential operator $\frac{\partial E}{\partial k_2}\frac{\partial}{\partial k_1} - \frac{\partial E}{\partial k_1}\frac{\partial}{\partial k_2}$.

Evidently (6-3) involves integrals of the form:

$$\int S^2 \frac{\partial f_o}{\partial E}\left[\frac{\partial E}{\partial k_2}\frac{\partial^2 E}{\partial k_1^2}\right]^2 d\tau \qquad (6\text{-}5)$$

under the simplest possible assumptions. For free electrons E is equal to $h^2k^2/2m$ and Equation (6-3) vanishes. If the Fermi surface is near a surface of the energy zone,

$$E = E^\circ + V_{kk'} ,$$

and the magneto-resistance coefficient (6-3) does not vanish. The most important contribution to B_t comes from the terms $\frac{\partial^2 E}{\partial k^2}$. If, for simplicity, it is assumed that B_t is a function of $\frac{\partial^2 E}{\partial k^2}$ only, a qualitative interpretation of the experimental curves of the magneto-resistance coefficient (Figure 21) in terms of the model suggested by the lattice parameter and resistivity results.

As the Fermi surface approaches the surface of the energy zone $\frac{\partial^2 E}{\partial k^2}$ assumes large values and hence the magneto-resistance is large. When contact between the Fermi surface and the energy zone occurs over a large area, fewer energy states with large $\frac{\partial^2 E}{\partial k^2}$ remain to participate in the conduction process and the magneto-resistance decreases. Approximately, then, the interpretation of contact between the Fermi surface and the (001) face of the energy zone, occurring with the addition of aluminum and gallium to titanium at about 2.8 percent solute, seems to explain the change in B_t with aluminum and gallium additions. The coefficient of magneto-resistance decreases rapidly with addition of silver, agreeing with the previous interpretation of a decreasing electron-atom ratio with silver additions. The decrease in the electron-atom ratio with silver addition results in a decreasing $\frac{\partial^2 E}{\partial k^2}$ and hence a decrease in B_t. Thus the behavior of the coefficient of magneto-resistance is qualitatively consistent with the lattice parameter and resistivity changes in the titanium alloys.

E. Hall Coefficient:

The Hall coefficient, like the coefficient of magneto-resistance, is difficult to express quantitatively except in a few very simple cases. Davis (75) finds for the Hall coefficient the relation:

$$R = -\frac{4\pi^3}{ce}\,\frac{I_7}{I_1 I_2} \quad , \qquad (6\text{-}6)$$

where I_1 and I_2 are given by (6-4), and I_7 is:

$$I_7 = -\int S \frac{\partial f_0}{\partial E} \frac{\partial E}{\partial k_2} \left(\frac{\partial E}{\partial k_2} \frac{\partial}{\partial k_1} - \frac{\partial E}{\partial k_1} \frac{\partial}{\partial k_2} \right) \left(S \frac{\partial E}{\partial k_1} \right) d\tau . \qquad (6\text{-}7)$$

The relation (6-6) is written for a single band, for conduction by holes in addition to electrons, the contribution to the Hall coefficient by holes must be included. Since the Hall coefficient of titanium is positive, the contribution to the Hall effect must be primarily due to holes participating in the conduction process.

The absence of a pronounced change in the Hall coefficient for aluminum concentrations of about 3 percent, analogous to the effect observed in the magneto-resistance coefficient is surprising at first, since both effects seem to be similarly dependent on E(k). The Hall coefficient, however, may be much more sensitive to crystallographic direction than the magneto-resistance coefficient, as Shockley suggests (77). A qualitative examination of the relation between Hall coefficient and crystallographic direction seems to indicate that the fact that polycrystalline specimens are employed in this study is responsible for the small change of the Hall coefficient with solute concentration. The empty corners of the zones together with the narrow region between the Fermi surface and the (001) zone faces probably contribute a large density of empty states for conduction in those directions. Thus the Hall coefficient for conduction along the (001) axis of the zone is large and positive. In the (100) direction the Fermi surface is not adjacent to faces of the energy zone; the

conduction is largely by electrons, and therefore the Hall coefficient can be assumed to be negative. The Hall coefficient in all crystallographic directions is averaged in the polycrystalline specimen with the result that while the Hall coefficient in the (001) direction may change significantly, the average in all directions may not be appreciably changed.

Further support to the suggested explanation of the Hall coefficient behavior is provided by the experiments of Shindler and Salkovitz on polycrystalline magnesium alloys (78). Shindler and Salkovitz found the Hall constant for magnesium changed approximately 10 percent over the range of solute additions in which the axial ratio exhibited anomalous behavior. The change in axial ratio in Mg alloys is interpreted by Hume-Rothery and Raynor (7), Raynor (9), and Busk (14) to be due to interaction of the Fermi surface and the energy zones of magnesium. Therefore, from the results of Shindler and Salkovitz and the present study, it is not clear whether a larger change in the Hall coefficient might not be expected in single crystal specimens, and the small change in magnesium alloys and titanium alloys is due to the use of polycrystalline specimens.

F. Magnetic Susceptibility:

Magnetic susceptibility of metals arises from two separate contributions: the diamagnetic susceptibility of the orbital (bound) electrons, and the paramagnetic susceptibility of the conduction

electrons. The diamagnetic contribution in most cases is very small compared to the paramagnetism of the conduction electrons, and therefore can be neglected. The conduction electrons contributing to the paramagnetism can only be those at the Fermi surface since the electrons occupying lower energy states are assumed to be paired spin-wise in each state, and hence contribute no net magnetic moment. Neglecting correlation and exchange effects of the conduction electrons, but including the diamagnetic contribution due to the translational motion of the conduction electrons, the susceptibility is:

$$\chi = \frac{4}{3}\mu_B^2 \left(\frac{dn}{dE}\right)_{Ef} \quad , \qquad (6\text{-}8)$$

where μ_B is the electron magnetic moment, and $\left(\frac{dn}{dE}\right)_{Ef}$ is the density of energy states at the Fermi surface. Equation (6-8) should be regarded as only approximate quantitatively for any real metal; however, (6-8) indicates the strong dependence of susceptibility on the density of energy states at the Fermi surface. Furthermore, additional refinements of the theory* (51, p. 576), do not remove this dependency on the density of energy states. The susceptibility predicted by Equation (6-8) is sensibly independent of temperature, since the temperature enters, in an expansion about T = o, as $\left(\frac{kT}{E_f}\right)^2$ and higher powers. At room temperature kT/E_f is about 0.005, hence

*Recently, Stoner (68) and Hume-Rothery and Coles (69) have presented the susceptibility in terms of the collective electron approximation. The relations given by these writers are similar in their dependence on $\left(\frac{dn}{dE}\right)_{Ef}$ to the expressions given in the text.

$\left(kT/E_f\right)^2 = 25 \times 10^{-6}$ so that χ can be expected to change by less than 0.0025 percent due to increasing the temperature from 0° K to 300° K.

The change in the paramagnetic susceptibility of titanium with solute addition is shown in Figure 23. The paramagnetic susceptibility of titanium (3.3×10^{-6}) is of the order of 10 times larger than predicted by Equation (6-8). This is not a serious objection, since Equation (6-8) is only approximate, but it is a troublesome discrepancy which alone might justifiedly be overlooked. A serious discrepancy between the theoretical predictions and experiment occurs in the effect of solute additions on the observed susceptibility. From the results of the experiments previously discussed, a strong dependence of susceptibility on solute additions would be expected. It is pertinent, therefore, to examine the expected susceptibility change with solute addition carefully before abandoning the explanation of the other experiments.

The total susceptibility of the conduction electrons is composed of Pauli (spin) paramagnetism and the translational diamagnetism. The relation is:

$$\chi_{total} = \chi_{spin} + \chi_{trans.}$$

$$\chi_{total} = 2\mu_B^2 \left(\frac{dn}{dE}\right)_{E_f} - \frac{2}{3}\mu_B^2 \left(\frac{dn}{dE}\right)_{E_f} . \qquad (6\text{-}9)$$

Evidently, the use of polycrystalline specimens cannot be responsible for the susceptibility behavior. The term χ spin is independent of crystallographic direction, since electron spin is not directly related to real space. Only the diamagnetic term $\chi_{trans.}$ can exhibit a

dependence on crystallographic direction, and this is not likely to be more than 50 percent of the value of $\chi_{trans.}$, or at most a 12 percent variation in χ_{total} with crystallographic direction.

According to the approximate theory, χ_{total} depends linearly on $(dn/d\varepsilon)_{Ef}$. If the interpretation of the previous experiments is correct, the Fermi surface increases with addition of aluminum and contacts the (001) face of the energy zone at about 2.5 percent aluminum. The density of energy states should increase in this range, due to the perturbation terms, to a sharp maximum; and decrease rapidly above 2.5 percent aluminum. Addition of silver decreases the electron-atom ratio causing the Fermi surface to shrink away from the (001) face of the energy zone. The density of energy states should therefore decrease gradually with addition of silver. Since the susceptibility is a linear function of density of energy states, χ should exhibit the same general behavior. Figure 29 shows, for comparison, this theoretical variation of susceptibility and the observed susceptibility. The theoretical values are adjusted to the observed value for pure titanium.

The complete lack of agreement between the calculated susceptibility of the conduction electrons and the observed susceptibility is of sufficient importance to require careful consideration. Therefore, from the susceptibility results it appears the following conclusions are possible:

(a) The interpretation of the previous experiments is incorrect,

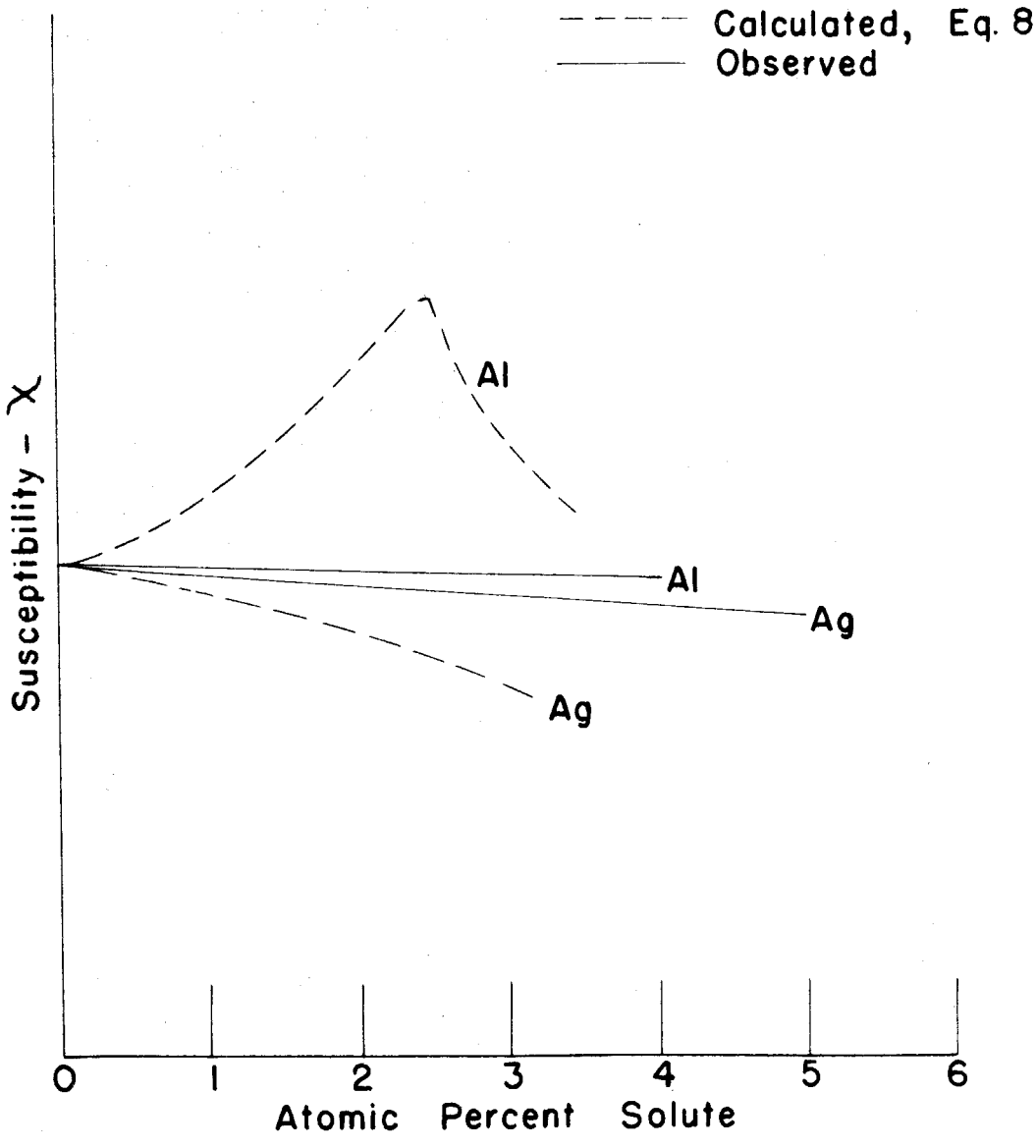

Figure 29 Calculated Susceptibility Of Conducting Electrons

Adjusted For Susceptibility Of Pure Titanium

(b) The apparent susceptibility is not due to the conduction electrons.

If (b) above is the correct interpretation of the susceptibility results, then the origin of the observed susceptibility must be in an electron energy band lying below the conduction band, but above the ionic states of the argon configuration. The energy levels in pure titanium must appear as shown in Figure 30. This hypothesis is not unreasonable on the basis of previous experiments; it provides an explanation of the observed valency effects of trivalent aluminum and gallium and monovalent silver by locating 2 electrons per atom of the 4 outer electrons of titanium below the conduction band so that the alloying valency is of the order of 2 electrons per atom, as previously assumed. The abnormally high resistivity of pure titanium can be explained in terms of transitions of conduction electrons to holes in the bound band as Seitz (51, p. 535) suggests. The resistivity-temperature curve, Figure 31, of pure titanium reported by Wyatt (42) is of the form to be expected from Seitz's analysis. In addition, the contribution to the specific heat by the electrons, as shown by the linear dependence of Cp on temperature near 0° K, is observed (68) to be smaller (by of the order of a factor of 10) than expected from the magnetic susceptibility of titanium. Since the electronic specific heat and the susceptibility due to the conduction electrons are dependent in the same way on the density of states, it is somewhat puzzling why the agreement is so poor.

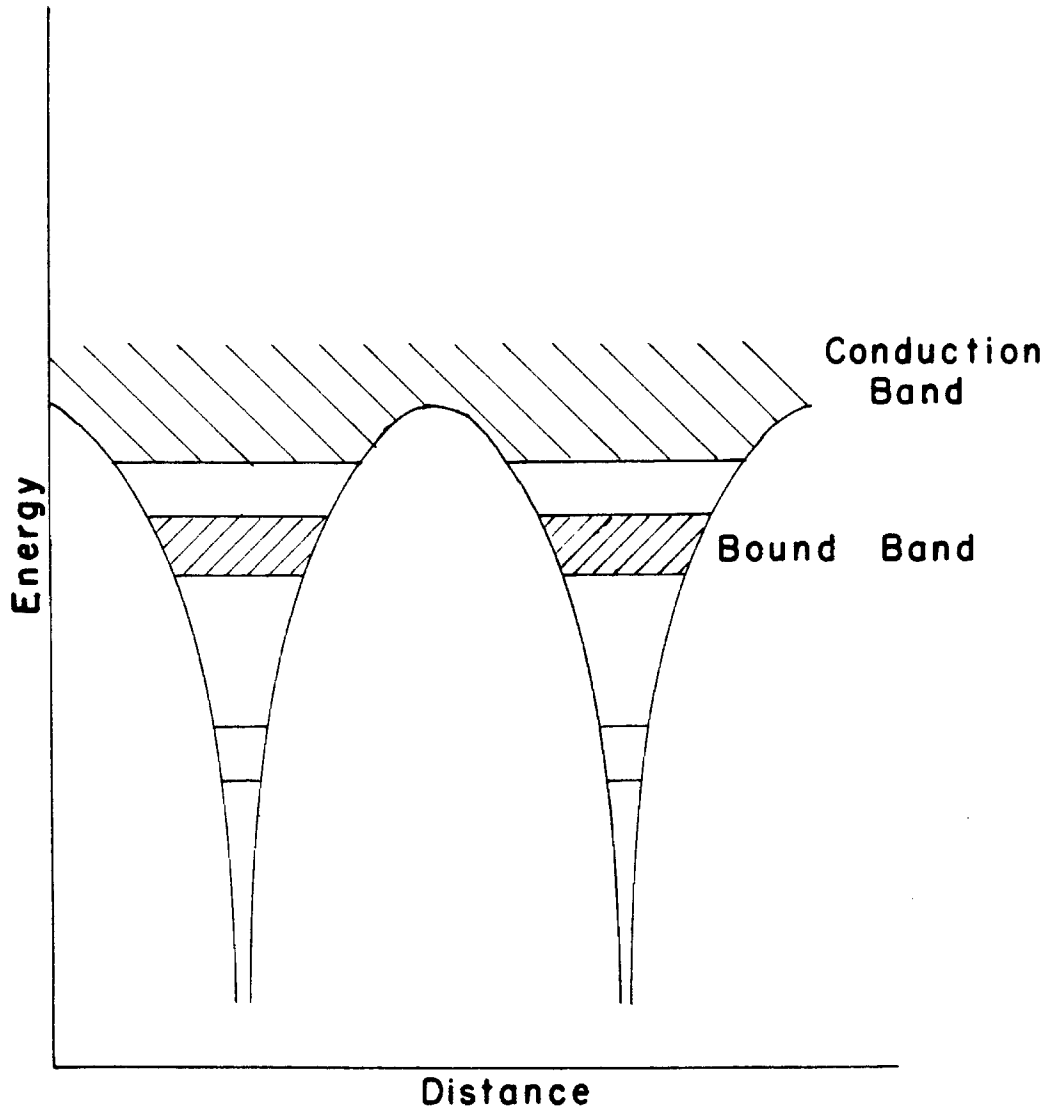

Figure 30 Proposed Energy Levels
In Titanium

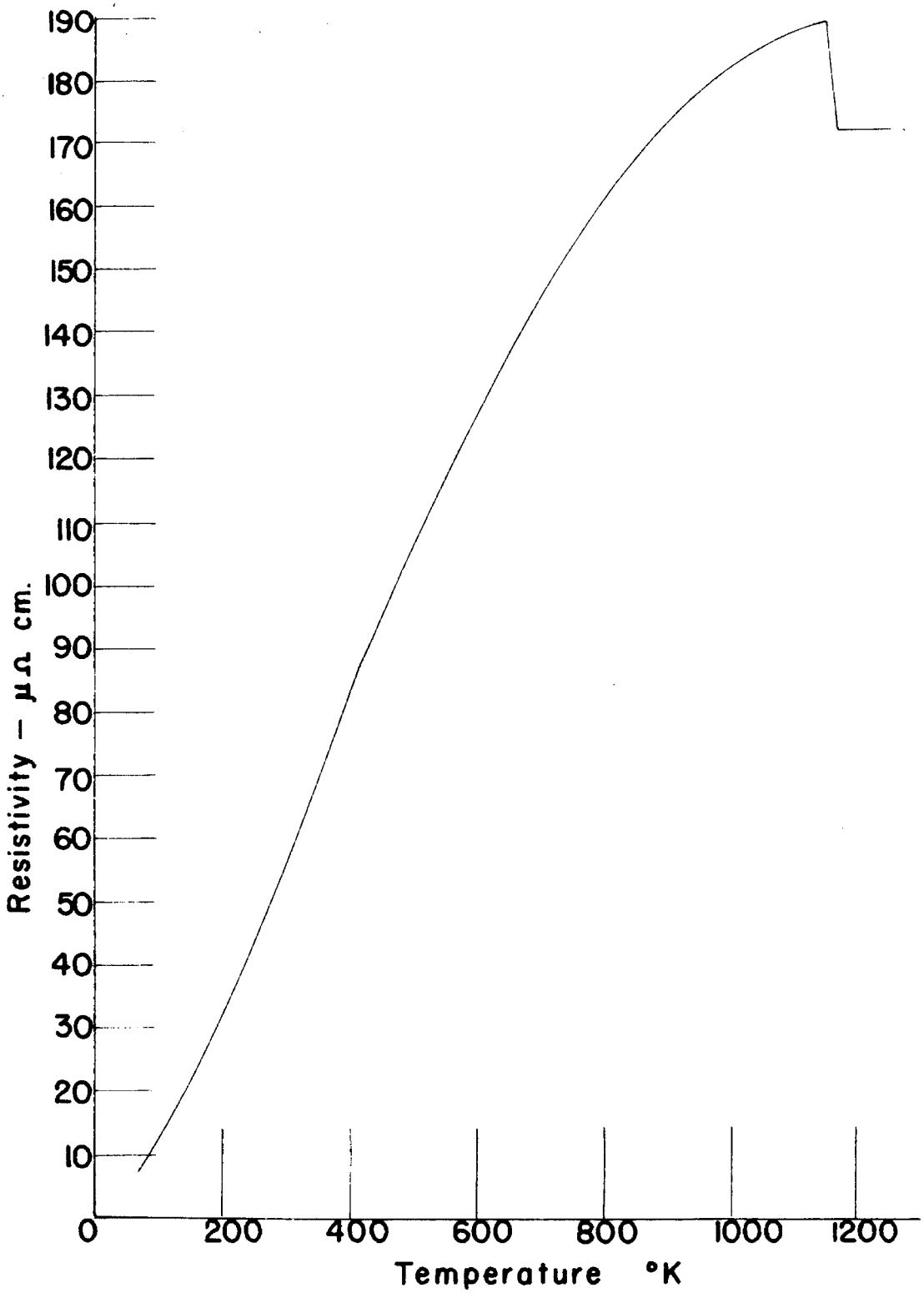

Figure 31 Resistivity Of Titanium (After Wyatt)

The ad hoc assumption of a bound energy band contributing heavily to the susceptibility requires some explanation about how this can occur. The wave functions for electrons in this band must strongly resemble the atomic 3d wave functions, since the electrostatic term of the Hamiltonian in this region cannot be severely perturbed from that for the free atom. The appropriate wave functions for these electrons, as a first approximation, may be constructed from atomic "d" wave functions; essentially this is the tight binding approximation of Bloch (57) and Jones and Mott (79). The cellular approximation of Wigner and Seitz (80), satisfying the symmetry properties of the lattice, may also be a suitable description of the wave functions in the bound band. Unfortunately the calculation is long and tedious and has never been done for titanium. The calculation for copper made by Krutter (81) has been extended by Slater (82) to the transition elements below copper in the periodic table. While there are a number of objections to extending Krutter's calculation to titanium, it is interesting to note that Slater's treatment of Krutter's calculation predicts a bound band in titanium, Figure 32.

Whether the tight binding or Wigner-Seitz approximations are used, it is clear that the wave functions will have the characteristics of "d" atomic wave functions. These wave functions of the electrons associated with one atom overlap the wave functions of the neighboring atoms, since the distance of separation is only 1.12 times the d-shell radius. Therefore, the exchange and correlation effects are certainly

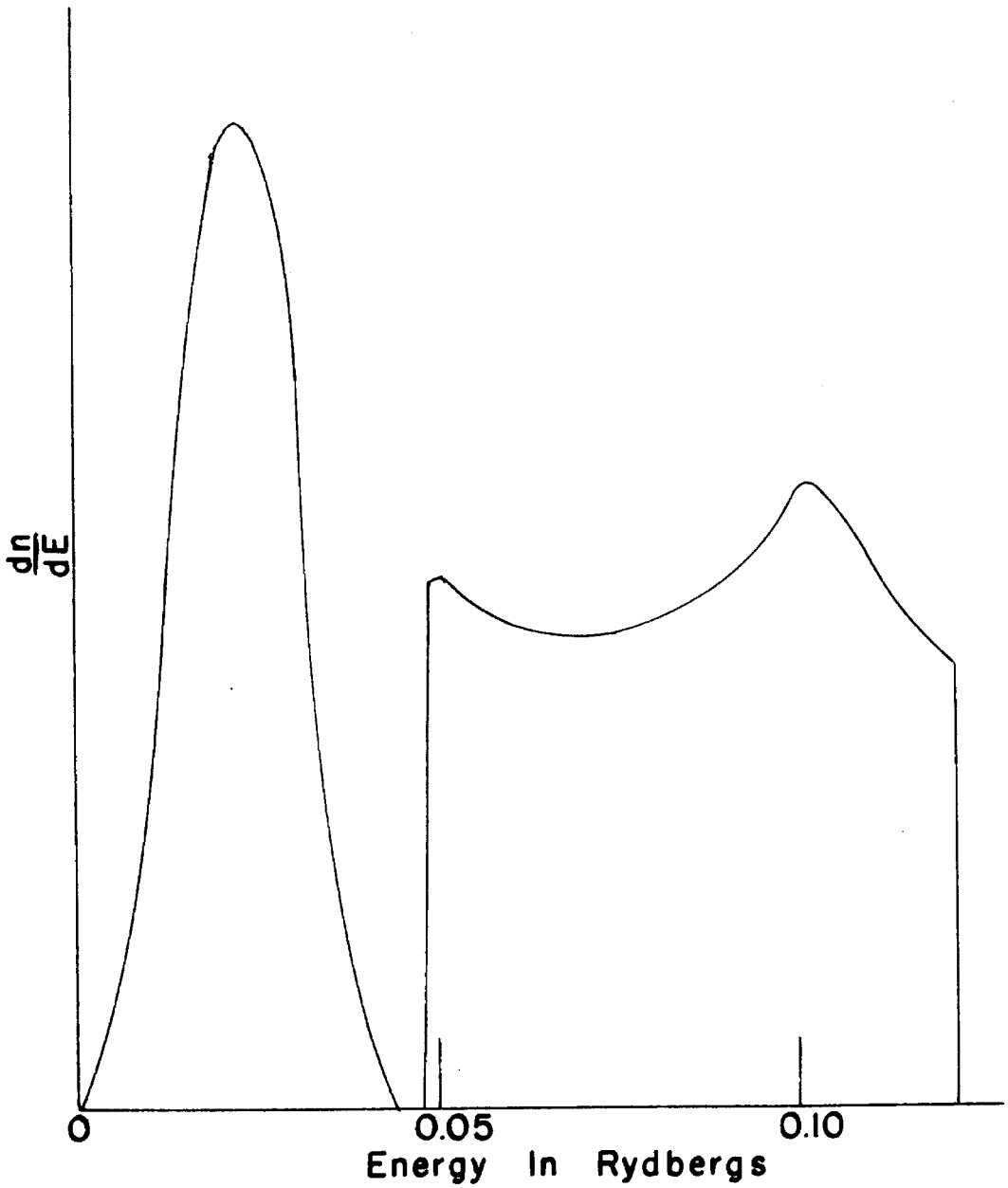

Figure 32 Density Of Energy Bands In Titanium (After Slater)

important contributions to the total energy. Zener (83) suggests that the exchange and correlation contributions insure antisymmetric spin coupling of these electrons, and therefore the d-function spins couple to form an antiferromagnetic exchange. In hexagonal close packed metals, according to Zener, the magnetic moments of the electrons are all aligned on any (001) plane, but the spins on adjacent (001) planes are aligned oppositely to the former. The magnetic lattice for titanium is simple hexagonal with, say, the + electron magnetic moment located at (000) and the - moment at (2/3, 1/3, 1/2), as shown in Figure 33.

Zener's antiferromagnetic model satisfies the requirements of the second (b) alternative resulting from the disagreement of susceptibility and the interpretation of the other experiments. An antiferromagnetic bound band can be expected to be occupied by the two outer electrons of titanium which, according to the interpretation, do not appear in the conduction band. The observed susceptibility is due largely (of the order of 90%) to the antiferromagnetic bound band, with a small (of the order of 10%) contribution from the conduction electrons in agreement with the electron specific heat. Confirmation of an antiferromagnetic structure in titanium could be immediately obtained from the detection of a simple hexagonal magnetic superlattice by neutron diffraction studies; however, neutron diffraction studies of titanium have not been reported. Studies of other properties in addition to those mentioned, which are less direct than neutron diffraction,

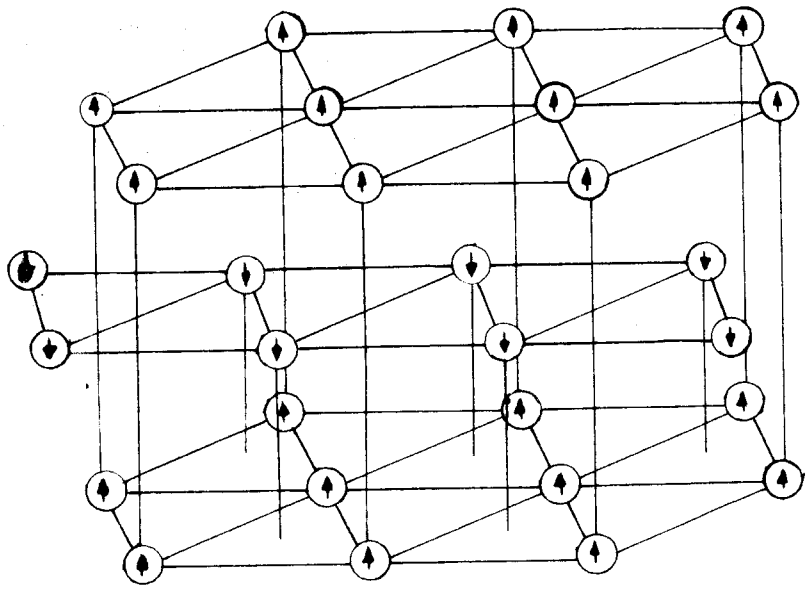

Figure 33 Antiferromagnetic Superlattice In Titanium

substantiate the assumed antiferromagnetic structure in titanium.

Van Vleck (64) from theoretical considerations predicts that the susceptibility due to antiferromagnetic coupling shows a temperature dependence. Van Vleck computes χ (T = 0°K) = 2/3 χ(T = T curie), and that χ(T) is nearly a linear function of temperature between 0° K and Tc. Van Vleck's theory agrees well with known antiferromagnetic crystals such as MnO. The variation of susceptibility with temperature for titanium found by Squire and Kaufmann (49) is shown in Figure 34, together with that predicted by Van Vleck's theory. The remarkable agreement between the experimental and theoretical curves probably is fortuitous, since the assumptions made by Van Vleck in developing the theory may not be entirely justified in titanium. The Squire and Kaufmann data, obtained by the less reliable Gouy method, nevertheless show excellent agreement with room temperature measurements made by the Fereday method in the present study, and are believed accurate.

Squire and Kaufmann, in their paper, quote J. C. Slater as suggesting that the titanium susceptibility may both show a temperature dependence and be due to the conduction electrons. The spin paramagnetism of the conduction electrons, Equation (6-8), may be strongly temperature dependent if the density $\left(\frac{dn}{d\mathcal{E}}\right)_{\mathcal{E}_f}$ is temperature dependent. Slater suggests that this may occur due to a slight splitting of the band which is sensitive to atomic spacing and hence to temperature. In this way $\left(\frac{dn}{d\mathcal{E}}\right)_{\mathcal{E}_f}$ is a function of temperature and not approximately

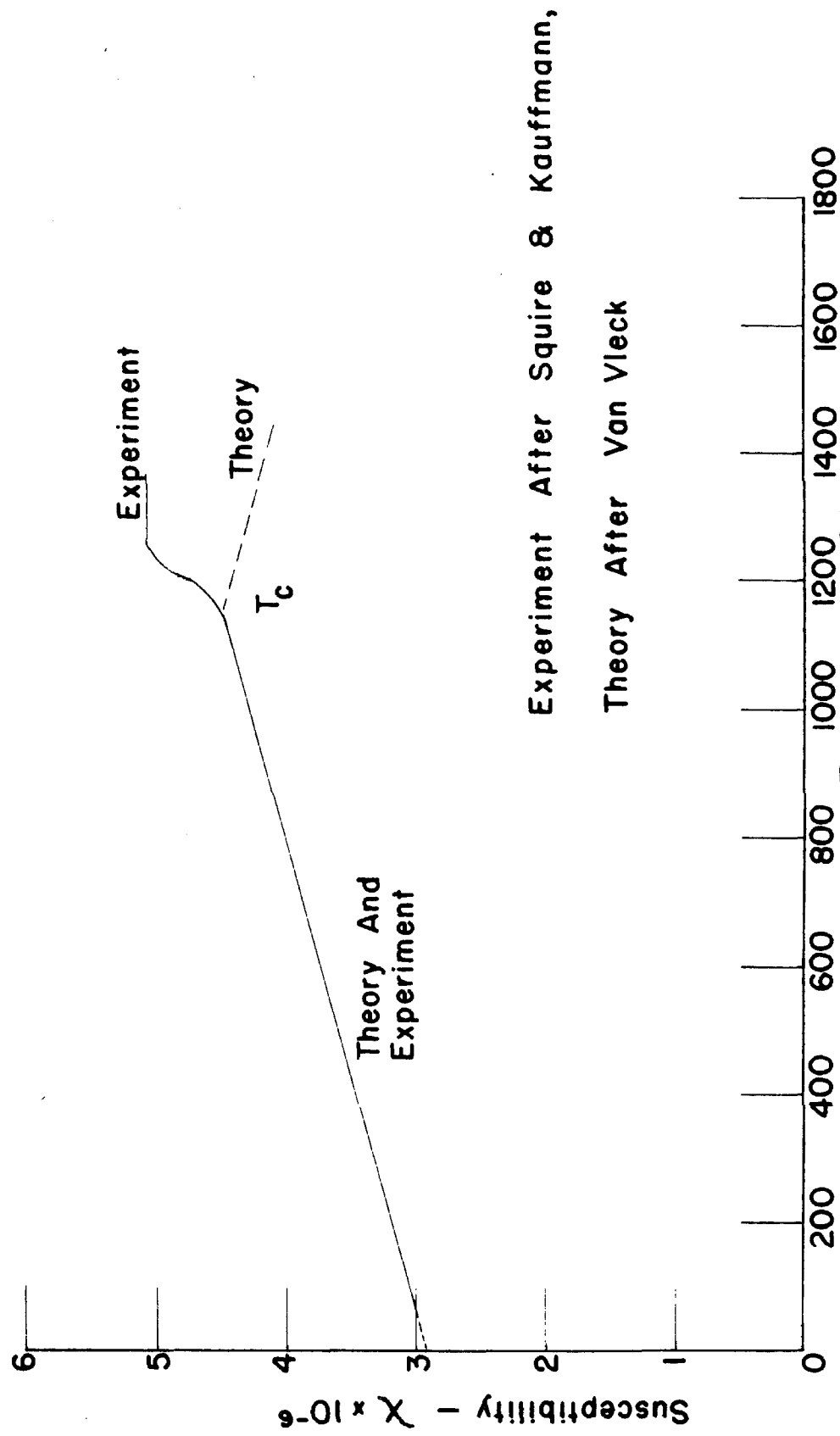

Figure 34 Susceptibility Of Titanium With Temperature

constant as assumed. The addition of solutes changes the electron-atom ratio and hence $\left(\frac{dn}{dE}\right)_{E_f}$, but causes no significant change in χ. Therefore Slater's suggestion is not correct; the assumed antiferromagnetic structure of titanium with Van Vleck's theory must be the correct interpretation of Squire and Kaufmann's data.

The addition of solutes can be expected to change $\left(\frac{dn}{dE}\right)_{E_f}$ less than 30 percent, and hence change χ spin due to the conduction electrons by less than 30 percent. χ spin of the conduction electrons is assumed to be of the order of 10 percent of the total susceptibility, from the electron specific heat, hence χ observed should change of the order of 3 percent or less due to solute additions. The observed susceptibility change, Figure 23, is approximately 3 percent or less in agreement with both the electron specific heat and the antiferromagnetic characteristics.

The evidence in favor of an antiferromagnetic structure due to a bound band occupied by 2 electrons per atom seems overwhelming. In lieu of neutron diffraction results, the evidence based on other experimental data seems adequate to conclude that the assumed antiferromagnetic structure does exist in titanium.

G. Electronic Structure:

The previously discussed experimental results appear to unambiguously suggest an electron structure in titanium consisting of two separate energy bands, each containing approximately two electrons.

The lower band, in which the electron wave functions are very nearly the same as the atomic 3d wave functions, is antiferromagnetic. The antiferromagnetic superlattice of the lower band, Figure 33, may have sufficient exchange energy associated with overlapping wave functions to be partly responsible for the low axial ratio c/a of titanium. This is not unreasonable on the basis of impurity effects on the axial ratio and susceptibility. Adsorbed oxygen, for example, increases the axial ratio (16) and markedly decreases the susceptibility. While the lower antiferromagnetic band is responsible for the susceptibility of titanium, it has little effect on the other properties studied. The addition of solutes, and the changes so produced, are largely the result of electronic effects in the upper, or conduction, band. The upper band appears to contain about 1.5 electrons per atom from a Bloch-Brillouin analysis of the physical properties. The wave functions in the upper band must be a mixture of "s" and "d" type functions with plane wave functions. The Bloch wave functions employed in this analysis are certainly no better than a rough approximation. A more sophisticated analysis, tight-binding, Wigner-Seitz, or the O.P.W. method described by Slater, might be expected to give a more reliable estimate of the number of electrons in the conduction band than the Bloch approximation. It is to be emphasized that the energy zones appear in some form in more elaborate methods, and the conclusions of energy zone interactions are probably much more accurate than the calculated density of energy states.

The energy band structure of pure titanium shown in Figure 30 is probably a good approximation to the actual band structure. However, the band structure is developed by somewhat indirect analysis in this study. Soft X-ray studies are necessary to more accurately establish the band structure.

Because of the double band structure of titanium, it is difficult to make any general statements of alloying valency. If titanium plays the role of the solvent in the alloy, the titanium valence in the alloy is about 2. If titanium is the solute atom, the valency may be either 2 or 4 electrons per atom depending on the potential near the solvent ions. The valency may, in addition, depend on the crystal structure of the alloy and on the lattice parameter. Certain compounds of titanium exhibit this double valency character, e.g., TiO and TiO_2. Titanium monoxide is a stable, electrically conducting compound indicating a valence of 2; while titanium behaves as if quadrivalent in titanium dioxide.

VII. SUMMARY AND CONCLUSIONS

The solid solution alloys consisting of solutes of aluminum, gallium, and silver in the titanium were investigated for changes in five physical properties due to the solute concentration in the alloys. In four of the five properties studied, lattice parameter, resistivity, coefficient of magneto-resistance, and Hall coefficient, evidence was obtained which indicates that: (1) the valency of the solute determines the manner in which these four properties change with solute addition; (2) the valency of titanium, as a solvent, is approximately 2 electrons per atom; and (3) analysis of the property changes in the alloys by the Brillouin-Bloch-Jones methods yields results consistent with experiment and indicates a solvent valency of titanium of 1.5 electrons per atom. The analysis of the data in the energy zone scheme requires that the correct energy zones be used. The energy zones for the close packed hexagonal lattice in both the extended and reduced schemes are developed by carrying out the perturbation calculation. The symmetry requirements of the point group and space group elements are discussed by methods due to Wigner, Seitz, and Herring, and the calculations for the hexagonal close packed lattice are presented. The form of the resulting energy zones differs from those given in the texts by Mott and Jones (53) and Wilson (52). These differences are shown to be due to symmetry requirements the latter zones do not satisfy.

The magnetic susceptibility does not exhibit any change with

solute additions. The Pauli spin paramagnetism of electrons in the conduction band is discussed to show that such changes are to be expected from the spin paramagnetism of the conduction electrons. It is concluded from the results of additional experiments of others, principally the temperature dependence of the susceptibility and the electron specific heat, together with absence of a solute effect on the susceptibility, that the major contribution to the observed susceptibility is from electrons in a bound energy band, containing 2 electrons per atom, below the conduction band. Van Vleck's theory of antiferromagnetic exchange coupling of the electrons in the bound band predicts susceptibility and electron specific heat effects which exhibit remarkable agreement with the observations. It is concluded on this basis that the metallic electronic structure of pure titanium consists of two bands: (1) the upper conduction band containing about 2 electrons per atom; and (2) a lower antiferromagnetic band containing 2 electrons per atom. This proposed electronic structure of titanium shows agreement with the present experimental studies and other pertinent data.

It is suggested that the lower antiferromagnetic band consists of anti-parallel spin coupling between neighboring planes of the form (001) in the hexagonal close packed titanium lattice. If the exchange coupling is as suggested, titanium must have a simple hexagonal magnetic superlattice. It is urged that neutron diffraction studies of pure titanium be executed to confirm the validity of this suggestion.

VIII. SUGGESTIONS FOR FURTHER WORK

The conclusion suggested by this study that titanium has an antiferromagnetic superlattice indicates the desirability of neutron diffraction studies. Experimental confirmation of the existence of a magnetic superlattice is extremely desirable. Soft X-ray emission spectroscopy is also desirable to determine the widths of the energy bands in titanium; however, the intensity of the X-rays will probably be uninterpretable due to the difficulty of calculating transition probabilities and the possibility of a significant Auger effect. The writer, in this respect, is grateful to Prof. J. H. Krumhansl of Cornell University for pointing out that the band widths might be obtained in an easier manner in this case by photoelectric emission.

The agreement between the lattice parameter anomalies and other physical property changes suggests further investigation in this direction. Among the properties which might be expected to exhibit similar behavior with solute additions in titanium are thermoelectric power and electronic specific heat. Additional interest is attached to thermoelectric power in these titanium alloys, since little experimental information is available to make direct comparison between thermoelectric power and electronic configuration in the metals. Thus thermoelectric power determinations in the titanium alloys may lead to a better understanding of the factors influencing thermoelectric power in alloys in general.

Investigation of ternary titanium solid solution alloys should be undertaken to determine the extent to which the analysis of the present study can be applied to alloys with two atomic species as solutes.

REFERENCES

(1) Hume-Rothery, W.; "Atomic Theory For Students of Metallurgy", Inst. of Metals, London, (1948).

(2) Pauling, L.; "Nature of the Chemical Bond", Cornell Univ. Press, Ithaca, N.Y., (1948).

(3) Jones, H.; "The Theory of Alloys in the Gamma-phase", Proc. Roy. Soc., A 144, 225 (1934).

(4) Jones, H.; "Applications of the Bloch Theory to the Study of Alloys and the Properties of Bismuth", Proc. Roy. Soc., A 147, 396 (1934).

(5) Peierls, R.; "Zur Theorie der elektrischen und thermischen Leitfahigkeit von Metallen", Ann. Physik 4, 121, (1930).

(6) Peierls, R.; "Zwei Bemerkungen zur Theorie der Leitfahigkeit", Ann. Physik 5, 244, (1930).

(7) Hume-Rothery, W. and Raynor, G.V.; "The Equilibrium and Lattice Spacing Relations in the System Mg-Cd", Proc. Roy. Soc., 174 A, 471 (1940); "The Apparent Sizes of Atoms in Metallic Crystals with Special Reference to Aluminum and Indium, and the Electronic State of Magnesium", Proc. Roy. Soc., 177 A, 27 (1940).

(8) Raynor, G. V.; "The Lattice Spacings of the Primary Solid Solutions of Silver, Cadmium, and Indium in Magnesium", Proc. Roy. Soc., 174 A, 457, (1940).

(9) Raynor, G. V.; "The Lattice Spacings of the Primary Solid Solutions in Magnesium of the Metals of Group IIIB and of Tin and Lead", Proc. Roy. Soc., 180 A, 107, (1942).

(10) Raynor, G. V.; "On the Solid Solutions of Chromium and Manganese in Aluminum", Phil. Mag., 36, 770, (1945).

(11) Raynor, G. V.; "The Constitution of the Aluminum Rich Al-Cr Alloys", Journal Inst. Met., 71, 493, (1945).

(12) Raynor, G. V.; "The Constitution of the Aluminum Rich Al-Co-Fe Alloys", Journal Inst. Met., 73, 397, (1947).

(13) Jones, H.; "The Effect of Electron Concentration on the Lattice Spacings in Magnesium Solid Solutions", Phil. Mag., 41, 663, (1950).

(14) Busk, R. S.; "Lattice Parameters of Magnesium Alloys", Trans. A.I.M.E., 188, 1460, (1950).

(15) Schramm, Gordon, and Kaufmann; "The Alloy Systems U-W, U-Ta, and W, Ta", Trans. A.I.M.E., 188, 195, (1950).

(16) Clark, H. T.; "The Lattice Parameters of High Purity Alpha Titanium; And the Effects of Oxygen and Nitrogen on Them", Trans. A.I.M.E., 185, 588, (1949).

(17) Bridgman, P. W.; Proc. Am. Acad. Arts Sciences, 60, 303-383, (1925).

(18) Carpenter, H. C. H.; Inst. Metals London, May Lecture, (1926).

(19) Jette, E. R., and Foote, F.; "Precision Determination of Lattice Constants", J. Chem. Phys., 3, 605, (1935).

(20) Spieser, R. ; private communication.

(21) Barrett, C. S.; "Structure of Metals", McGraw-Hill Book Co., New York, 1943, p. 125.

(22) Fereday, R. A.; "Comparison of Small Magnetic Susceptibilities", Proc. Phys. Soc., London, 42, 251, (1930).

(23) Davy, N.; "The Design of Pole Pieces of Electromagnets and the Forces Acting on Small Bodies Placed in Their Magnetic Fields", Phil. Mag., 33, 575, (1942).

(24) Cohen, M. U.; "Precision Lattice Constants from X-ray Powder Photographs", Rev. Sci. Inst., 6, 68, (1935).

(25) Hoel, P. G., "Introduction to Mathematical Statistics", John Wiley & Sons, New York, 1949.

(26) Cramer, H.; "Mathematical Methods of Statistics", Princeton University Press, Princeton, 1946.

(27) Saini, H.; "Coefficient of Expansion of Silver by X-Ray Method", Helv. Phys. Acta, 6, 597, (1933).

(28) Buerger, M. J.; "X-Ray Crystallography", John Wiley & Sons, New York, 1942.

(29) Jette, E. R., and Foote, F.; "Precision Determination of Lattice Constants", Rev. Sci. Inst., 10, 277, (1939).

(30) Cohen, E. R.; "Nonindependent Observational Equations in the Theory of Least Squares", Phys. Rev., 81, 162, (1951).

(31) Birge, R. T.; "Errors by Least Squares Method", Phys. Rev., 40, 207, (1932).

(32) Peierls, R.; "Theory of the Change of Resistance in Magnetic Fields", Ann. Phys., Lpz. (5), 10, 97, (1931).

(33) Page, L.; "Introduction to Theoretical Physics", Van Nostrand, New York, 1928.

(34) Hutchison, T. S., and Reekie, J.; "An Electrodynamic Balance for the Measurement of Magnetic Susceptibilities", J. Sci. Inst., 23, 209, (1946).

(35) McGuire, T. R., and Lane, C. T.; "Magnetic Susceptibility Balance for Use at Liquid Helium Temperatures", Rev. Sci. Inst., 20, 489, (1949).

(36) Honda, K.; "Magnetization of Alloys in Relation to Their Composition and Temperature", Ann. Phys., Lpz., 32, 1048, (1910).

(37) Owen, M.; "Thermomagnetic Properties of the Elements", Ann. Phys., Lpz., 37, 657, (1912).

(38) Vogt, E.; "Atomic State in Metallic Lattices from the Basis of Magnetic Measurements", Ann. Phys., Lpz., 14, 1, (1932).

(39) Bumps, E. S., Kessler, H. D., and Hansen, M.; "Titanium-Aluminum System", A.I.M.E., J. of Metals, 4, 609, (1952).

(40) Adenstedt, H. K., and Freeman, Jr., W. R.; "The Tentative Titanium-Silver Binary System", WADC Technical Report 52-109, Part I, April 1953.

(41) Worner, H. W.; "The Structure of Titanium-Silver Alloys in the Range 0 - 30 At. % Silver", J. Inst. Metals, 82, 222, (1954).

(42) Wyatt, J. L.; "Electrical Resistance of Titanium Metal", A.I.M.E., J. of Metals, 5, 903, (1953).

(43) Matthiessen, A.; Pogg. Ann., 103, 428, (1858).

(44) Matthiessen, A., and Holzmann, H.; Pogg. Ann., 110, 222, (1860).

(45) Guertler, W.; "Electrical Conductivity of Alloys", Ztsch. anorg. allgem. Chemie, 51, 397, (1906).

(46) Linde, J. O.; "Electrical Properties of Gold Alloys", Ann. Physik, 10, 52, (1931); "Electrical Properties of Silver Alloys", Ann. Physik, 14, 353, (1932); "Electrical Properties of Dilute Solid Solutions. Part III. Resistance of Copper and Gold Alloys. Regularities in the Resistance Increments", 15, 219, (1932).

(47) Scovil, G. W.; "The Hall Effect in Titanium", J. App. Phys., 24, 226, (1953).

(48) Foner, S.; "Hall Effect in Pure Titanium, Vanadium, and Chromium", Phys. Rev., 91, 447 (A), (1953).

(49) Squire, C. F., and Kaufmann, A. R.; "The Magnetic Susceptibility of Ti and Zr", J. Chem. Phys., 9, 673, (1941).

(50) de Boer, J. H., Clausing, P., and Fast, J. D.; "Transition of Hexagonal to Cubic Titanium", Rec. Trav. Chim, 55, 450, (1936).

(51) Seitz, F.; "Modern Theory of Solids", McGraw-Hill Book Co., New York, 1940.

(52) Wilson, A. H.; "The Theory of Metals", Cambridge Univ. Press, London, 1953.

(53) Mott, N. F., and Jones, H.; "Theory of the Properties of Metals and Alloys", Oxford Univ. Press, London, 1936.

(54) Drude, P.; Ann. Physik, 1, 566, (1900).

(55) Lorentz, H. A.; Amsterdam Proc., 1904-1905; "The Theory of Electrons", G. P. Stechert & Co., New York, 1923.

(56) Sommerfeld, A.; "Electron Theory of Metals on the Basis of the Fermi Statistics", Z. Physik, 47, 1, (1928).

(57) Bloch, F.; "Quantum Mechanics of Electrons in Crystal Lattices", Zeits. f. Physik, 52, 555, (1928).

(58) Brillouin, L.; "Die Quantenstatistik", J. Springer, Berlin, 1931. Also: Compt. Rend., 191, 198, (1930); 191, 292, (1930); Jour. Phys. (VII), 1, 377, (1930).

(59) Wigner, E.; "Constitution of Metallic Sodium", Gott. Nachr., 1932, 546, (1932).

(60) Herring, C.; "Effect of Time-Reversal Symmetry on Energy Bands of Crystals", Phys. Rev., 52, 361, (1937).

(61) Seitz, F.; "Matrix-Algebraic Development of Crystallographic Groups", Ann. of Math., 37, 17, (1936).

(62) Herring, C.; "Accidental Degeneracy in the Energy Bands of Crystals", Phys. Rev., 52, 365, (1937).

(63) Bouckaert, C., Smoluchowski, R., and Wigner, E.; "Theory of Brillouin Zones and Symmetry Properties of Wave Functions in Crystals", Phys. Rev., 50, 58, (1936).

(64) Hund, F.; "Symmetry of a Crystal Lattice and the States of its Electrons", Zeits. f. Physik, 99, 119, (1936).

(65) Pines, David; Private communication.

(66) Wigner, E. P.; "Interaction of Electrons in Metals", Phys. Rev., 46, 1002, (1934); "Effects of Electron Interaction on Energy Levels in Metals", Trans. Faraday Soc., 34, 678, (1938).

(67) Pines, David; "A Collective Description of Electron Interactions", Phys. Rev., 82, 625, (1951); "A Collective Description of Electron Interactions II", Phys. Rev., 85, 338, (1952); "A Collective Description of Electron Interactions III", Phys. Rev., 92, 609, (1953); "A Collective Description of Electron Interactions IV", Phys. Rev., 92, 626, (1953).

(68) Stoner, E. C.; "The Magnetic Susceptibility and Electronic Specific Heat of Transition Metals in Relation to Their Electronic Structure", Acta Met., 2, 250, (1954).

(69) Hume-Rothery, W., and Coles, B. R.; "The Transition Metals and Their Alloys", Adv. in Physics, (Suppl. Phil. Mag.), 3, 149, (1954).

(70) Goodenough, J. B.; "A Theory of the Deviation from Close Packing in Hexagonal Metal Crystals", Phys. Rev., 89, 282, (1953).

(71) Duwez, P. E.; "Atomic Diameters of Metallic Elements", Metal Progress, 61, 348 B, (1950).

(72) Hume-Rothery, W., and Andrews, K. W.; "The Equilibrium Diagram of the System Silver-Gallium", J. Inst. Met., 68, 133, (1942).

(73) Owen, E. A., and Rowlands, V. W.; "Solubility of Certain Elements in Copper and Silver", J. Inst. Met., 66, 361, (1940).

(74) Hibbard, W. R.; "Electrical Resistivity of Dilute Binary Terminal Solid Solutions", Trans. A.I.M.E., 200; J. Met., 6, 594, (1954).

(75) Davis, L.; "Change of Resistance in a Magnetic Field", Phys. Rev., 56, 93, (1939).

(76) Sondheimer, E. H., and Wilson, A. H.; "The Theory of the Magneto-resistance Effects in Metals", Proc. Roy. Soc., A 190, 435, (1947).

(77) Shockley, W.; "Electrons and Holes in Semiconductors", Van Nostrand Co., New York, 1950.

(78) Schindler, A. I., and Salkovitz, E. I.; "Brillouin Zone Investigation of Mg Alloys. I. Hall Effect and Conductivity", Phys. Rev., 91, 1320, (1953).

(79) Jones, H., and Mott, N. F.; "Electronic Specific Heat and X-Ray Absorption of Metals and Other Properties Related to Electron Bands", Proc. Roy. Soc., 162 A, 49, (1937).

(80) Wigner, E., and Seitz, F.; "Constitution of Metallic Sodium", Phys. Rev., 43, 804, (1933); "Constitution of Metallic Sodium. II.", Phys. Rev., 46, 509, (1934).

(81) Krutter, H. M.; "Energy Bands in Copper", Phys. Rev., 48, 664, (1935).

(82) Slater, J. C.; "Ferromagnetism of Nickel", Phys. Rev., 49, 537, (1936); "Electronic Structure of Alloys", J. App. Phys., 8, 385, (1937).

(83) Zener, C.; "Interaction between the d-shells in the Transition Metals", Phys. Rev., 81, 440, (1951); "Interaction between the d-shells in the Transition Metals. II. Ferromagnetic Compounds of Manganese with Perovskite Structure", Phys. Rev., 82, 403, (1952); "Interaction between the d-shells in the Transition Metals. III. Calculation of the Weiss Factors in Fe, Co, and Ni", Phys. Rev., 83, 299, (1952); "Interaction between the d-shells in the Transition Metals. IV. The Intrinsic Antiferromagnetic Character of Iron", Phys. Rev., 85, 324, (1953).

(84) Van Vleck, J. H.; "On the Theory of Antiferromagnetism", J. Chem. Phys., 9, 85, (1941).